

MODELING AND INVERSION OF MAGNETIC AND  
IP/RESISTIVITY DATA FOR DELINEATING  
FAVOURABLE TARGET AREAS FOR URANIUM  
MINERALIZATION IN CHHOTA UDAIPUR, AJMER  
DISTRICT, RAJASTHAN

*by*

CHINNAMILI RAMANJANEYULU

ENGG1G201801005

**Bhabha Atomic Research Centre, Mumbai**

*A thesis submitted to the  
Board of Studies in Engineering Sciences*

*In partial fulfillment of requirements*

*for the Degree of*

MASTER OF TECHNOLOGY

*of*

**HOMI BHABHA NATIONAL INSTITUTE**

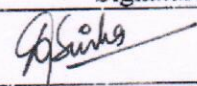
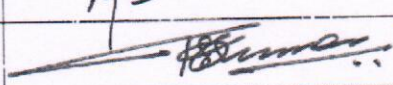
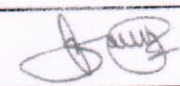
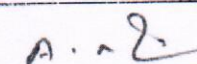
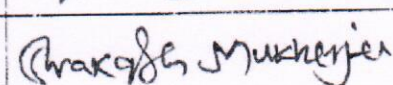
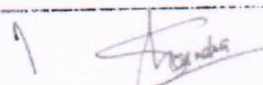
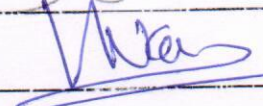


**February, 2021**

# Homi Bhabha National Institute

## Recommendations of the Thesis Examining Committee

As members of the Thesis examining Committee, we recommend that the thesis prepared by Chinnamalli Ramanjaneyulu entitled "Modeling and inversion of Magnetic and IP/Resistivity data for delineating favourable target areas for Uranium mineralization in Chhota Udaipur, Ajmer district, Rajasthan" be accepted as fulfilling the thesis requirement for the Degree of Master of Technology.

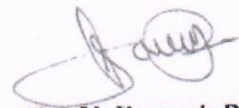
	Name	Signature
Member-1	Dr. D. K. Sinha	
Member-2	Dr. T. S. Sunil Kumar	
Member-3	Dr. V. Ramesh Babu	
Member-4	Dr. A. Rama Raju	
Technical Advisor	Prakash Mukherjee	
Examiner	Dr. Subhash Chandra	
Guide & Convener	Dr. V. Ramesh Babu	
Chairman	Prof. Vivekanand Kain	

Final approval and acceptance of this thesis is contingent upon the candidate's submission of the final copies of the thesis to HBNI.

I hereby certify that I have read this thesis prepared under my direction and recommend that it may be accepted as fulfilling the thesis requirement.

Date: 11-02-2021

Place: Hyderabad



(Dr. V. Ramesh Babu)  
Guide

## DECLARATION

I, hereby declare that the investigation presented in the thesis has been carried out by me. The work is original and has not been submitted earlier as a whole or in part for a degree / diploma at this or any other Institution / University.

*CH Ramanjaneyulu*  
(Chinnamilli Ramanjaneyulu)

## ACKNOWLEDGEMENT

My greatest appreciation goes to my project Guide, Dr. V. Ramesh Babu, Adjunct Professor, HBNI for his valuable support and decisive guidance throughout this thesis work. His support in suggesting valuable reference books, in sharing his field and research experience contributed greatly to enrich my thesis.

I have great pleasure in acknowledging my gratitude to my technical advisor Shri Prakash Mukherjee, SO/D, Exploration Geophysics group, AMD, Jaipur for his honest and constructive comments in data processing and interpretation.

I am grateful to Dr. D. K. Sinha, Director, Atomic Minerals Directorate for Exploration & Research (AMD), Department of Atomic Energy (DAE) who has given me the opportunity to do M. Tech Degree course from HBNI through BARC training school.

I also wish my thanks with deeper sense of gratitude to Additional Director (OP-I), Additional Director (OP-II), Additional Director R & D for their guidance and support.

I would also like to thank Regional Director, AMD, WR and Deputy Regional Director AMD, WR for his continuous support and discussions at various steps during this thesis work and help for submitting thesis within given time frame.

My special thanks go to Shri A. Markandeyulu, Incharge, EGP Group, AMD-Hyderabad and Shri Subash Ram, Incharge, EGP Group, AMD-Jaipur.

I would like to thank Shri Roshan Ali Shaik (SO/D), Y. Siva Krishna (SO/D), Shri Deepak Kumar (SO/D), Shri Rajesh Kumar Verma (SO/D), D. Damodhar (SO/C), Shri D. Raghavender (SO/C), of EGPG, AMD, WR and Shri B. Srinivas Rao (SO/E), Shri T. Manoj Kumar (SO/C) of AMD, SR, Shri Harsha Yalla, SO/D (ASRS) for their support and helpful discussions.

I would also like to thank incharge Petrology laboratory and XRF laboratory, AMD, WR for their support and My acknowledgement would be incomplete without thanking Incharge and Head BARC Training School, AMD Campus, Hyderabad for their support and for ensuring the optimum academic environment that has helped me in completion of the project.

I am also thankful to the competent authority of HBNI for providing the opportunity to pursue the M. Tech. degree.

I also thankful to my colleagues, all technical and non-technical staff who have supported me directly or indirectly in the completion of my project work

# CONTENTS

<b>SYNOPSIS</b>	iv
<b>LIST OF FIGURES</b>	v
<b>LIST OF TABLES</b>	ix
<b>CHAPTER 1 INTRODUCTION</b>	
1.1 General	1
1.2 Geophysical methods for uranium exploration	2
1.2.1 Magnetic method	3
1.2.2 Induced polarization (IP) and Electrical resistivity methods	4
1.3 Study area	4
1.3.1 Objective of the study	4
1.3.2 Location and accessibility of the study area	5
1.3.3 Previous work	6
<b>CHAPTER 2 GEOLOGY OF THE STUDY AREA</b>	
2.1 Introduction	11
2.2 Regional geology of the area	12
2.2.1 Banded Gneissic Complex	13
2.3 Detailed geology of the study area	14
<b>CHAPTER 3 MAGNETIC METHOD OF EXPLORATION</b>	
3.0 Introduction	17
3.1 Theory of magnetic method	18
3.2 Instruments	19
3.3 Magnetic Data Acquisition	20
3.4 Physical property measurement	21

3.5 Magnetic Data processing	22
3.5.1 Diurnal correction	23
3.5.2 Correction for cultural noise	24
3.5.3 Data visualization	24
3.5.4 Filtering techniques	24
3.6 Interpretation of Magnetic Data	25
3.6.1 Qualitative interpretation	26
3.6.1.1 Total Magnetic Intensity Anomaly Map	26
3.6.1.2 Reduced to Pole Magnetic Anomaly Map	27
3.6.1.3 Upward continuation filter	29
3.6.1.4 First Vertical Derivative Filter	30
3.6.1.5 Tilt Derivative or Tilt angle method	32
3.6.2 Quantitative interpretation of magnetic data	33
3.6.2.1 Euler deconvolution	34
3.6.3 Modeling and Inversion of Magnetic Data	36
3.6.3.1 2-D Forward Modeling	36
3.6.3.2 3-D Modeling	39
3.6.3.3 Forward modeling in 3D	43

## **CHAPTER 4 INDUCED POLARIZATION AND RESISTIVITY METHOD OF EXPLORATION**

4.1 Introduction	47
4.2 Theory of Induced polarization	48
4.2.1 Membrane polarization	49
4.2.2 Electrode polarization	49
4.3 Measurement of Induced Polarization	50
4.4 Theory of DC Resistivity method	51

4.5 Data Acquisition of IP and Resistivity Data	54
4.5.1 Instrumentation	54
4.5.2 Gradient array	54
4.5.3 Data acquisition	55
4.6 Processing and interpretation of IP and Resistivity Data	57
4.6.1 Apparent Resistivity Map	57
4.6.2 Apparent Chargeability Map	58
4.6.3 Decay curve analysis of IP data	60
4.7 Inversion of IP/Resistivity Data	64
<b>CHAPTER 5 INTEGRATED INTERPRETATION</b>	
5.1 Petrographic Study	69
5.2 Hydrogeochemical study	70
5.3 Geochemical analysis	72
5.4 Profile analysis of Magnetic and IP/Resistivity data	75
<b>CHAPTER 6 CONCLUSIONS</b>	81
PUBLICATION TITLE	83
REFERENCES	85

## SYNOPSIS

This thesis for the M. Tech project through HBNI deals with the systematic application of Magnetic and IP/Resistivity methods to identify the subsurface target areas for uranium mineralisation in and around Chhota Udaipur, Ajmer district, Rajasthan. The study area is located around 9 km south-east of Kishangarh which is a part of the banded gneissic complex (BGC) of Archaean age. Radioactive anomalies with high uranium concentration were reported during geological investigation in 1997-98 by AMD. The study area gained more importance as it is located within the albitite zone in its southern part which is important in the NDFB for its correlation with U mineralization in several areas like Rohil-Ghateswar sector of Sikar district, Rajasthan. Magnetic and IP/Resistivity methods are applied to delineate the structural features like faults/fractures, shear zones and conductive bodies which form the ideal environment for U-mineralization.

Magnetic data was acquired over the 30 sq.km area which facilitated in demarcating faults/fractures in E-W, NE-SW and NW-SE directions. Three significant high magnetic anomalies have been observed in the middle and towards southeastern side of study area, interpreted as mafic intrusion/ magnetite mineralization in BGC. 2-D and 3-D magnetic models enabled in deciphering the location and geometry of the structures in the study area. From IP/Resistivity data over 7.5 sq.km area, three high chargeability zones have been delineated, zone-M<sub>1</sub> has NE-SW strike length of around 600 m with width of 90 to 130 m and zone-M<sub>2</sub> has strike length of 1.5 km with width of 300 to 350 m in NNE-SSW direction in the eastern side of the study area. The high chargeability zones are correlatable with low to moderate resistivities which are interpreted as the fractures filled with disseminated sulphides in BGC. Laboratory analysis of rock samples and water samples were carried out for better correlation with the observed geophysical anomalies with laboratory values.

Integrated interpretation of geophysical data including petrographic study, geochemical and hydro geochemical studies reveal that high chargeability zones are well correlated with the moderate to low resistivity and moderate to high magnetic zones. These zones are favorable target areas for sub-surface uranium mineralization in this area.

## LIST OF FIGURES

<b>Figure No.</b>	<b>Description</b>	<b>Page No.</b>
1.1	Location of the study area, Chhota udaipur village, Ajmer district, Rajasthan	5
1.2	Survey block over toposheet No. 45J/14 & 15, Chhota udaipur area, Ajmer district , Rajasthan	6
1.3	Previous geophysical Total magnetic anomaly map, Chhota Udaipur area, Ajmer district, Rajasthan	8
1.4	Previous geophysical apparent chargeability contour map, Chhota Udaipur area, Ajmer district, Rajasthan	9
2.1	Three sub-basins of North Delhi Fold Belt, two sub-parallel albitite zone present in the Khetri Sub-Basin and BGC	13
2.2	Geological map of Tilonia-Nasirabad area, Ajmer district, Rajasthan	16
3.1	GEM Systems, GSM 19T Proton Precision Magnetometer used for Data Acquisition in the survey area	19
3.2	Magnetic profile layout map, Chhota Udaipur area, Ajmer district, Rajasthan	20
3.3	Diurnal variation of geomagnetic field on 17 <sup>th</sup> December 2019	23
3.4	Total magnetic intensity anomaly map, Chhota Udaipur area, Ajmer district , Rajasthan	27
3.5	Reduced to pole anomaly map, Chhota Udaipur area, Ajmer district , Rajasthan	28
3.6	Upward continued magnetic (RTP) map of 400m level, Chhota Udaipur area, Ajmer district, Rajasthan	30

3.7	FVD of TMI anomaly map, Chhota Udaipur area, Ajmer district, Rajasthan	31
3.8	Tilt-Angle map of the RTP grid, Chhota Udaipur area, Ajmer district , Rajasthan	33
3.9	Euler solutions over TMI map, Chhota Udaipur area, Ajmer district , Rajasthan	35
3.10	Profile AB over TMI map for 2D modeling	37
3.11	2D geological model of profile AB, Chhota Udaipur area, Ajmer district , Rajasthan	38
3.12	3-D Inverted Magnetic model of Chhota Udaipur area, Ajmer district , Rajasthan	41
3.13	Inverted magnetic model highlighting the high susceptibility bodies overlaid on the rtp map, chhota udaipur area, Ajmer district, Rajasthan	42
3.14	Horizontal depth slices of inverted magnetic model at a depth of 200m, 400m and 600m	43
3.15	TMI map and 3D modelled TMI map response	44
3.16	3D forward modeling for observed TMI response	45
4.1	(A) Membrane polarization (B) Electrode polarization	50
4.2	IP measurement	51
4.3	Schematic diagram for the resistivity( $\rho$ ) when current passes through a material	52
4.4	General electrode configuration used in resistivity survey	53
4.5	Multi electrode IRIS IP Receiver	54

4.6	IRIS IP Transmitter	54
4.7	Gradient array configuration	55
4.8	IP/Resistivity Profiles layout over RTP map, Chhota Udaipur area, Ajmer district , Rajasthan	56
4.9	Apparent resistivity map, Chhota-Udaipur area, Ajmer district, Rajasthan	58
4.10	Apparent chargeability map, Chhota-Udaipur area, Ajmer district, Rajasthan	60
4.11	Chargeability decay curve analysis of IP data station near RW <sub>1</sub>	62
4.12	Chargeability decay plot analysis of IP data station near RW <sub>2</sub>	62
4.13	Bivariate plot of Chargeability (a) & Decay Time constant( $\tau_1$ )	63
4.14	Bivariate plot of Chargeability(b) & Decay Time constant( $\tau_2$ )	63
4.15	2D-Inverted depth sections (P) resistivity (Q) Chargeability of IP/Resistivity data along the traverse S8E	66
4.16	2-D Inverted depth-sections of Chargeability along the traverses S6, S7 and S8, Chhota Udaipur area, Ajmer district, Rajasthan	67
4.17	2-D Inverted depth-sections of Resistivity along the traverses S6, S7 and S8, Chhota Udaipur area, Ajmer district, Rajasthan	68
5.1	Petrographic study of radioactive sample	69
5.2	Petrographic study of grab sample	70
5.3	Petrographic study of grab sample	70
5.4	Water sample locations over the RTP map of Chhota Udaipur area, Ajmer district , Rajasthan	71

5.5	Correlation of major oxides	74
5.6	Primitive Mantle normalized spider plot	74
5.7	Profiles over RTP and Apparent chargeability maps	75
5.8	Profile analysis of magnetic and IP/Resistivity data along RW <sub>1</sub> line	76
5.9	Profile analysis of magnetic and IP/Resistivity data along RW <sub>2</sub> line	77
5.10	(a) Integrated structural features and high chargeability zones over FVD of RTP map (b) Resistivity contour map of Chhota Udaipur area, Ajmer district, Rajasthan	78

## LIST OF TABLES

<b>Table No.</b>	<b>Description</b>	<b>Page No.</b>
2.1	Stratigraphic Classification of Bhilwara Supergroup	15
3.1	Physical properties of various rock samples from Chhota Udaipur, Ajmer district, Rajasthan	22
3.2	Different rock types and their magnetic susceptibility for the model of AB profile	39
3.3	Inversion parameters of 3D magnetic voxel model	40
4.1	Inversion parameters of chargeability and resistivity depth section of S8E line	64
4.2	Inversion parameters of chargeability and resistivity depth sections of S6, S7 and S8 lines	65
5.1	Hydrogeochemical analysis of water samples from Chhota Udaipur area, Ajmer district, Rajasthan	73



# CHAPTER 1

## INTRODUCTION

### 1.1 General

Fossil fuel sources are gradually declining, leading to a potential global scarcity of energy. Nuclear power is a long-term, low-carbon and cleaner solution to meet the requirements of increasing population in our country and it has a very significant economic and operational advantages over other conventional sources of power. It produces energy via nuclear fission rather than chemical burning and it contributes 34% reduction in carbon intensity per MW than renewable (world nuclear news 2020), the noxious element of global warming. A pellet of nuclear fuel weighs approximately 6 grams. However, that single pellet yields the amount of energy equivalent to that generated by a ton of coal, 120 gallons of oil or 17,000 cubic feet of natural gas, making nuclear fuel much more efficient than fossil fuels (<https://www.world-nuclear.org>). Uranium is the raw material mostly used to create fuel for nuclear power and its atomic number 92 and atomic weight 238 which is highest atomic number found naturally in significant quantity. The average abundance of uranium in crustal rocks is 2.7 ppm (2-4 ppm various estimates) (IAEA Vienna, 1988). As demand for the energy is steeply increasing, uranium consumption is also increasing and hence, it has become mandatory to find new uranium reserve in our country.

Geophysical techniques have been successfully employed worldwide for delineation of mineral resources. Geophysical methods are indirect tools for uranium exploration which play a vital role in the identification of subsurface structural features and possible conducting horizons as favorable locales for uranium mineralization.

The most obvious technique to explore for uranium deposits is the radiometric method that directly records the response of uranium and other radioactive elements by

measuring gamma rays. Anomalous concentration may be detected by radiometric surveys using scintillometers and Geiger-muller counters over the subsurface structures containing radioactive materials in the top 30 cm of the earth's cover as gamma rays emanating from the earth's surface below 30 cm will not be detected by surface measurements of radioactivity. Therefore, geophysical methods are applied as an indirect tool to explore the concealed of uranium mineralization at depths, even up to 1 km.

Geophysical methods are successfully employed in discovery of the world-famous uranium deposits like Olympic dam deposit (Esdale Donald et al., 2003) and McArthur River mine (Tuncer et al., 2006), Millennium zone (Powell et al., 2007) of Athabasca basin.

## **1.2 Geophysical methods for uranium exploration**

Uranium minerals does not occur in appreciable quantity to alter the physical properties of rock to provide detectable geophysical anomaly. However, like any other minerals uranium gets deposited where it finds the suitable environment for precipitation. Geophysical methods utilized to detect subsurface geological targets often associated with uranium mineralization, for example fracture, faults, lithological contacts. The geometry of the subsurface structural features with appreciable physical property contrast can be mapped well by application of geophysical methods. The geophysical methods which are widely used are gravity, magnetic methods in the regional and semi-regional scales; and, electromagnetic and geoelectrical methods which include Induced Polarization technique for detailed investigations on prospect scale. In general, the choice of any geophysical method for uranium exploration largely depends upon the local geology of the area under investigation. The utility of any geophysical methods depends on the physical property contrast between the geological object sought and its host rocks. Although, a wide range of geophysical methods are available for uranium exploration, the most useful methods are the magnetic, electrical, gravity and electromagnetic.

However, based on the geological problem magnetic and IP/Resistivity methods are opted for the present study and their applicability discussed briefly below.

### **1.2.1 Magnetic method**

Magnetic method is a versatile, easy and inexpensive geophysical tool that can be executed fast. It is a useful technique both for reconnaissance and detailed investigations such as geological mapping and delineation of structural features. Intrusive bodies can be effectively delineated by the magnetic method. The magnetic method of prospecting is based on the study of local geomagnetic field produced by the variations in intensity of magnetization of rock formations. The magnetization of rocks is partly due to induction in the earth's magnetic field and to some extent due to remnant magnetization of the underlying formations. The induction component depends on magnetic susceptibility ( $k$ ) of rocks and on the intensity of magnetic field. The variable concentration of ferrimagnetic minerals plays a key role in determining the magnetic properties of the rock that are significant geologically and geophysically. While the magnetizing field remains constant over a small area, the remnant magnetic intensity and its variation for a given rock type also remain the same. In turn, the variation in the measured magnetic field can be attributed to the presence of various rock types with different susceptibilities. Therefore, magnetic method can be used effectively for geological mapping and structural studies. Therefore, zones favourable for uranium accumulation can be identified by surface magnetic observations. The successful application magnetic method to delineate the subsurface structural features like faults, fractures, shear zones and alteration zones for uranium exploration in India discussed by Dash et al., 2006, Ramesh babu et al., 2007, Satyanarayana et al., 2014, and Shrajala et al., 2015. World class ore bodies like the Olympic dam (Esdale Donald et al., 2003), Ernest Henry (Austin et al., 2019) of Australia and Bayon Obo (Hong et al., 2016) associated with iron oxide related mineralisation were established based on magnetic method.

### **1.2.2 Induced polarization (IP) and Electrical resistivity methods**

Among all geophysical techniques, electrical methods are considered to be the most widely used for studies related to uranium exploration. The prime objective of electrical surveys is to determine the subsurface resistivity distribution by making measurements on the ground surface. The ground resistivity is related to various geological parameters such as the mineral and fluid content, porosity and degree of water saturation in the rock (Loke et al., 2000). Formations which are structurally disturbed give rise to change in the apparent resistivity of the rocks. The induced polarization is one of the electrical methods, makes use of the capacitive action of the subsurface to locate zones where conductive minerals are disseminated within their host rocks. Disseminated sulphides are the main target for this method as their presence indicates the suitable reduction environment for uranium mineralization. Shrajala et al., 2015, Srinivasa Rao et al., 2018, Srinivasa Rao et al., 2016 Vijaya Kumar et al., 2015 are successfully applied IP and Resistivity techniques to delineate the structural features and disseminated sulphide mineralisation in uranium exploration.

In view of the successful applications of geophysical methods for uranium exploration elsewhere, an attempt was made to map the basement fractures hosting uranium mineralisation by employing the magnetic and IP/Resistivity methods in and around Chhota Udaipur area of Ajmer district, Rajasthan.

## **1.3 Study area**

### **1.3.1 Objective of the study**

The objective of the present study is to decipher the subsurface geological structures, alteration zones from the interpretation of magnetic data, sulphides rich zones associated with fractures and/or shear zones from IP/Resistivity data. Integrated interpretation to identify the favorable subsurface target areas for uranium mineralization.

### 1.3.2 Location and accessibility of the study area

The study area falls in/ around Chhota Udaipur, Ajmer district, Rajasthan which is located around 9 km SE of Kishangarh city and 110 km SW of the Jaipur. The area is bounded by coordinates (489000 E, 2927700 N), (489000 E, 2933600 N) (482800 E, 2933600 N) (482800 E, 2927700 N) of UTM 43N (26°28'-26°31'30" Latitude and 74°50'-74°53'20" Longitude) and covers a total area of about 30 sq. km.

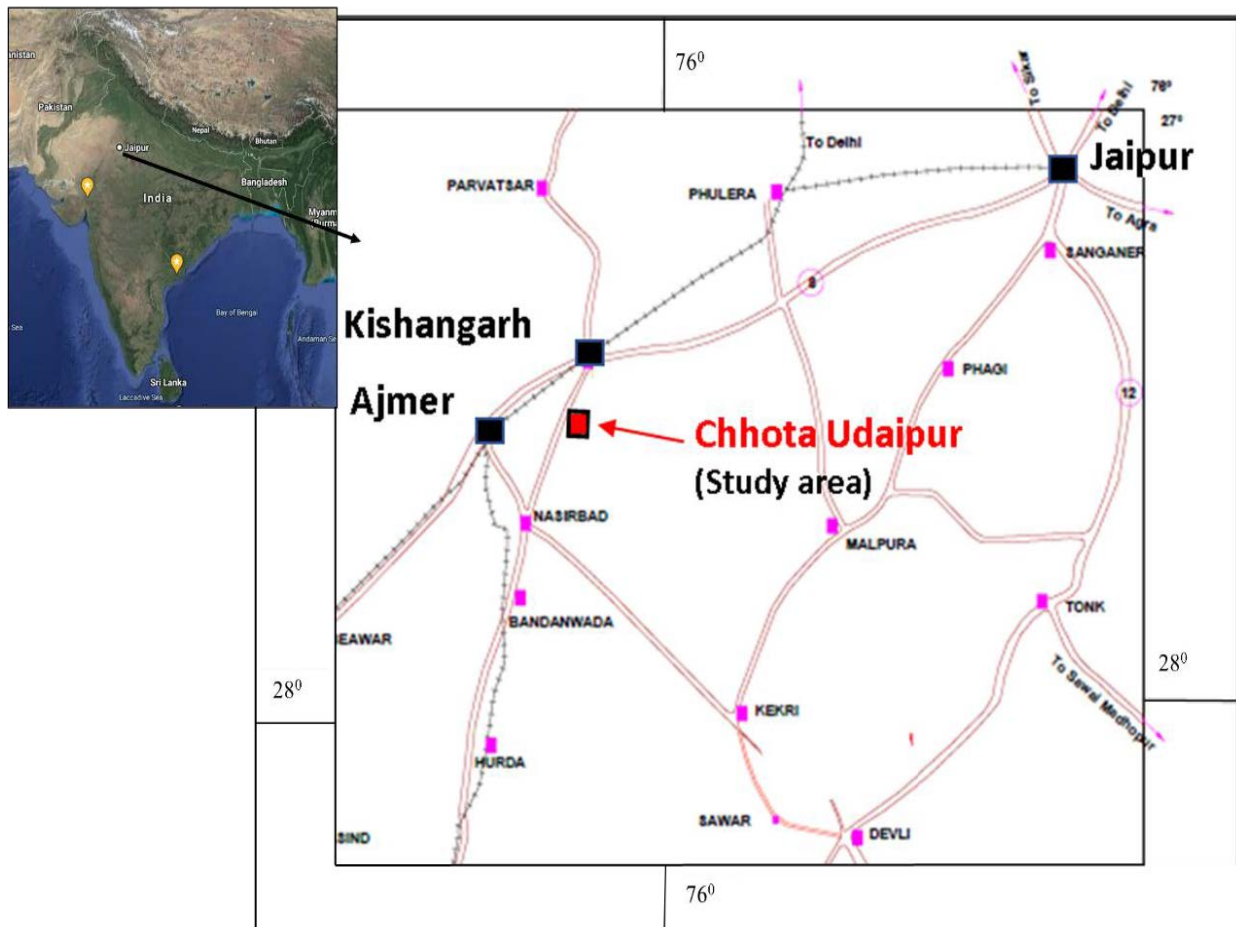


Figure 1.1 Location of the study area, Chhota udaipur village, Ajmer district, Rajasthan

(Source Google maps and GSI)

The study lies in toposheet nos. 45J/14 & 45J/15 as shown in the Figure 1.2. The survey block has the western boundary as National highway NH 79A which connects Nasirabad - Kishangarh-Jaipur (Figure 1.1). The nearest railway station is Kishangarh on the Jaipur-Ahmedabad broad gauge line. The nearest airport is Jaipur.

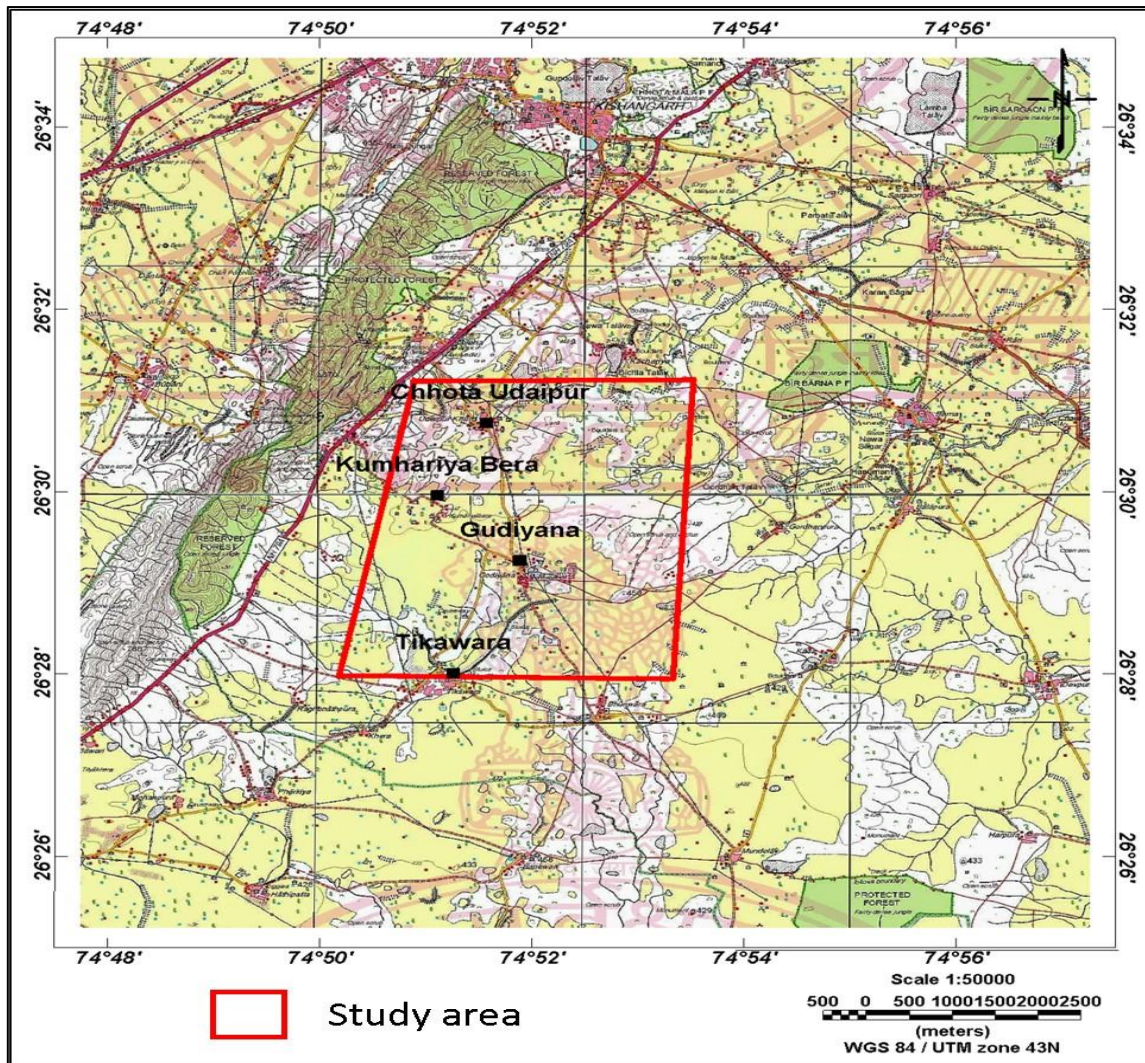


Figure 1.2 Survey block over toposheet No. 45J/14 & 15, Chhota udaipur area, Ajmer district, Rajasthan (Source SOI)

### 1.3.3 Previous work

Uraniferous polymetallic veins are reported in the gneisses of Sandmata Complex of Archaean age by Sinha et al., 2002, from two adjoining dug well dump samples near Chhota Udaipur village. These samples are analyzed by laboratory studies of gamma-ray spectrometry, fused pellet fluorimetry for uranium along with physical and chemical methods. Laboratory studies revealed that the presence 1.62 % of  $eU_3O_8$ , approximately 10% of ThO and Cu, Mo, and Pb vary from 0.41 to 10.64%, 0.03 to 0.46% and <0.02 to 0.11% respectively and also some samples were analyzed more than 1% of sulphides (Sinha et al., 2002). These results

shown that samples have a polymetallic character and as the two dug wells are separated by 210 m distance in NE-SW direction, indicates a possible subsurface strike continuity.

Geophysical studies comprising magnetic, IP/Resistivity and EM-Turam surveys were carried out earlier by Subash Ram et al., (1999) to trace the subsurface sulphide bearing zones towards NE direction of radioactive anomaly location over an area of 4 Sq. Km near Chhota Udaipur area, Ajmer district, Rajasthan. The study indicated the presence of high magnetic linear with 300-1500 nT amplitude and which is truncated at many places, by N-S trending local displacements. High chargeability zones with amplitude 16 mV/V were observed with a background of 5 mV/V as isolated pockets by the Induced polarization/ Resistivity survey. The geophysical signatures are interpreted to be due to the fault/fractures filled with sulphides in a high resistive environment like banded gneissic complex (BGC) of Archaean age. In view of the encouraging results obtained from the earlier geophysical surveys, magnetic and IP/Resistivity techniques are adopted to delineate the favourable zones of uranium mineralization in the area.

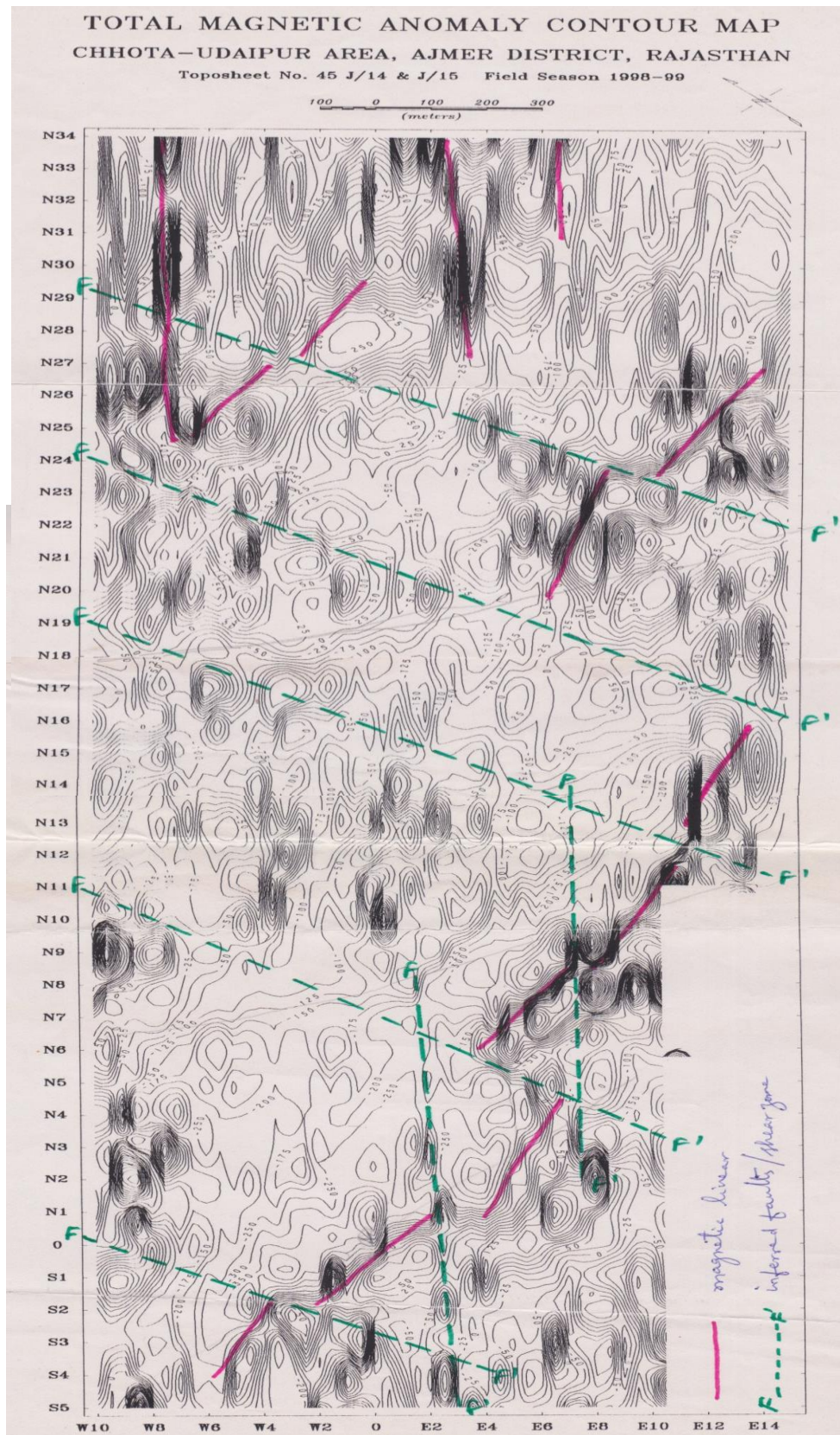


Figure 1.3 Previous geophysical Total magnetic anomaly map, Chhota Udaipur area, Ajmer district, Rajasthan (after Subash Ram et al.,1999)

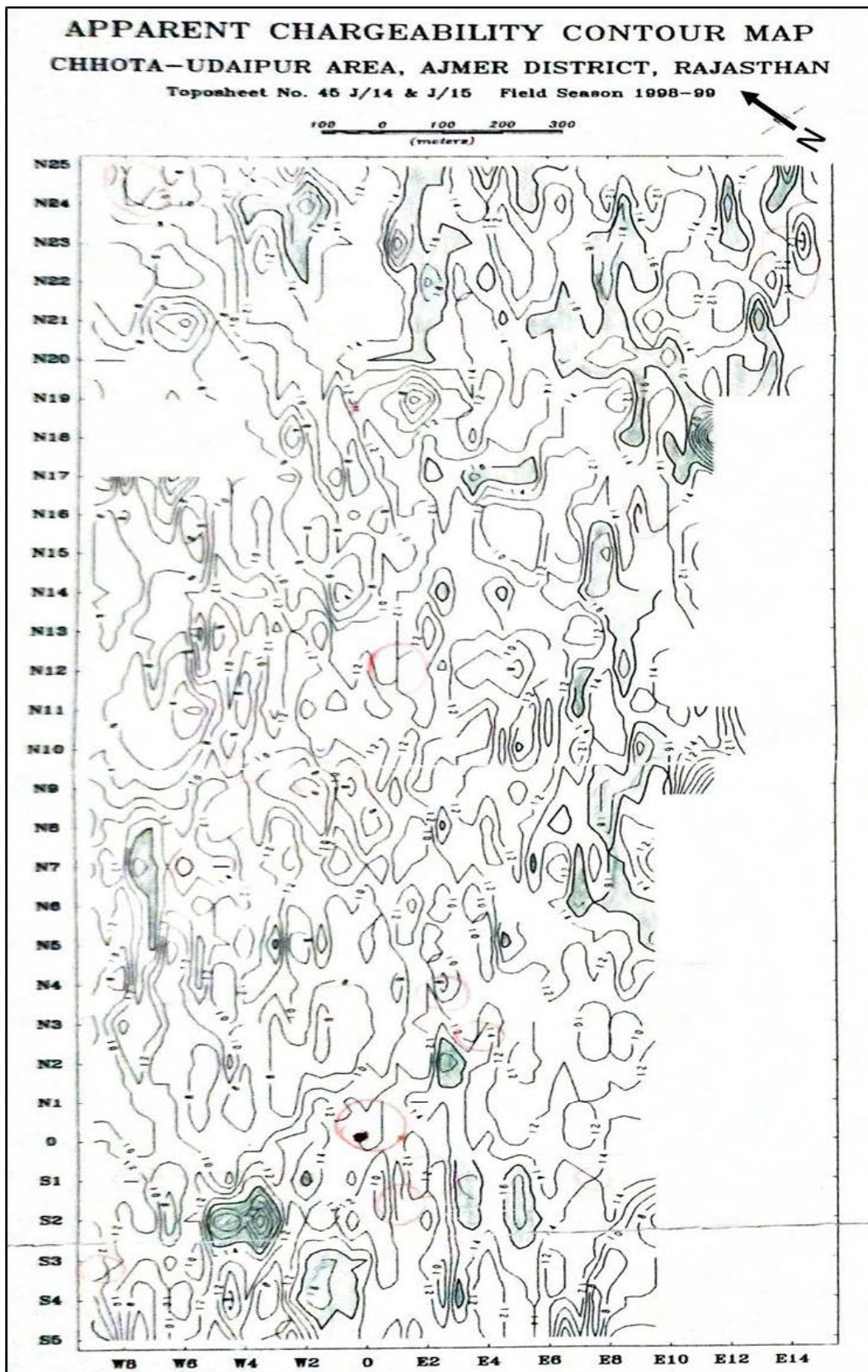


Figure 1.4 Previous geophysical apparent chargeability contour map, Chhota Udaipur area, Ajmer district, Rajasthan (after Subash Ram et al.,1999).



## CHAPTER 2

### GEOLOGY OF THE STUDY AREA

#### 2.1 Introduction

North-western Indian Craton (NWIC) presents varied geological and tectonic process of over 3500 million years. The NWIC is bounded by Great Boundary Fault (GBF) in the east and Thar Desert in the west. It is separated by the SONATA (Son-Naramada-Tapti) lineament from the Central Indian Tectonic Zone in the south and Indo-Gangetic alluvium in the north (Ramakrishnan et al., 2010; Dhirenda Kumar Pandey et al., 2014). It hosts variety of metallic and non-metallic and mineraloid deposits of sizeable mineral reserves (Sumit Kumar Ray et al., 1987). The terrain consists of wide variety of litho-units from Archaean to Holocene. The oldest geological record is contained within Banded Gneissic Complex (BGC) formed during the Archaean period. Aravalli Basin and Delhi Basin formed during Proterozoic period due to repeated period of crustal rifting, development of intracontinental rift basins, subsequent oceanic trough and depositions of sediments of different facies. The formation of folded belts associated with multi deformation and polyphase metamorphism of the rock sequences. During the late Proterozoic period, crustal deformation and associated thermal regime caused large scale anatexis and emplacement of number of granite plutons and wide spread acidic and local basic volcanism and associated mineralisation. During Phanerozoic period the extent of geological activity has reduced substantially except the development of separate basins. The period is followed by the episodes of extensive basaltic volcanism, Deccan traps during Late Cretaceous to Early Tertiary period which is present on the southern part of the craton. Finally, depositions of fluvial sediments, formation of aeolian land forms are prevailed during the Holocene period (Sinha and Roy, 1998).

## 2.2 Regional geology of the area

The Banded Gneissic complex of Archean age forms the basement and comprises of high grade metamorphic and migmatite rocks (Heron, 1953) overlain by the cover sequences of Middle Proterozoic Delhi Supergroup of rocks, which forms a narrow belt extending from Haryana in the north to Gujarat (Deri-Ambaji) in the south. The Delhi fold belt roughly divides the Aravalli craton into two parts. The eastern part is composed dominantly of basement rocks, Aravalli Supergroup and its equivalent cover sequences, while the western part is essentially a volcanic province (Malani), with Late Proterozoic cover sequences (Marwar) and Mesozoic-Cenozoic sedimentary basins. This belt has been further divided into North Delhi Fold Belt (NDFB) and South Delhi Fold Belt (SDFB). This subdivision is based largely on the Rb–Sr whole rock isochron data from syn-kinematically emplaced granites in the NDFB and SDFB, which have been dated to 1.65–1.45 Ga and ~0.85 Ga, respectively (Crawford et al., 1970). These belts are separated by a migmatitic gneiss track around Ajmer, the SDFB is developed from Ajmer (Rajasthan) to NW Gujarat, while the NDFB is developed in Khetri-Alwar-Ajabgarh-Bayana in northern Rajasthan. (Sinha –Roy et al., 1998).

The NDFB is constituted of three sub-basins designated as Khetri, Alwar and Lalsot-Bayana sub-basins from west to east respectively. The Khetri sub-basin is known for the uranium occurrences and polymetallic mineralization, which is characterized by the presence of broad zones of albitization. The albitite intrusives are wide spread along the NE-SW trending zone with an extent over 170 km and maximum width of about 10km following Khetri lineament in northeast and Kaliguman lineament in southwest (Sumit Kumar Ray et al., 1987). Uranium occurrences in Khetri sub basin are broadly associated with two NE-SW trending (eastern and western) albitite zones. Rohil, Guman Singh Ki Dhani, Narsinghpuri, Maota, Jahaz, Bagholi uranium occurrences are associated with western albitite zone, while Buchara,

Ladi Ka Bas, Geratiyon Ki Dhani, Kalatopri, Rela-Ghasipura are associated with eastern albitite zone (Kamlesh Kumar et al., 2018).

The present area of study forms the part of the Banded gneissic complex and hence it is described in detail.

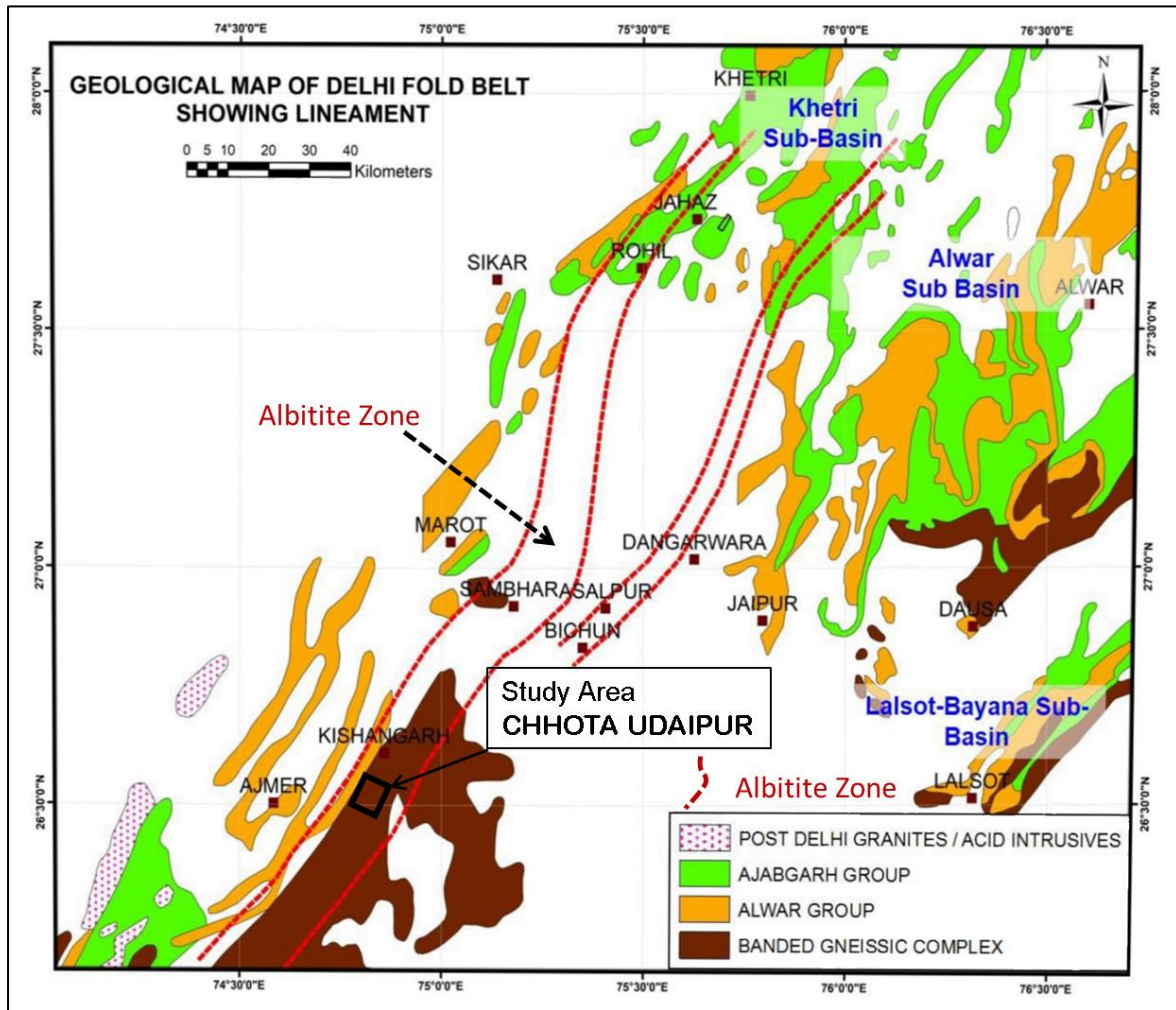


Figure 2.1 Three sub-basins of North Delhi Fold Belt, two sub-parallel albitite zone present in the Khetri Sub-Basin and BGC (Modified after GSI,1995)

### 2.2.1 Banded Gneissic Complex

Banded Gneissic Complex (BGC) represents the oldest geological record in Rajasthan and forms the basement for the Proterozoic fold belts, comprising various types of gneisses, migmatites, high-grade schist and metabasic rocks in the gneissic terrains of Sandmata Complex, Mangalwar Complex and the Hindoli Group. These represent the early Precambrian

crust formed through the process of granite-granulite greenstone accretion. Mangalwar Complex and Hindoli Group forms greenstone type basins and result of the deformation in oldest, elongated sedimentary basins formed in rifted ensialic crusts. Large scale acidic and intermediate magmatic emplacements such as granite, granodiorite and tonalite plutons have happened due to tectonic activity at about 2900 Ma. Sandmata Complex contains the high-grade equivalent of rocks up to granulite facies. The Archaean-Proterozoic boundary in Rajasthan is marked by a prominent phase of acid igneous activity and emplacement of Berach Granite and equivalent granite plutons at about 2500 Ma.

### **2.3 Detailed geology of the study area**

The study area is in and around Chhota Udaipur village, Ajmer district, Rajasthan and it is partially soil covered and is located in the SW continuity of albitite line. It is a part of Sandmata complex of Archaean age (2500 Ma). The western boundary is marked by the Delhi Supergroup which overlies the Sandmata Complex along tectonised unconformity, kaliguman lineament which separates the BGC from Delhi group of rocks and has the eastern boundary with the Mangalwar Complex. The study area contains rocks of Badnor and Shambhugarh Formations of Sandmata Complex and Gyangarh-Asind acidic igneous intrusive rocks of granitic to granodioritic in composition.

The Sandmata complex is represented by biotite schist, gneisses and older mafic enclaves comprising pyroxenite, amphibolite, hornblende schist, chlorite schist and epidiorite of Badnor formations and migmatites and gneisses of Shambugarh formation. The uraniferous polymetallic veins have been reported in Sandmata complex intruded by Gyangarh Asind acidic igneous suite at two dug wells of Chhota Udaipur area, Ajmer district, Rajasthan. These two dug wells are separated by 210m in NE-SW direction and indicates the possible subsurface strike continuity towards the south-west of Chhota-Udaipur area.

Table 2.1 Stratigraphic Classification of Bhilwara Supergroup (after Gupta et al., 1997)

ARCHAEAN	INTRUSIVES	Berach Granite and Gneiss (2585 Ma),
		Untala and Gingla Granites (2860 Ma), Ultramafics, Giyangarh-Asind acidic rocks.
	HINDOLI GROUP	Nangauli Formation
		Sujanpura Formation
		Bhadesar Formation
	MANGALWAR COMPLEX	Potla/Rajmahal Formations
		Lasaria/Suwana Formations
		Kekri Formation
		Mando-ki-Pal Fm.
		Sarara Formation
		Baranch Formation
	SANDMATA COMPLEX	Badnor Formation
		Shambhugarh Formation.

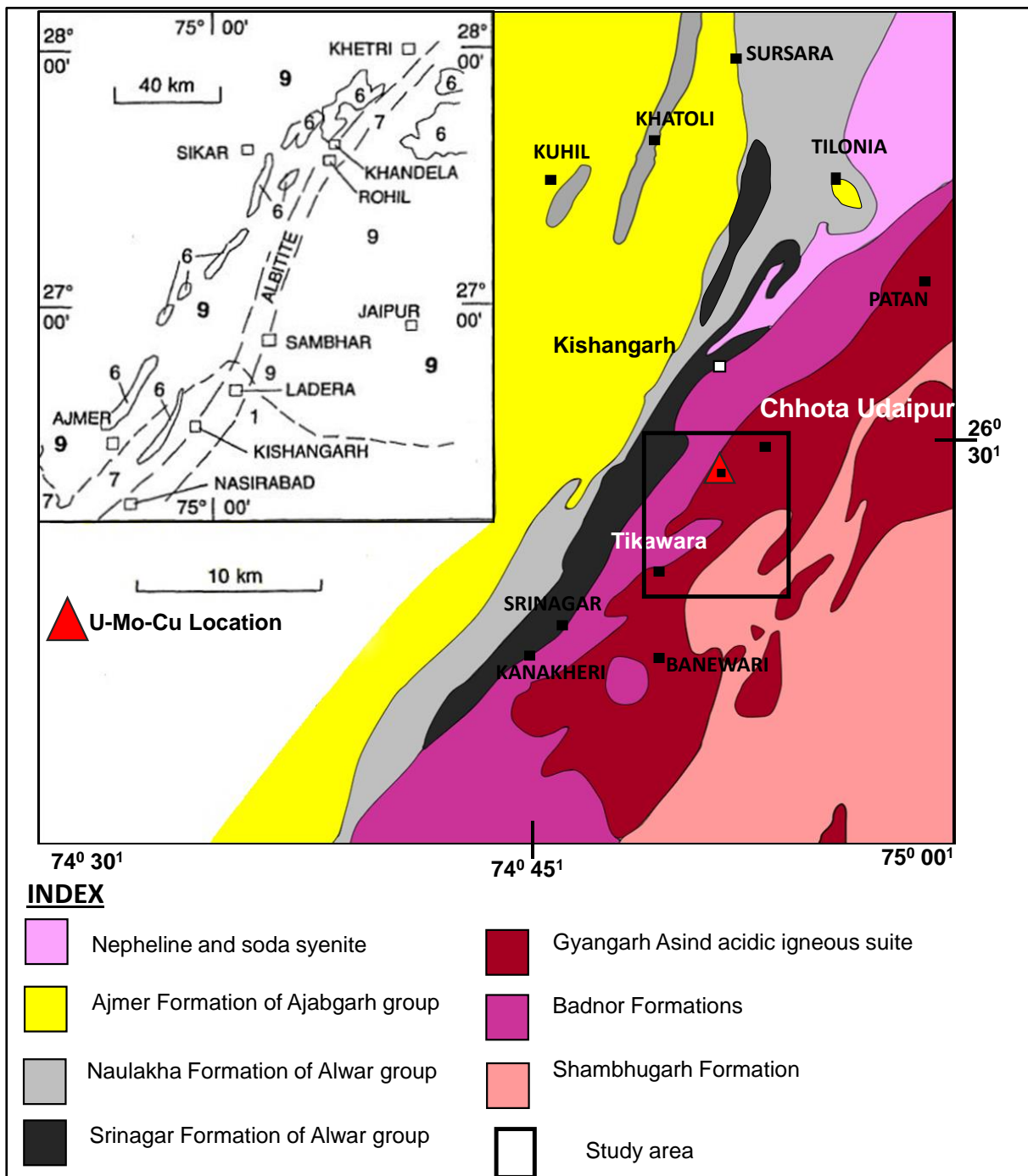


Figure 2.2 Geological map of Tilonia-Nasirabad area, Ajmer district, Rajasthan (modified after Sinha et al., 2002)

## CHAPTER 3

### MAGNETIC METHOD OF EXPLORATION

#### 3.0 Introduction

Magnetic method is the oldest and passive geophysical method. It was developed for mineral exploration, primarily for iron ore searching and it is one of the most widely used geophysical method in exploration programme as a reconnaissance tool to understand the subsurface structural features (Paterson and Reeves, 1985) which is relatively cost-effective technique and rapid to employ. The method is based on the measurement of the lateral variations in magnetic field which are magnetic expressions of the subsurface geological features. For successful application of magnetic method, lateral variation in the magnetic susceptibility is essential. Magnetic susceptibility of rocks varies with the variations in the concentration of magnetite and other ferro, ferri-magnetic minerals in crustal rocks formed below the Curie point temperature. As temperature increases, thermal energy begins to breakdown the ordering of a ferromagnetic material and above the Curie temperature, spontaneous magnetization ceases. Since temperature in the Earth increases with depth, there exists a depth below which materials cannot behave as ferromagnetic. Thus, only rocks at shallow depths (approximately less than 20km) in the Earth can exhibit remnant magnetization which is a permanent magnetism of rock acquired when it was formed, in the direction of the earth's magnetic field at that time. So, the local magnetic anomalies are arising from variation in magnetization contrast of crustal rocks which reflects the subsurface lithology and structural fabric. In general, igneous and metamorphic rocks have higher magnetic susceptibilities as compared to sedimentary rocks, the subsurface geological structures and lithological contacts, such as basic dyke intrusives with high susceptibilities (Roberts and Smith, 1994) and prominent fault and fractured zones with low susceptibilities, can be usefully picked up (Clark et al., 1992; Henkel and Guzman et al., 1977; Cull and Massi et a.l, 2002 and Lopez-Loera et

al., 2010; Ramesh Babu et al., 2007; Srinivasa Rao et al., 2016; Vijay Kumar et al., 2015). As such, to acquire precise subsurface information and to resolve the ambiguity in potential field interpretation, magnetic surveys are to be followed by other geophysical methods like gravity electrical resistivity, electromagnetic or seismic survey.

### **3.1 Theory of magnetic method**

Geomagnetic field has different physical origins and can be found both below (in the form of electrical currents and magnetized material) and above the Earth's surface. Each source happens to produce a contribution with rather specific spatiotemporal properties. The crustal rocks are too weak to produce the observed magnetic field in the absence of external field and mantle rocks also existed at high temperature environment so their contribution could be nominal. According to dynamo theory earth's main magnetic field is generated and maintained by system of electrical currents in outer core, which are generated by the motion of the conducting fluids (Radhakrishna murthy et al; 1978).

In principle, magnetic method has the ability of greater depth of investigation, thereby magnetic surveys give 3D geological information. The fundamental non-uniqueness of potential field source distribution is a crucial limitation of 3D interpretations of magnetic surveys. By constraining models only ambiguity in source geometry can be estimated. Magnetic properties governs the reliability of magnetic models, besides that factors which determine magnetisation, intensities and directions of the geological units in an area of investigation are essential for solving geological ambiguity in acquiring reliable interpretation.

Ore bodies in the world such as Olympic dam (Esdale Donald et al., 2003), Ernest Henry (Austin et al., 2019) of Australia and Bayan Obo (Hong et al., 2016) of China associated with iron oxide related mineralisation were identified by using magnetic method and also corridor of likely mineralisation delineated by mapping of the structures using magnetic method.

### 3.2 Instruments

Two GEM make (<http://www.gemsys.ca/versatile-proton-magnetometer>) Proton Precision Magnetometers (PPM) were used in the magnetic survey, one for recording the diurnal variations at base and the other for field use as a rover. PPM measures the Earth's magnetic field independent of its direction to a resolution of 0.01 nT and with an accuracy of  $\pm 0.2$  nT.



Figure 3.1 GEM Systems, GSM 19T Proton Precision Magnetometer used for Data Acquisition in the survey area ([www.gemsys.ca](http://www.gemsys.ca))

PPM is a light-weight, less cumbersome equipment having a sensor, console and GPS antenna. It can be operated in three operating modes, Walking, Mobile, and Base. These magnetometers are integrated with inbuilt Global positioning system (GPS) receiver for recording spatial locations along with magnetic data. Spatial horizontal accuracy of GPS is 0.6 m. It has inbuilt memory of 20 Mb to store the acquired data.

### 3.3 Magnetic Data Acquisition

Magnetic data was acquired at the station interval 25 m and traverse spacing of 100 m and 200 m as shown in the Figure3.2.

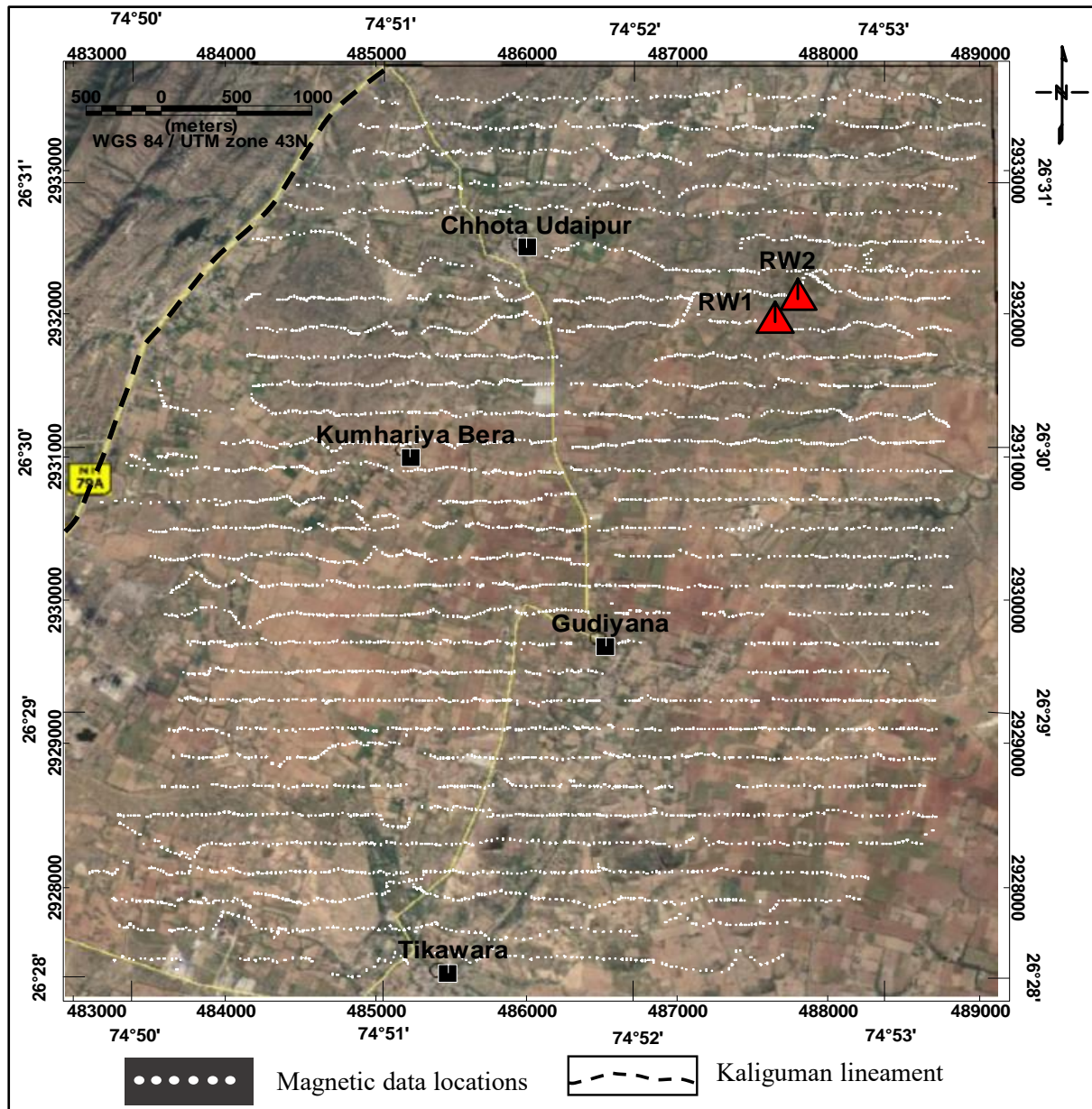


Figure 3.2 Magnetic profile layout map, Chhota Udaipur area, Ajmer district, Rajasthan

Geological features have a NE-SW trend hence, east-west traverses were selected based on the accessibility of the study area (Figure3.2). Total of 30 sq. km area was covered in and around the Chhota Udaipur area with the above specified survey parameters. Diurnal variation of the Earth's magnetic field was recorded at every 60 seconds using a base station established

in the cultural noise free and low magnetic gradients in the area near Chhota Udaipur village (486384N, 293200E).

### 3.4 Physical property measurement

For geological mapping and geophysical prospecting, information about physical properties of rocks are important for a plausible geological interpretation. The ultimate result of any geophysical survey is to interpret the anomaly in terms of the geology. The magnetic susceptibility of rocks in the study area are helpful to the interpretation of magnetic data. The induced magnetization in a material when placed in external magnetic field depends on its magnetic susceptibility. Susceptibility is defined as the ratio of magnetization ( $M$ ) to magnetizing field ( $H$ ), given as

$$\mathbf{M} = \mathbf{kH} \text{ or } \mathbf{k} = \frac{\mathbf{M}}{\mathbf{H}} \quad \dots\dots\dots (3.1)$$

The units of  $M$  and  $H$  are same and hence  $k$  is dimensionless. Measurement of magnetic susceptibility( $K$ ) helps to understand the magnetic nature of the geological formations and in the modeling of the anomaly.

Magnetic susceptibility is measured using the portable handheld (kappa) KT-10 v2 susceptibility meter (<https://www.yumpu.com/user/terraplus.ca>). The instrument is working based on the fact that the alternating magnetic field produced by Helmholtz coil induces a magnetic field in the specimen which is proportional to the rate of change of its magnetic moment. Knowing the magnetic field and the volume of the specimen, its susceptibility is calculated. Measured susceptibility values are shown in table 3.1.

Table 3.1 Physical properties of various rock samples from Chhota Udaipur, Ajmer district, Rajasthan

S. No	Rock type of the Sample	No. of samples	Susceptibility (K *10 <sup>-3</sup> SI)	Radioactivity (μR/hr)	Density (g/cc)
1.	Radioactive samples (Magnetite bearing Quartz biotite gneiss)	4	25 – 570	180-234	2.78
2.	Quartz mica schist	4	1.9 – 2.5	11	2.84
3.	Magnetite bearing Biotite gneiss	3	25 –30	12	2.75
4.	Albitized biotite gneiss	5	2.9 – 7.34	12	2.67
5.	Biotite gneiss	4	0.5 – 1.5	13	2.78
6.	Acidic rock (Granodiorite)	4	0.02 – 0.03	10	2.62
7.	Quartzo-felspathic rock	4	0.01 – 0.04	10	2.62
8.	Hornblende gneiss	5	3 – 10	10	2.76
9.	Pure Quartz vein	3	0.041-0.004	-----	2.63

### 3.5 Magnetic Data processing

Geophysical data processing is the most important step and which is an intermediate stage between data acquisition and interpretation of the data. The aim of the data processing is to enhance the data quality by suppressing or removing the different noise present in the data. During processing, the observed data are corrected for natural and instrumental variations. Ground magnetic data processing includes corrections for diurnal variations of the geomagnetic field, single spike reading, and IGRF (International Geomagnetic Reference Field) correction to remove background/normal geomagnetic field. IGRF correction is important correction in airborne as well as ship born magnetic surveys. However, in a limited area the

background/normal magnetic field variation is very less and insignificant; hence IGRF correction is not required in detailed/semi-detailed ground magnetic surveys.

### 3.5.1 Diurnal correction

Diurnal variations are subject to amplitude and phase changes, depending on the geographic location of the observer. The variations earth's magnetic field are recorded by a base station magnetometer located in the survey area. The measured magnetic field by using rover magnetometer is then corrected for the diurnal variation through a direct subtraction of field data from the corresponding time synchronized base magnetic data using GEM link software. Variations in the geomagnetic field due to magnetic storms can be so rapid, unpredictable, and of such large amplitude. Magnetic surveying is suspended under these conditions. The amplitude of the diurnal variations of geomagnetic field in solar quite day is 10-30 nT and during magnetic storms is up to 1000nT (William Lowerie, 2007). Figure 3.3 represents the diurnal variations that of recorded by base magnetometer on a typical day during the survey and variation of 14.3 nT was observed.

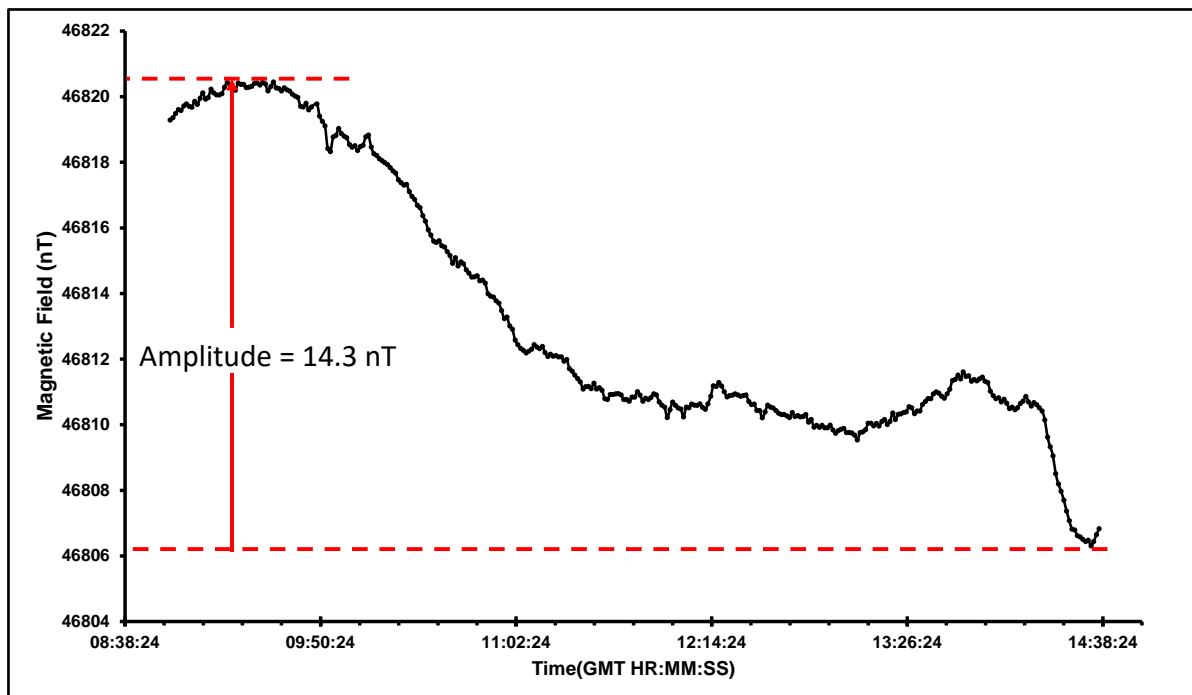


Figure 3.3 Diurnal variation of geomagnetic field on 17<sup>th</sup> December 2019

### **3.5.2 Correction for cultural noise**

Magnetic anomalies caused by man-made features are defined as cultural noise in magnetic survey. Cultural noise interferes with the magnetic anomalies of interest arising from subsurface. The sources of cultural noise are ferrous objects such as drill holes lined with steel casing, steel buildings, pipelines, bridges, tank farms, metallic fencing, power lines etc. Generally cultural noise has high frequency (short wavelength). There is no method to completely eliminate the cultural noise from the observed magnetic anomalies but frequency domain techniques can suppress this noise to some extent.

In the present study, the base station has been established in such a way to avoid cultural noise as far as possible. The observed profile data also has been thoroughly checked and single peaks, point anomalies caused by the cultural noise are filtered. Further, fourth difference of the anomalies has been calculated and a non-linear filter is applied to smoothen the data.

### **3.5.3 Data visualization**

After applying all the corrections to the raw data which are mentioned above, the data was gridded using minimum curvature gridding method with a cell size of 30 m. Minimum curvature gridding method (Briggs, 1974) is a very popular gridding algorithm and it takes into account surface of minimum curvature. The results are presented in the form of shaded relief images map for better visualization. The gridded data are used for further processing and matched filtering using frequency domain through Fourier Transform. For effective interpretation of the acquired magnetic data, further data enhancement techniques are applied using various transformations such as; upward continuation, reduced to pole and derivatives.

### **3.5.4 Filtering techniques**

The initial stage of magnetic data interpretation generally involves the application of mathematical filters to processed data with an objective to enhance anomalies of interest and to gain some preliminary information on source location.

Different mathematical filtering techniques have been applied on the gridded data to enhance the information of interest. Most of the filtering techniques are mathematically more complex to apply in time/space domain, but these techniques having simple mathematical operations in frequency domain. Filtering operations in frequency domain improves the efficiency of the filter and decreases the run time. Hence, Fourier transformation is used to transform the data into frequency/wavenumber domain. After applying filtering technique in frequency domain, this data is transformed back into time/wavelength domain using inverse Fourier transformation.

### **3.6 Interpretation of Magnetic Data**

The magnetic anomaly of a finite body invariably contains positive and negative anomalies arising from the bipolar nature of magnetism. Magnetic interpretation is classified as qualitative interpretation and quantitative interpretation methods. The aim of the qualitative interpretation is a visual inspection of the shape and trend of the magnetic anomalies such as sharpness of anomalies, elongation and areal extends of the contours, +ve and -ve peaks of the anomalies to delineate the strike of the formations, structural trends, and regional tectonics. Generally, in contoured maps, when the lines are close together, they represent a steep gradient and high-density contours indicates litho-contact, faults/fractures. When contour lines are widely spaced, they represent shallow gradient or slow change in magnetic value. Closed contours are associated with three-dimensional body in the subsurface, while the elongated contour indicates two-dimensional body with strike along the contours trend. The breaks and offset in the contours also a key feature in the identification of faults/fractures. Quantitative interpretation includes estimation of depth to the top of the source body, 2D/3D profile modelling and Inversion. Interpretation is ambiguous even in the case of high-quality data because the observed anomaly can be replicated by an infinite number of source distributions shallower or possibly deeper than the actual source of the anomaly and moreover potential field

measured at the surface can be considered as integral of potential fields from all depth. There is no depth control in potential fields and it is up to center of the Earth in case of gravity and up to Curie's temperature in case of magnetics. The ambiguity is not relieved by additional measurements of the magnetic field and its various components or by observations at different levels, because these are not independent measurements. Thus, geological information, borehole information and/or other geophysical data is required for the successful interpretation of magnetic anomalies.

### **3.6.1 Qualitative interpretation**

#### **3.6.1.1 Total Magnetic Intensity Anomaly Map**

Total magnetic intensity (TMI) anomaly map (Figure 3.4) has been prepared by applying minimum curvature gridding technique with a 30 m cell size using Geosoft software (<http://www.geosoft.com>). The amplitude of TMI anomaly varies from -359 nT to 1102 nT. The contour pattern of the anomaly indicates the general trend of geological features in the study area as NE-SW direction. Two strong bipolar magnetic signatures have been observed towards central and south-eastern part of study area indicating the presence of ENE-WSW trending high magnetic bodies. Interpretation on TMI map for structural features and litho-contacts is complex because of the bipolar nature of the magnetic field. In order to remove the inclination ( $41.682^\circ$ ) and declination ( $1.07^\circ$ ) effects of Earth's magnetic field, reduced to pole (RTP) filter was used.

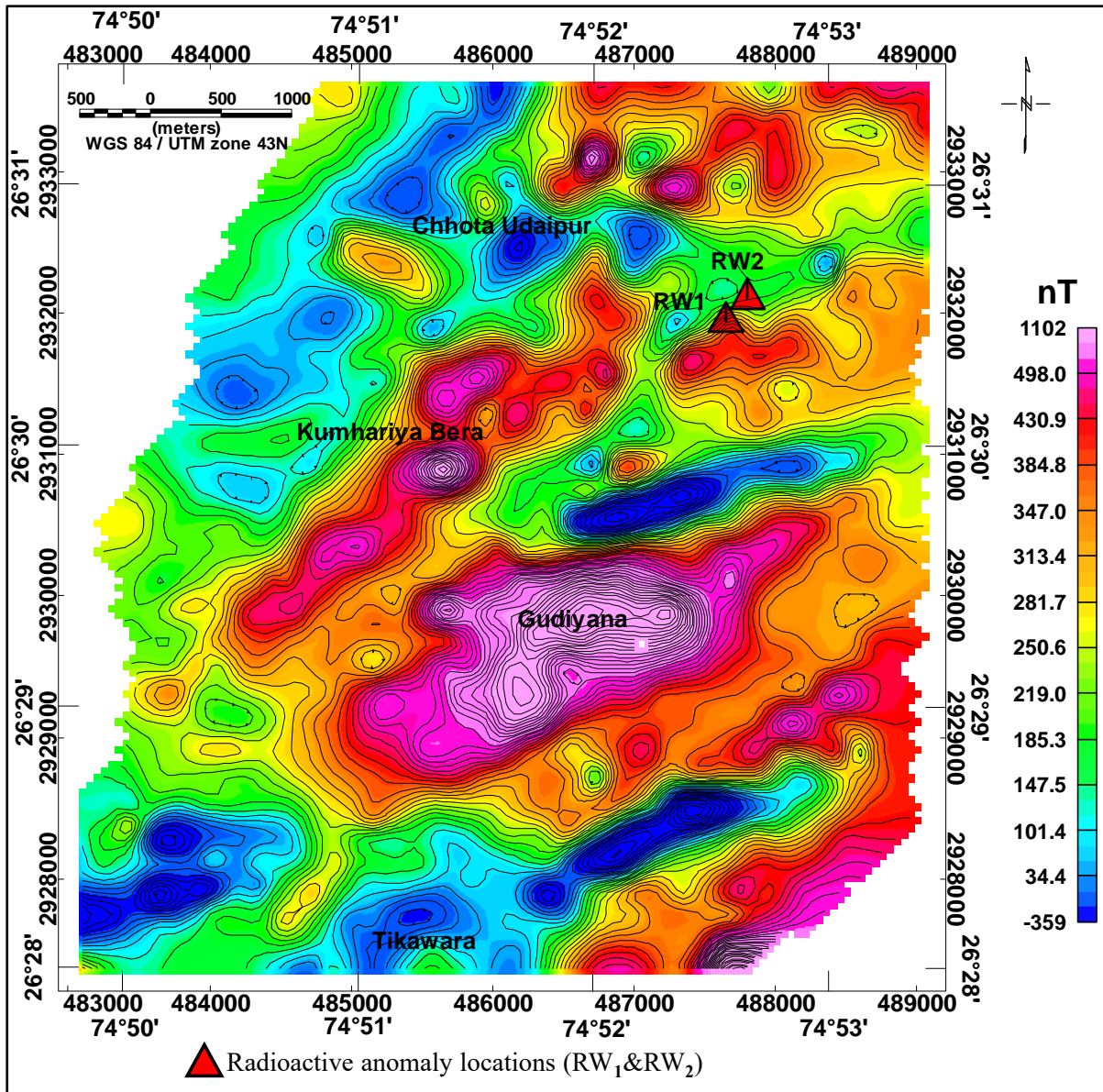


Figure 3.4 Total magnetic intensity anomaly map with contour interval of 20nT of Chhota Udaipur area, Ajmer district, Rajasthan

### 3.6.1.2 Reduced to Pole Magnetic Anomaly Map

Reduced to pole (RTP) magnetic anomaly map has been prepared so that anomalous features can be precisely located for better interpretation. Figure 3.5 shows the RTP map of the study area with improved spatial location of anomalies associated with subsurface geological formations than compared to TMI map.

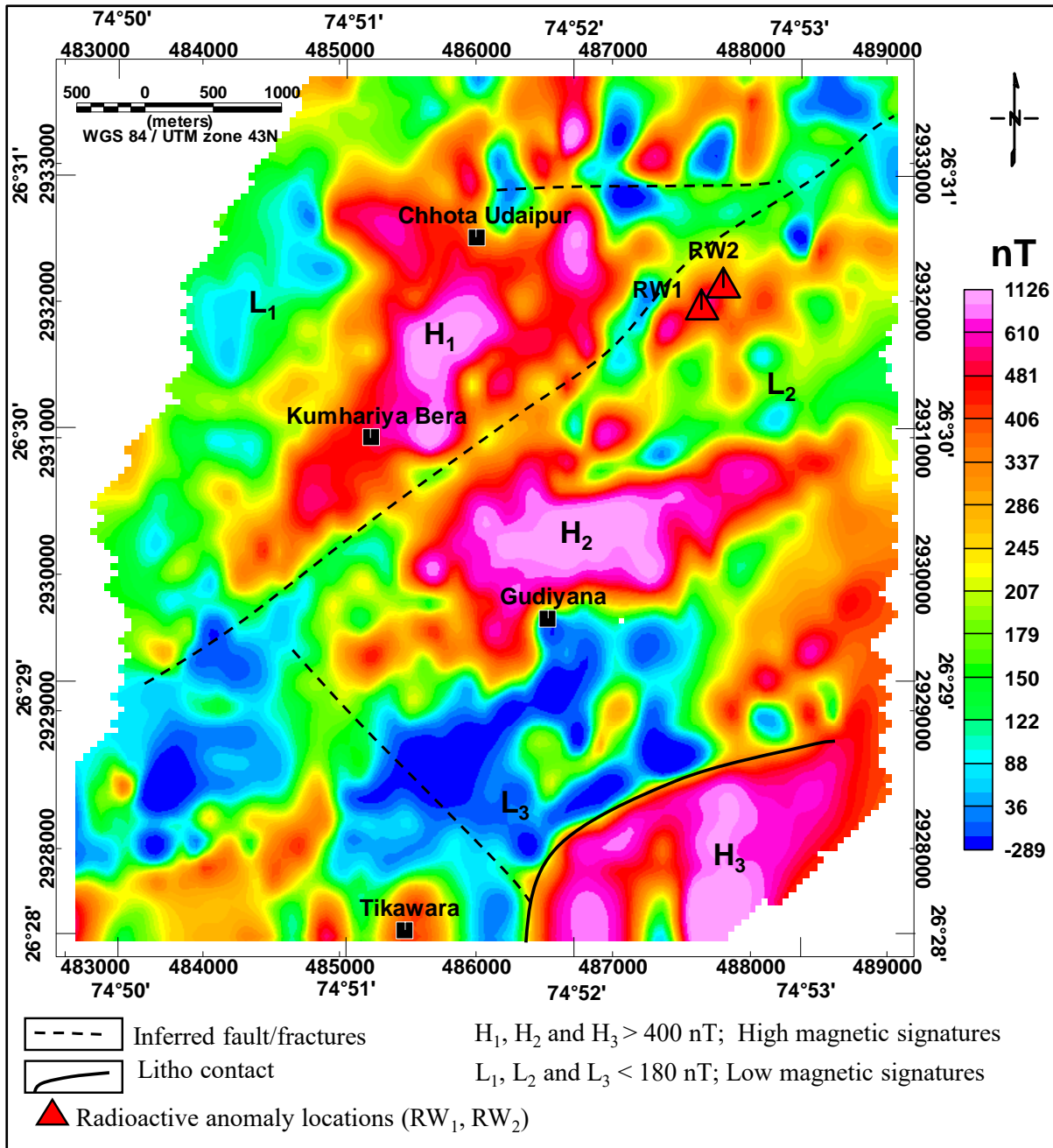


Figure 3.5 Reduced to pole anomaly map, Chhota Udaipur area, Ajmer district, Rajasthan

The trend and disposition of magnetic anomaly sources are clearly demarcated in reduced to pole map as shown in Figure 3.5. Based on variation in anomaly trend and amplitude, prominent NE-SW, E-W and NW-SE trending subsurface fault/fractures have been delineated in the study area. The low magnetic signature L<sub>1</sub> observed in the north western part of the map is because of the presence of low susceptibility quartz-mica-schist and it is observed that the strike of the formation changes from NE-SW to ENE-WSW direction. The moderate low

magnetic signature L2 in the eastern side of study area is attributed to the country rock hornblende gneiss. The very low magnetic signature L3 towards the southern side of the Gudiyana village may interpreted as injection of the Gyangarh Asind acidic igneous intrusives within BGC.

The previously reported Chhota Udaipur radioactive anomaly is associated with the moderate high magnetic (>460 nT on RTP map) signature. The high magnetic signature H<sub>1</sub>(> 400 nT) near kumariya bera village, is due to the presence of magnetite bearing biotite gneiss. The high magnetic signatures H<sub>2</sub>, H<sub>3</sub> in the center and south-eastern part of the study area are possibly due to the mafic intrusives (Pyroxenite's) of Badnor formation or association of gneiss with magnetite mineralisation, since there is no rock exposure in this area to certainly attribute to magnetic anomaly. Many small spatially limited magnetic anomalies with relatively moderate amplitude have been observed in the north and eastern side of the study area, which could be due to polymetallic injections in BGC.

### **3.6.1.3 Upward continuation filter**

Upward continuation is a mathematical technique that project data taken at an elevation to a higher elevation. The effect is that short wavelength features are smoothed out because one is moving away from the anomaly (Radhakrishna murthy et al., 1978). Upward continuation is a way of enhancing large scale (usually deep) features in the survey area and tends to accentuate anomalies caused by deep sources at the expense of anomalies caused by shallow sources.

Upward continuation filter has been applied to the RTP grid at 400 m level of height. As stated earlier several small magnetic anomalies with relatively moderate amplitude in the north and eastern side of the study area (Figure 3.5) are attenuated in 400m upward continued map which indicates that the anomalies have originated from shallow sources. The prominent the high magnetic signatures H<sub>1</sub>, H<sub>2</sub>, H<sub>3</sub>

in the study area showing strong high amplitudes even at 400m (Figure 3.6) and above continued heights which indicating that these high magnetic bodies have greater depth extension in the BGC.

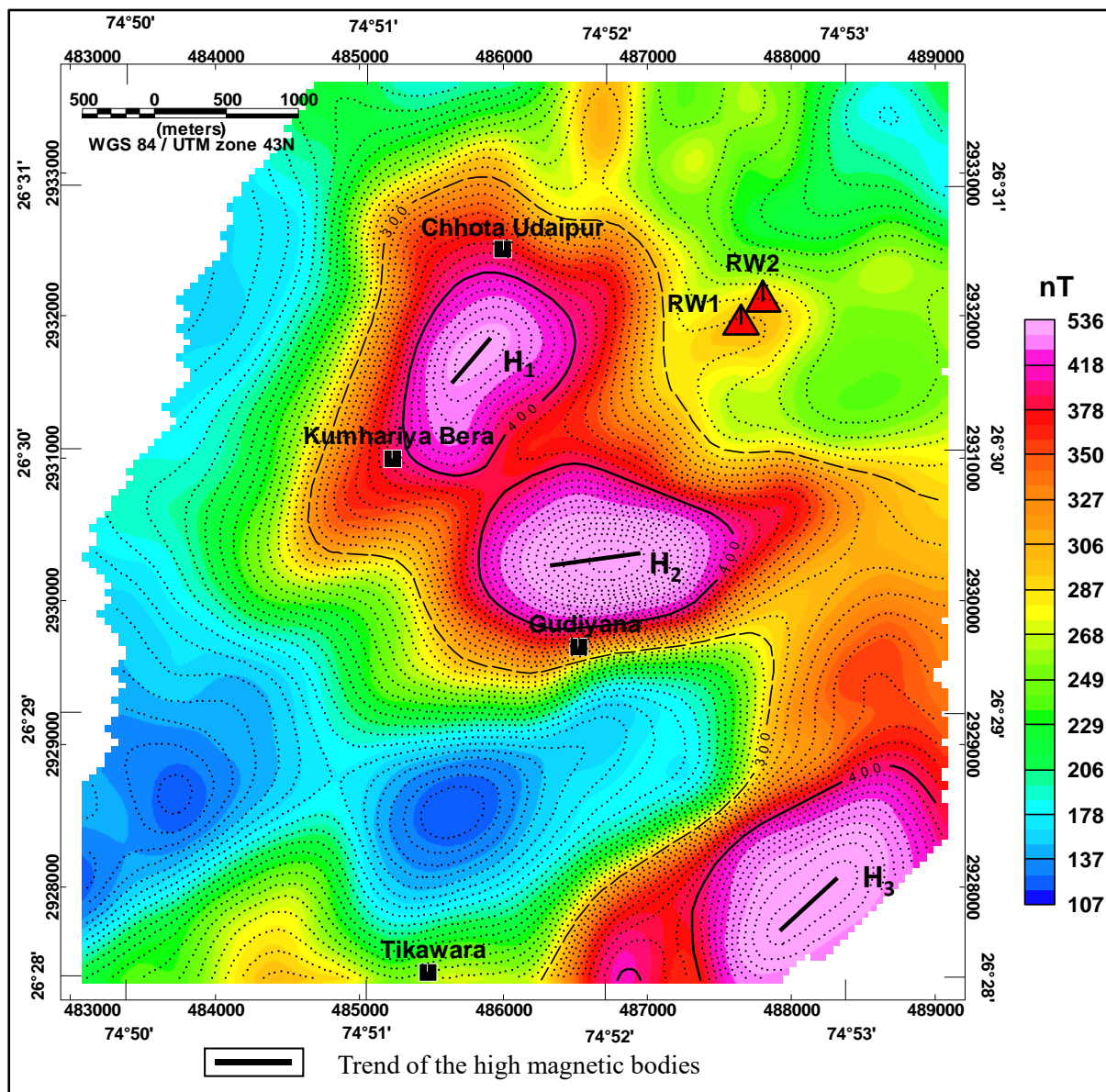


Figure 3.6 Upward continued magnetic (RTP) map of 400m level, Chhota Udaipur area, Ajmer district, Rajasthan

### 3.6.1.4 First Vertical Derivative Filter

First Vertical Derivative (FVD) is the first order differentiation of observed anomalies with depth which emphasizes the contributions from shallow sources at the expense of those from the larger and deep-seated sources. It is also used to sharpen the shallow contacts and

structural features (Telford et al., 1990; Lowrie et al., 2007; Radhakrishna murthy et al., 1978).

FVD filter has been applied over RTP grid.

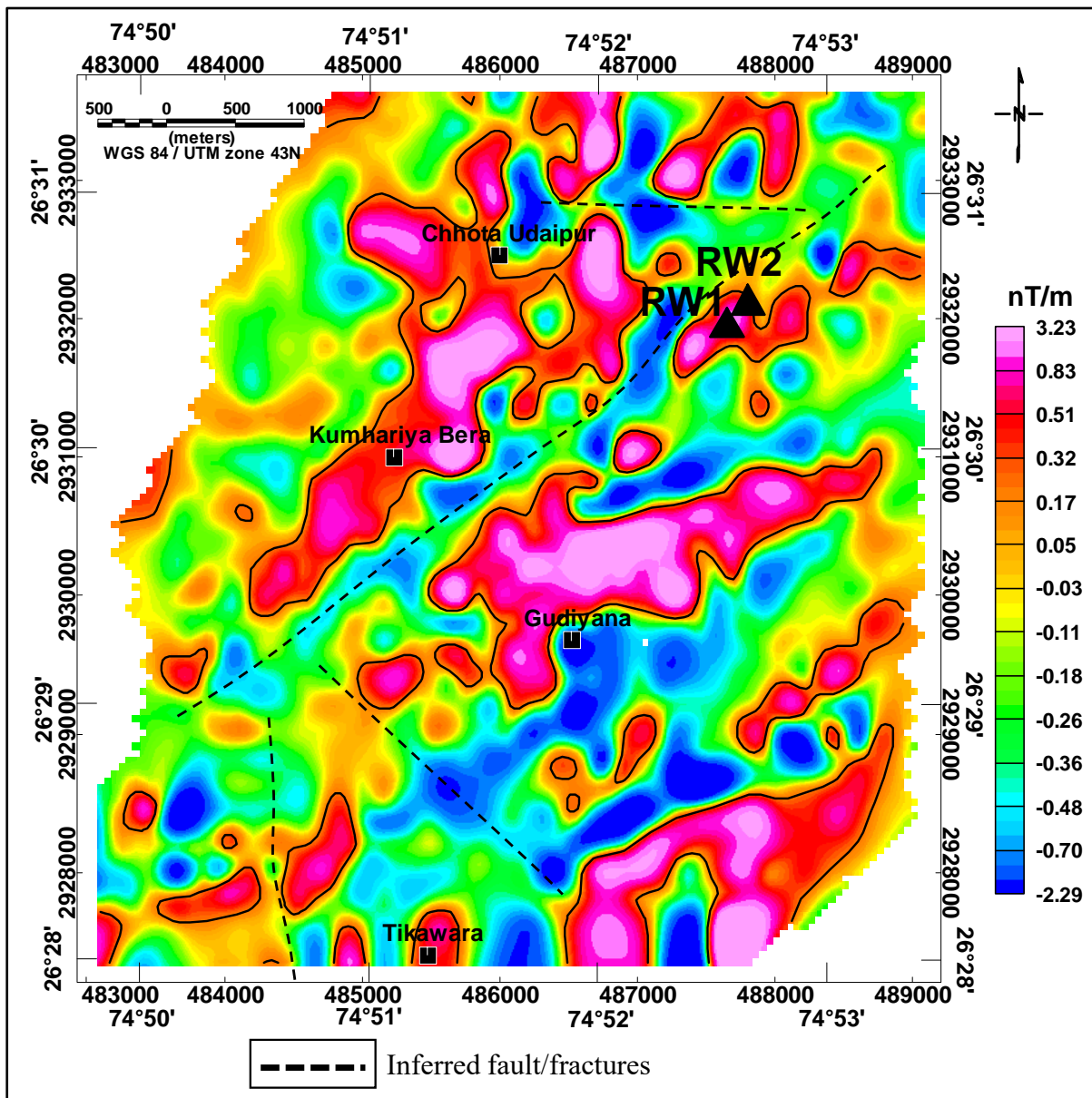


Figure 3.7 FVD of RTP anomaly map, Chhota Udaipur area, Ajmer district, Rajasthan

From the FVD filtered map (Figure 3.7), it has been observed that the high magnetic anomalies are enhanced and closely-spaced anomalies are better resolved. Based on variation in anomaly trend and amplitude, prominent subsurface structural features trending NE-SW, E-W and NW-SE fault/fractures have been demarcated in the study area as shown in Figure 3.7.

### 3.6.1.5 Tilt Derivative or Tilt angle method

Tilt Derivative (TDR) method proposed by Salem et al. (2008) has come into wide use as an aid for interpreting magnetic gridded data. High TDR values are commonly associated with lateral contrasts in magnetization and may represent dikes. The low TDR values may represent nonmagnetic or alteration zones, fractures or faults within the country rock. The tilt angle technique is the ratio of the vertical derivative to absolute value of the total horizontal derivative of the magnetic field

$$\text{TDR}_\theta = \tan^{-1} \left( \frac{\frac{\partial T}{\partial z}}{|\text{THDR}|} \right) \quad \dots\dots (3.2)$$

Where T is the total magnetic field,  $\frac{\partial T}{\partial z}$  is the vertical derivative of the magnetic field

$$|\text{THDR} = \frac{\partial T}{\partial x} + \frac{\partial T}{\partial y}| \text{ absolute value of the total horizontal derivative of the magnetic field}$$

The tilt angle amplitudes are restricted to values between  $-\pi/2$  and  $+\pi/2$ ; thus, the method limits the amplitude variations into a certain range therefore it functions like an automatic-gain-control filter which responds equally well to shallow and deep sources. The amplitude of the tilt angle is positive over the magnetic sources, crosses through zero at or near the edge of the source, and is negative outside the source (Miller and Singh, 199; Salem et al 2007). The half-distance between  $+45^\circ$  and  $-45^\circ$  contours provide an estimate of the source depth for vertical contacts. Tilt derivative map of the study area clearly demarcated the contacts between high magnetic and low magnetic bodies with zero (radians) contour and also brought out prominent NE-SW, NW-SE and east west fracture zones in the survey area as shown in Figure 3.8. Low TDR values have been observed towards the southern portion of the study area, which could be due to the alteration of gneissic rocks by the intrusion of Gyangarh Asind acidic igneous rocks. The depth to sources are estimated from tilt angle technique, the high

magnetic signature H<sub>1</sub> has the range of 50 to 180m and high magnetic signature H<sub>2</sub> has the sources lying at in the range of 150 to 320m depth.

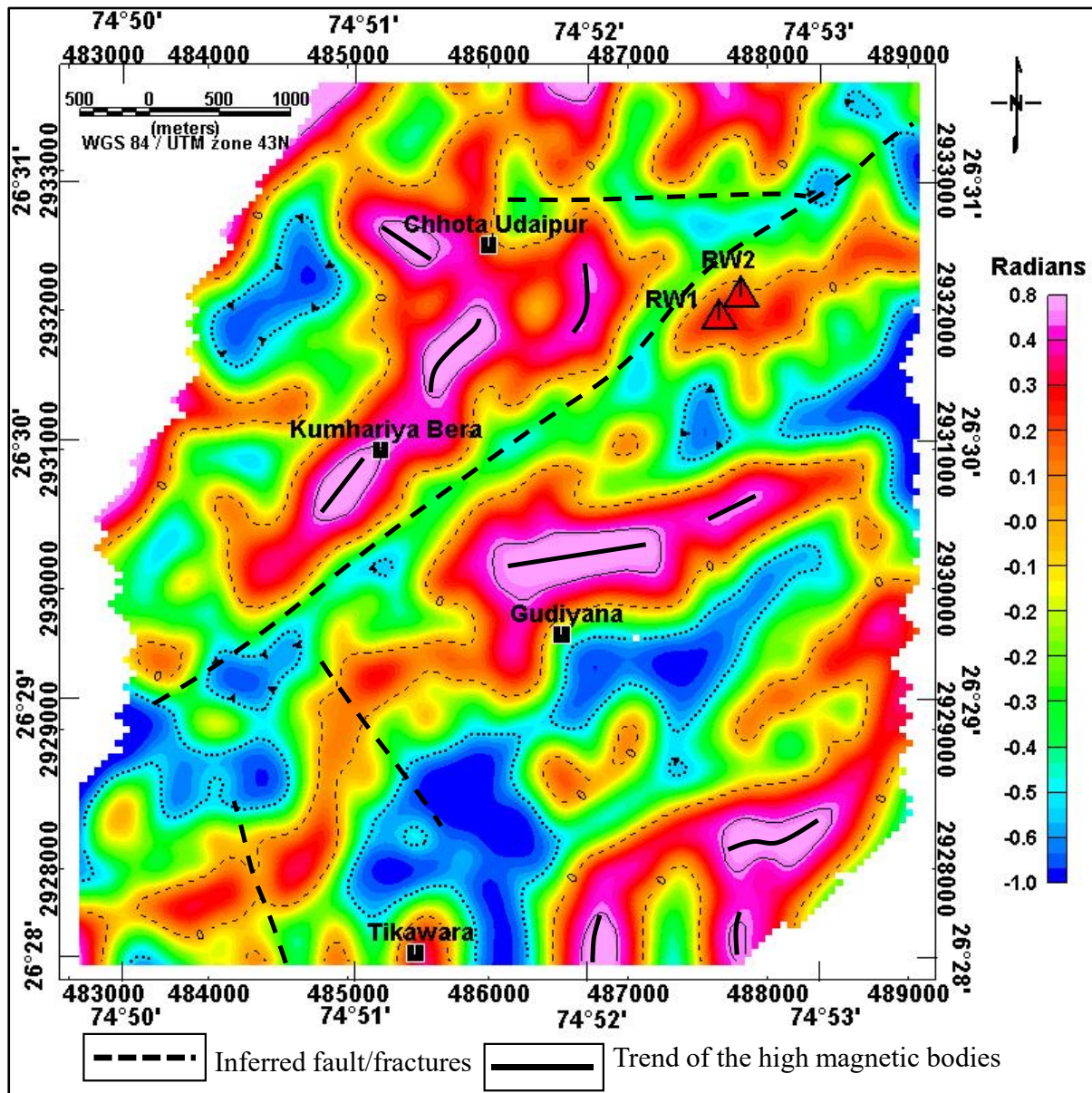


Figure 3.8 Tilt angle map of the RTP image, Chhota Udaipur area, Ajmer district, Rajasthan

### 3.6.2 Quantitative interpretation of magnetic data

Quantitative interpretation includes providing information about the source body geometry such as depth to the top, dip, thickness of the source bodies. In the following section, different methods used in quantitative interpretation are discussed.

### 3.6.2.1 Euler deconvolution

Thompson et al.,1982 proposed a technique for analysing magnetic data based on Euler relation for homogeneous functions. The Euler deconvolution technique uses first-order x, y, and z derivatives to determine location and depth for various idealized targets (sphere, cylinder, thin dike, contact), each characterized by a specific structural index (SI). A structural index is an exponential factor corresponding to the rate at which the field falls off with distance, for a source of a given geometry. SI for different source geometries are as follows

<b>SI</b>	<b>Source geometry</b>
0	Contact / Step
1	Sill / Dyke
2	Cylinder / Pipe
3	Sphere

Although theoretically the technique is applicable only to a few body types which have a known constant structural index, the method is applicable in principle to all body types. Reid et al., (1990) extended the technique to 3D data by applying the Euler operator to windows of gridded data sets. The Euler deconvolution technique is insensitive to magnetic inclination, declination and remanence.

In this study, the Euler deconvolution technique was applied over the TMI grid for location and depth determination of causative anomalous bodies from observed magnetic field data. Different structural indexes and window lengths have been tested for cluster of Euler solutions, eventually structural index  $SI=0$  where Window of 10 x 10m data points proved to be most suitable and is used for depth estimation.

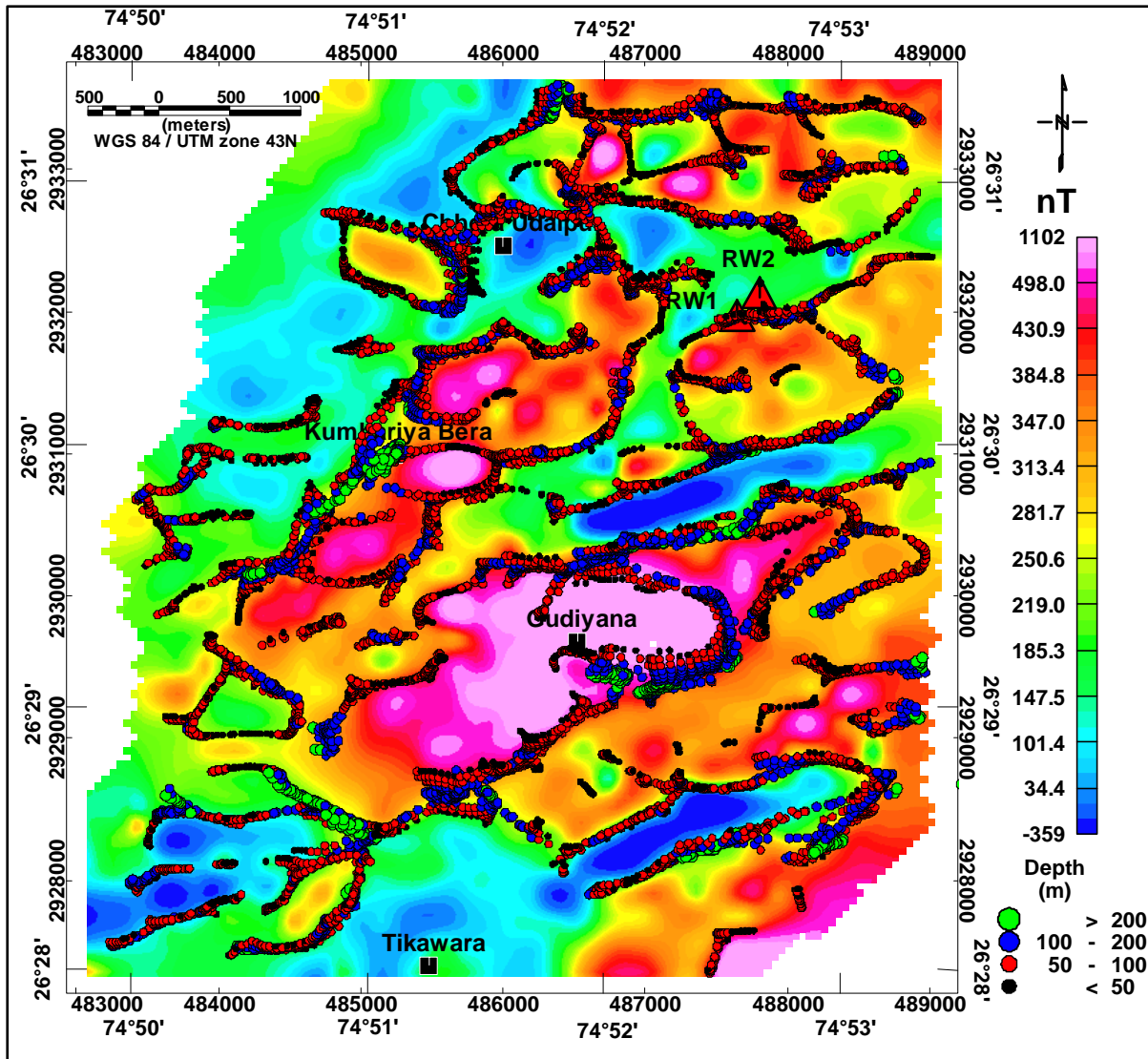


Figure 3.9 Euler solutions over TMI map, Chhota Udaipur area, Ajmer district, Rajasthan

The minimum and maximum source depth ranges obtained by this method are 50 m to 350 m and solutions with depths to source above the error tolerance levels are rejected. These solutions are plotted over TMI map as shown in Figure 3.9. The center of the plotted circles represents the location ( $x_0$  &  $y_0$ ) of the interpreted source. Similarly, depths are displayed using color variation to represent 4 different ranges. From the figure, it is observed that in the northern part of the study area depth solutions are predominantly shallower (<50m) to intermediate (50 m-100 m) and contacts near earlier reported radioactive anomalies are giving depth solutions in this range. The solutions for relatively deeper depths from 100m to 200m and more are located in the western and southern part of the study area. It is also observed that the high magnetic signature

H<sub>2</sub> is associated with deeper depth solutions than compared with that of high magnetic signature H<sub>1</sub>. It is observed from Figure 3.9 that the Euler solutions clearly indicate the magnetic sources are relatively shallower in the northern portion of the study area than compared to the southern side.

### **3.6.3 Modeling and Inversion of Magnetic Data**

Modeling and inversion refers to the assumption of geophysical models and parameters based on known geology and modifying in an iterative approach such that the observed anomalies and theoretical anomalies fit closely. All the inversion schemes are iterative and utilize one or the other form of optimization techniques. Quantitative interpretation refers to drawing geologic conclusions from the inverted models. As is typical for geophysical inverse problems, a purely mathematical solution of magnetic inversion is nonunique. In inversion, a model is parameterized to describe either source geometry or the distribution of a physical property such as magnetic susceptibility.

#### **3.6.3.1 2-D Forward Modeling**

Forward modeling refers to the computation of theoretical magnetic anomalies for assumed geometry and shape parameters which is useful in understanding the magnetic anomalies in terms of subsurface geology. Two dimensional (2D) forward modeling studies have been carried out using GM-SYS module of Oasis Montaj software along a representative profile 'AB' (Figure 3.10). This profile has been extracted from TMI grid in the NNW-SSE direction in such way to represent all the major litho-units in the study area. Results from Euler depth solutions and susceptibility values measured from different geological rock units have been utilized as input and the ambiguity in the modeling of magnetic data has been minimized.

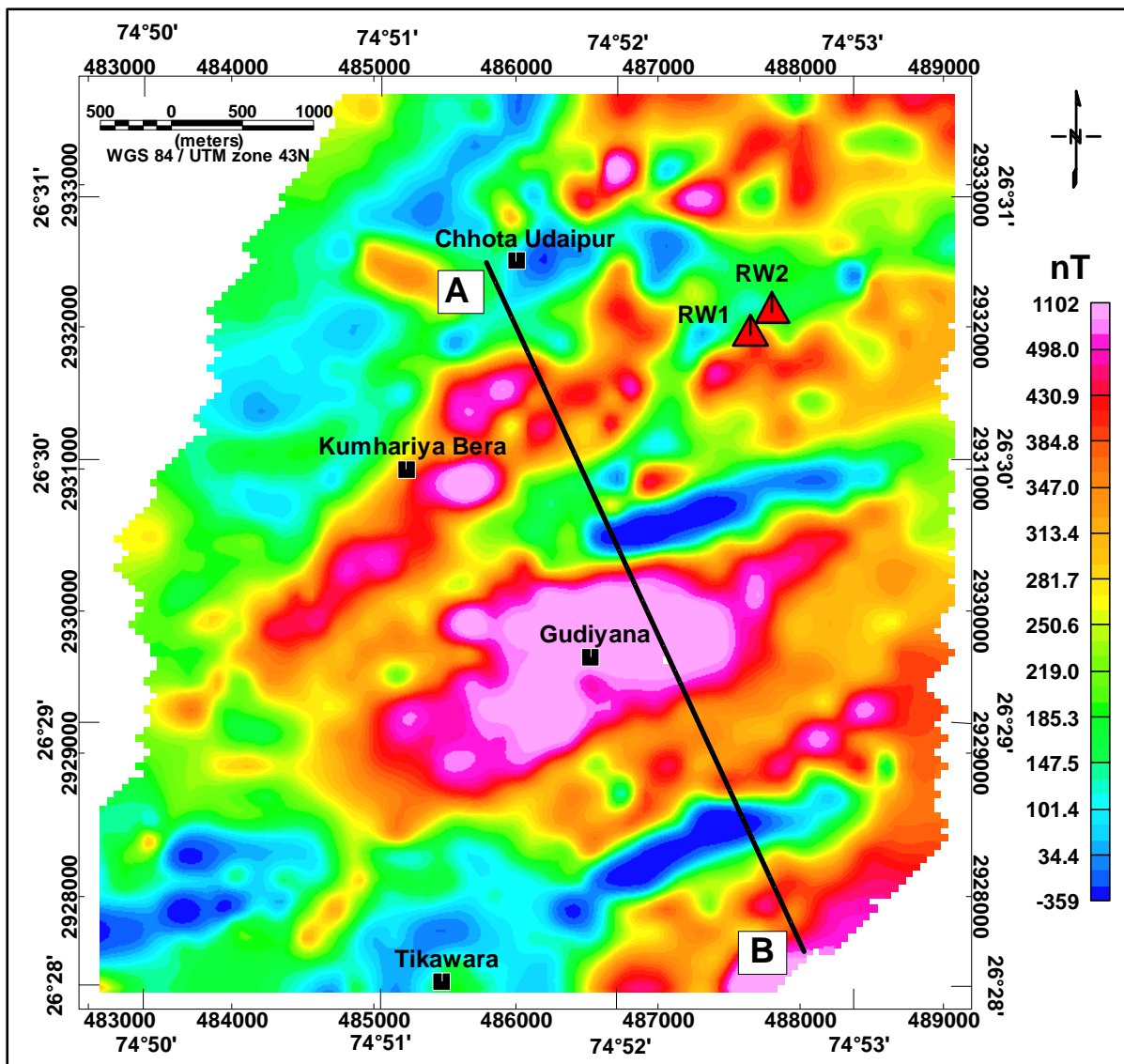


Figure 3.10 Profile AB over TMI map for 2D modeling

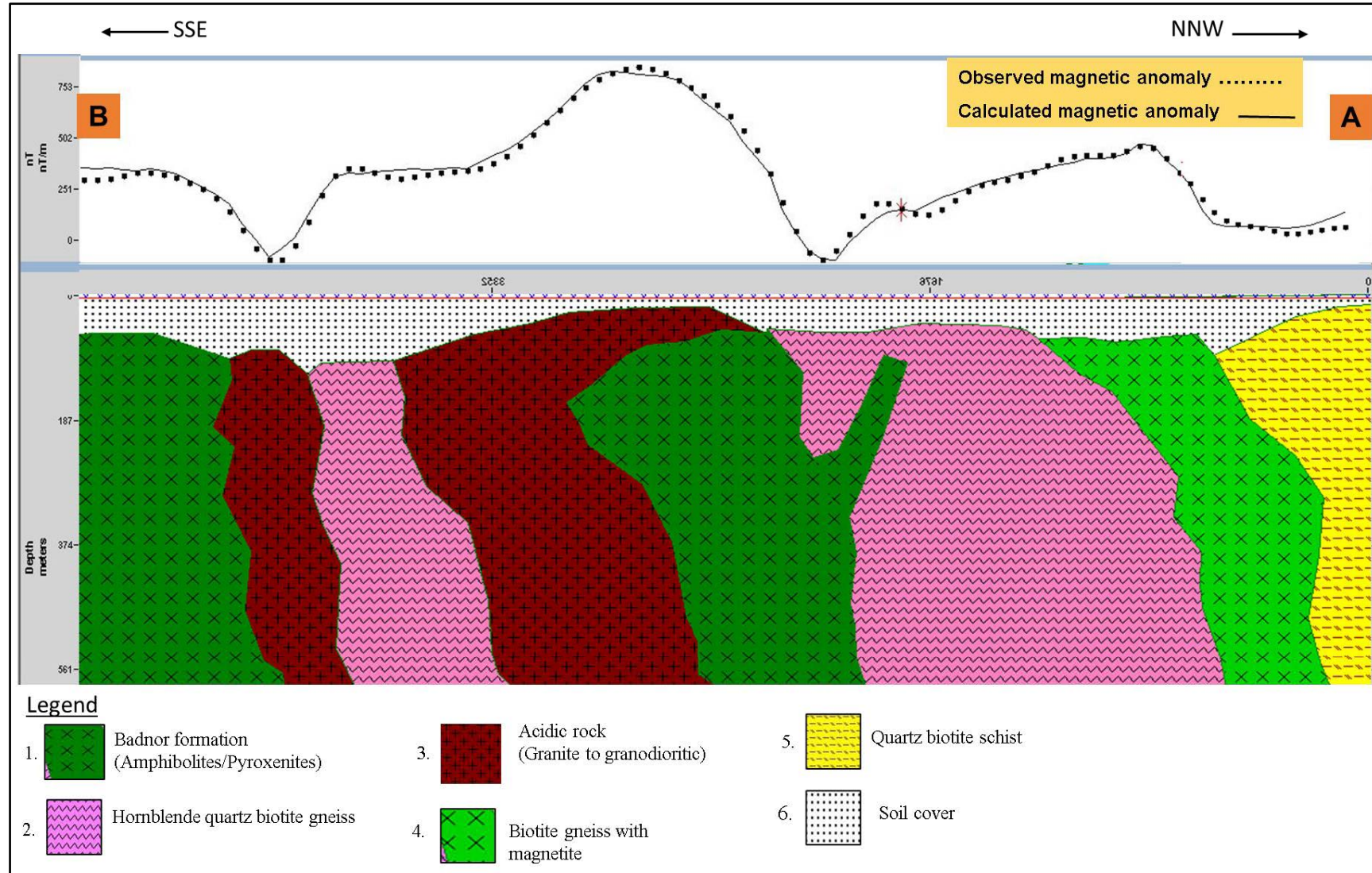


Figure 3.11 2D geological model of profile AB, Chhota Udaipur area, Ajmer district, Rajasthan

Table 3.2 Different litho units and their magnetic susceptibility from the model-AB

S. No	Rock types	Magnetic susceptibility
1.	Badnor formation (Amphibolite's/Pyroxenites)	0.0314 SI units
2.	Hornblende quartz biotite gneiss	0.010 SI units
3.	Acidic rock (Granodiorite)	0.00012 SI units
4.	Biotite gneiss with magnetite	0.032 SI units
5.	Quartz Biotite Schist	0.005 SI units
6.	Soil cover	0.03 mSI units

Figure 3.11 shows the probable subsurface model along 5.2 km long NNW-SSE a profile line A-B. It is clearly observed that the soil thickness varies between 10 to 50 m from north to south and at some places basement gneissic rocks are exposed. The model (Figure 3.11) has revealed the presence of quartz biotite gneiss associated with magnetite having high susceptibility ( $K= 0.032$  SI) values (shown as light green color). The Mafic intrusive bodies(pyroxenite's) of Badnor formation possess high order of magnetic susceptibility values ( $K= 0.0314$  SI) and are responsible for high magnetic signature in the center of the study area. The quartz-biotite-schist in NW of study area is having low susceptibility ( $K= 0.005$  SI) (which is represented with yellow color). The country rock biotite gneiss and migmatites are having moderate susceptibility ( $K = 0.010$  SI) because of the presence of hornblende mineral. The low magnetic signature in the southern side of the study area is due to the younger Gyangarh Asind acidic intrusive igneous rocks within the banded gneissic complex, of granitic to granodioritic composition having very low susceptibility ( $K = 0.00012$  SI).

### 3.6.3.2 3-D Modeling

2D model gives the subsurface configuration along a profile while the 3D modeling is important for better conceptualization of subsurface and to visualize the lithological unit in

three dimensional (3D). 3D modeling of magnetic data provides 3D distribution of magnetic susceptibility in the subsurface. To allow maximum flexibility for the model to represent it in geologically realistic structures, we discretize the 3-D model region into a set of rectangular cells, each having a constant susceptibility. The number of cells is generally far greater than the number of the data available, thus problem is underdetermined which is solved by minimizing a global objective function composed of the model objective function and data misfit. The algorithm can incorporate a priori information into the model objective function by using one or more appropriate weighting functions. The model for inversion of susceptibility a positivity constraint is imposed to reduce the non-uniqueness and to maintain physical reliability. We assume that there is no remanent magnetization and that the magnetic data are produced by induced magnetization only while inverting the data. An attempt has been made to invert the magnetic data using UBC MAG3D ([www.eoas.ubc.ca](http://www.eoas.ubc.ca)) which resulted to the susceptibility distribution in 3D.

Table 3.3 Inversion parameters of 3D magnetic voxel model

<b>S. No</b>	<b>Parameter Description</b>	<b>Parameter value</b>
1	Total no. of data points	5035
2	Total no. of cells in X-direction	200
3	Total no. of cells in Y-direction	102
4	Total no. of cells in Z-direction	53
5	Total no. of cells	1081200
6	Number of iterations	27
7	Sensitivity of the model	Min: 4.24E-09 and Max: 3.78E-08
8	achieved relative error	8.9554E-02

Inverted 3D magnetic susceptibility distribution of magnetic data using UBC MAG3D is shown in Figure3.12 but it was a completely mathematical model. The first order trend (regional) has been removed from the observed magnetic data for the enhancement of residual anomaly before doing the 3D-inversion which resulted the subtle anomalies to be more clearly

visible. The high magnetic signature  $H_1$  (Figure 3.5) near Chhota Udaipur village gets truncated at places by fault/fractures and discrimination of low susceptibility NE-SW fracture are clearer in inverted model. The high magnetic signature  $H_2$  near Gudiyana village showing displacement in its eastern extension may be due to fault/fracturing which is not clear in RTP map as compared to 3D inverted model. and 3D model illustrates the SW continuity high susceptibility distribution of the magnetic anomaly  $H_2$ .

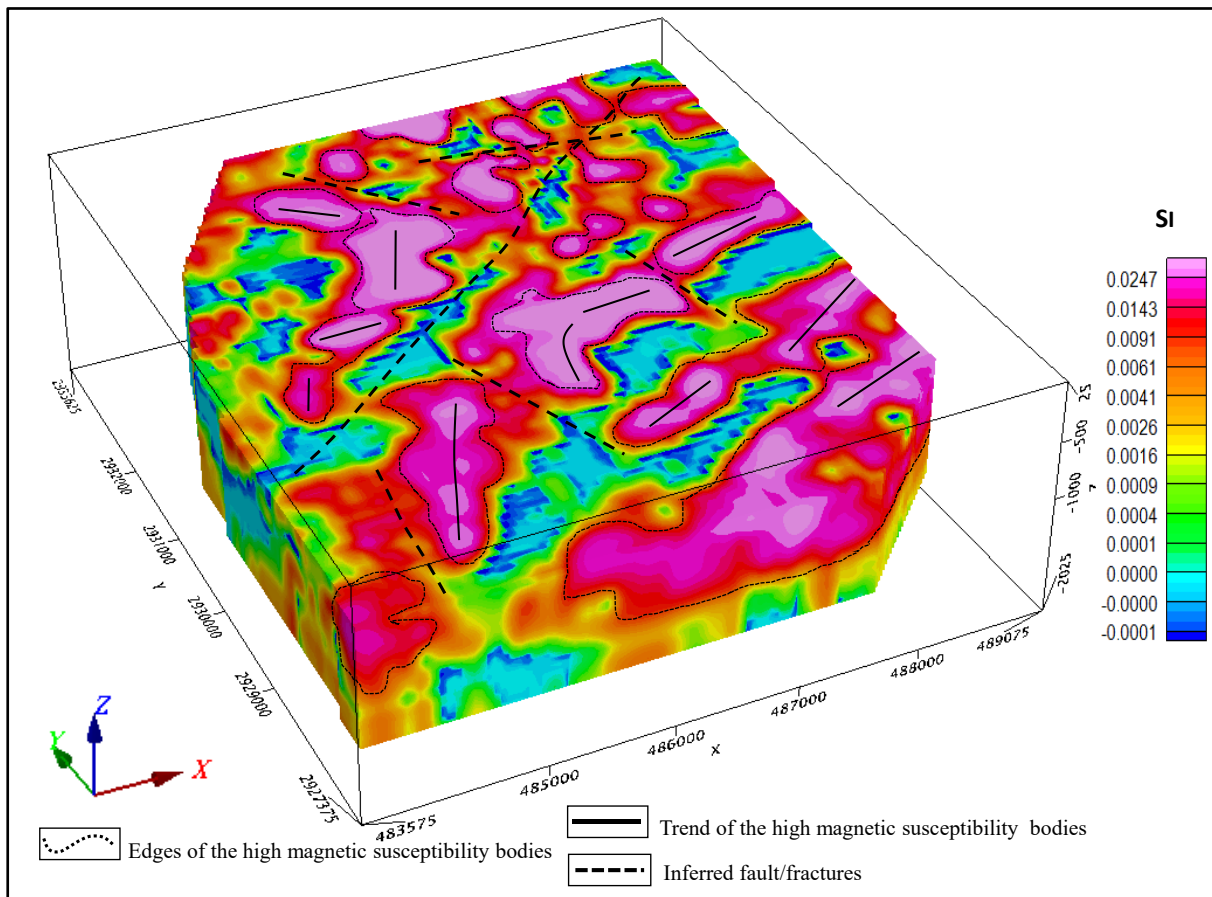


Figure 3.12 3-D Inverted Magnetic model of Chhota Udaipur area, Ajmer district, Rajasthan Magnetic susceptibility measurement of rock samples forms a basis for the interpretation about type and nature of magnetic sources. The susceptibility of magnetite bearing biotite gneisses are having around 30 mSI units and responsible the high magnetic signature  $H_2$  ( $> 400\text{nT}$ ) near kumariya bera village. Iso surfaces of 30 mSI susceptibility have been prepared to understand the distribution of particular susceptibility value implies the rock type and overlaid on the RTP

map (Figure 3.13). The iso surface of 30 mSI magnetic susceptibility representing magnetite bearing biotite gneiss is well resolved in the depth range of 80 m to 650m and correlates with the high magnetic signatures in RTP map.

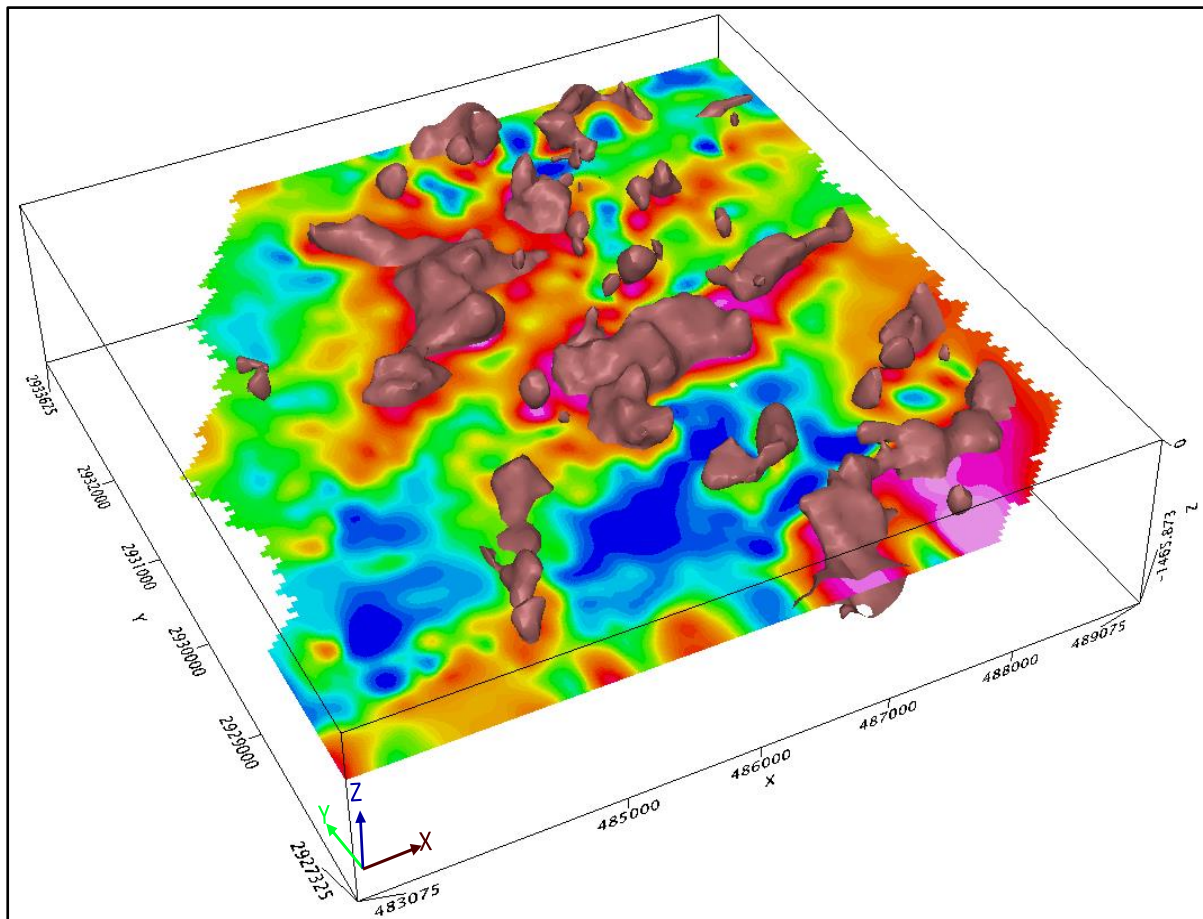


Figure 3.13 Inverted magnetic model highlighting the high susceptibility iso-surface (K= 30 mSI unit) overlaid on the RTP map, Chhota Udaipur area, Ajmer district, Rajasthan

Different Depth slices of magnetic susceptibility distribution at the levels 200 m, 400 m and 600 m are shown in Figure 3.14. Depth slice at 200 m indicates the presence of many small high magnetic susceptibility sources (magnetic susceptibility > 15 mSI) in the western and north eastern part of the survey area. Depth slice at the level of 400 m and 600 m, shows features which are attributed to mafic bodies/ magnetite mineralisation within the gneisses of Sandmata complex having the depth extension.

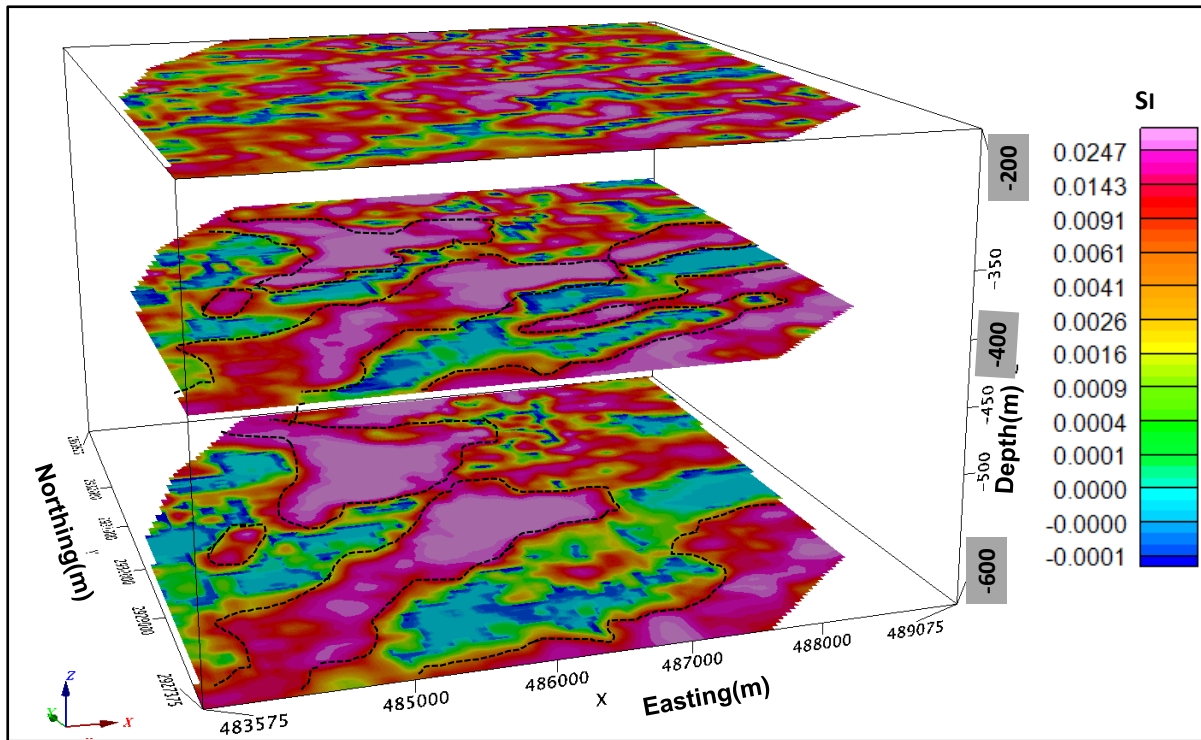


Figure 3.14 Horizontal depth slices of magnetic model at a depth of 200m, 400m and 600m

### 3.6.3.3 Forward modeling in 3D

3-D modeling of the magnetic data was carried out using Model Vision pro software ([www.tensor-research.com.au](http://www.tensor-research.com.au)) A model that approximately matches a complete anomaly is likely to be more reliable than the one that matches only a single profile all through. Detailed modeling studies should therefore focus on matching the observed data as closely as possible. Again, for computational convenience, the available 50 x 50 m gridded data was used in modeling the data. Multiple bodies were chosen for 3-D modeling based on the earlier generated 2-D models. Magnetic responses for these bodies were computed by manipulating the parameters in such a way that the observed and computed models fit as close as possible. The forward model is shown along with observed and computed data images (Figure 3.15).

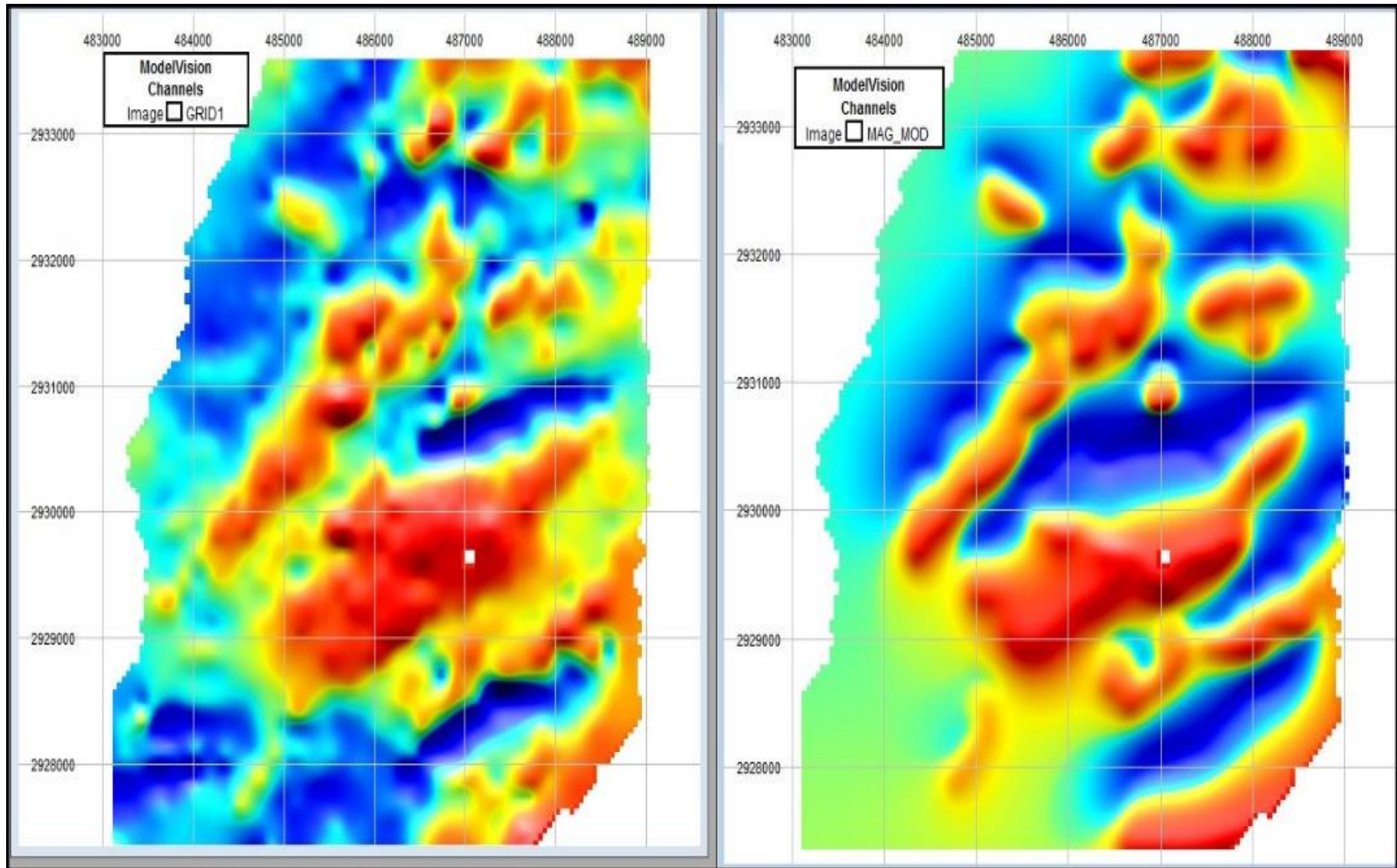


Figure 3.15 TMI map and 3D modelled TMI response

The response of 3D subsurface bodies is shown in Figure 3.16. From 3D modeling it is observed that the high magnetic source of anomaly H<sub>2</sub> is not continuous, has irregular distribution and high magnetic intrusive body in SW of Gudiyana village is better resolved from these modeling studies. Apart from the three prominent high magnetic anomalies, there are several moderate magnetic anomalies with limited spatial and depth extension which are interpreted as polymetallic injections in BGC.

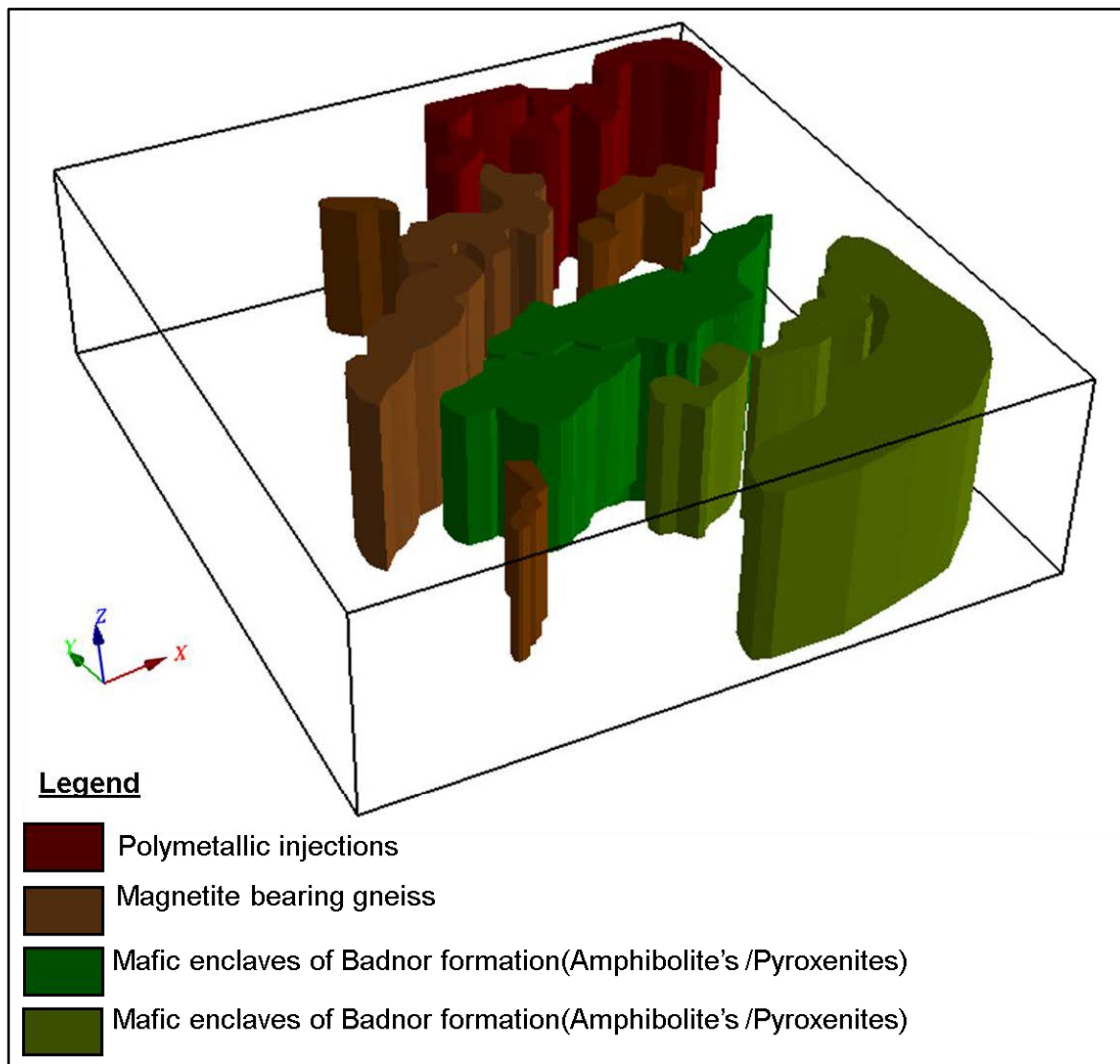


Figure 3.16 3D forward modeling for observed TMI response



## CHAPTER 4

# INDUCED POLARIZATION AND RESISTIVITY METHOD OF EXPLORATION

### 4.1 Introduction

Resistivity survey is extensively used in mineral exploration with an objective of direct detection of electrically anomalous targets, in particular sulphides and metal oxide mineralization as it provides information about distribution of electrical conductivity, a measure of the ease with which electrical currents flow within the subsurface. From the resistivity survey we can get the information about the geometry and electrical characteristics of the source of anomalies. The Induced Polarization (IP) survey is similar to electrical resistivity method, is a relatively new technique in geophysics, and has been employed mainly in base-metal exploration and to a minor extent in groundwater search (Seigel et al., 1997)

IP refers to a resistive blocking action in earth materials and the process is most pronounced in fluid-filled pores next to metallic minerals. IP is a current-induced electrochemical phenomenon observed as delayed voltage response in earth materials for exploring subsurface mineral deposits. The IP effect is therefore observed to be strongest near rocks containing metallic luster minerals (Marshall and Madden, 1959; Sumner, 1976). The IP anomalies are mainly caused by the metallic minerals such as disseminated sulphides and graphite or by the oxides such as magnetite (Telford, 1990). The IP phenomenon is measured by passing a controlled inducing current through a substance and observing resultant voltage changes with time or with variations of inducing frequency.

Field measurements of the I.P. effect may be divided into two main groups, the frequency domain and time domain methods. In the frequency-domain methods, the dispersive nature (or effect as a function of frequency) of the phenomenon is observed and is measured at

least two frequencies, for example at 1 Hz. and 10 Hz expressed as units of "percent frequency effect" or PFE. In the time domain method, measured the decay of the potential after switching off a d.c. current. Time domain IP has been extensively used for mapping subsurface metallic ore bodies, environmental problems and permeability imaging (Borner et al.,1996; Oldenburg et al., 1997).

Satyanarayana et al., 2018 effectively utilized the IP and Resistivity methods in search of base metal exploration. Vijaya Kumar et al., 2015; Shrajala Pitla et al., 2015; Srinivasa Rao et al., 2016 and Srinivasa Rao et al., 2018 have successfully applied the IP and Resistivity techniques to delineate the fractures, faults, shear zones and conductive horizons for uranium exploration in NDFB, Rajasthan.

#### **4.2 Theory of Induced polarization**

The principal cause of induced polarization in mineralized rocks is a current-induced electron transfer reaction between electrolyte ions and metallic-luster minerals. When metallic minerals block or are next to electrolyte-filled pore paths and an electric current flow through the rock, an electrochemical over-potential (overvoltage) builds up at the interface between the electron-conducting mineral and the pore solution. These electrochemical forces that oppose current flow are described as polarizing the interface and the increase in voltage required to drive current through the interface is called the overvoltage (Marshall and Madden, 1959; Sumner, 1976). Even after removal of applied current, voltage does not come to zero instantaneously it will take finite time to decay to zero. The effect of induced polarization mainly caused by the metallic minerals such as disseminated sulphides and graphite or by the oxides such as magnetite (Telford, 1990). The IP effect is most pronounced near rocks containing dispersed metallic mineral grains. Polarization can increase with fluid content and decreases with pore space. Induced polarization can be expressed relatively in percentage (%) as the ratio of secondary voltage to applied primary voltage ( $V_p$ ). Measurements are taken at a

number of discrete time intervals during the charge decay and stacked using repeats to improve the signal to noise ratio. The IP effect is caused by two main mechanisms, which are membrane polarization and the electrode polarization effects.

#### **4.2.1 Membrane polarization**

Membrane polarization is caused by presence of clay minerals and constriction within the pore channel. The effect decreases with increasing salinity of the pore fluid. Electrolytic conduction is the predominate factor in most rocks when no minerals are present and the frequency is low. Most of the rock forming minerals have a net negative charge on their outer surfaces in contact with the pore fluid and attract positive ions onto this surface from pore fluid. The concentration of positive ions extends about 100  $\mu\text{m}$  into the pore fluid, and if this distance is of the same order as the diameter of the pore throats, the movement of ions in the fluid resulting from the impressed voltage is inhibited (Telford, 1990). Negative and positive ions thus build up on either side of the blockage and, on removal of the impressed voltage, return to their original locations over a finite period of time causing a gradually decaying voltage.

#### **4.2.2 Electrode polarization**

When metallic minerals are present in a rock, an alternative, electronic path is available for current flow. Figure 4.1(b) shows a rock in which a metallic mineral grain blocks a pore, when a voltage is applied to either side of the pore space, positive and negative charges are imposed on opposite sides of the grain. An electro chemical reaction takes place at the interface between the grain surface and pore fluid. Negative and positive ions then accumulate on either side of the grain which are attempting either to release electrons to the grain or to accept electrons conducted through the grain. The rate at which the electrons are conducted is slower than the rate of electron exchange with the ions. Consequently, ions accumulate on either side

of the grain and cause a build-up of charge. When the impressed voltage is removed the ions slowly diffuse back to their original locations and cause a transitory decaying voltage.

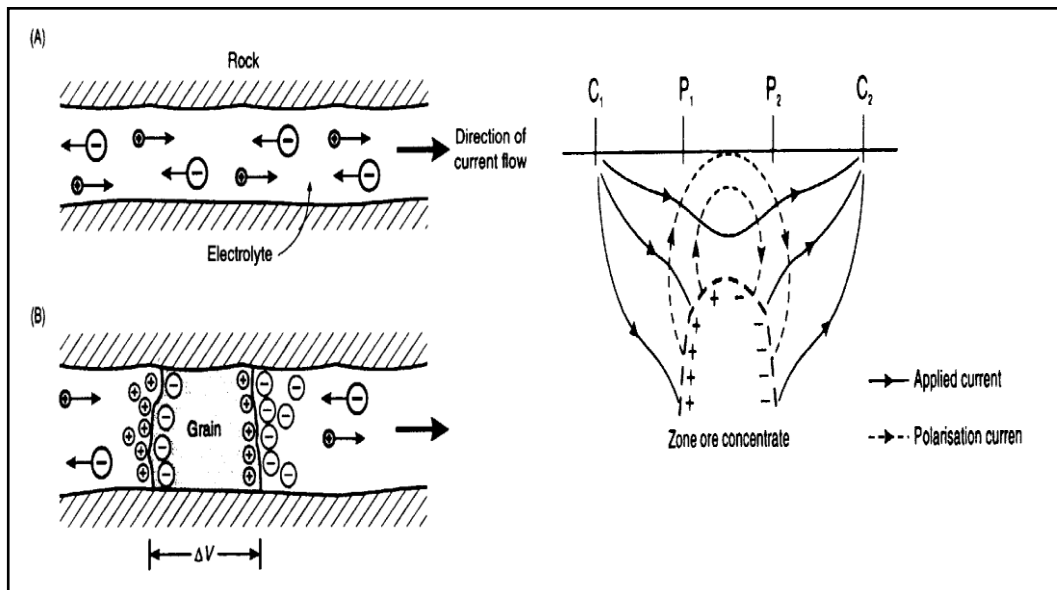


Figure 4.1(A) Membrane polarization (B) Electrode polarization (after Telford et. Al., 1990)

In the present study IP data has been acquired in time domain (TDIP) mode, hence measurement of IP response in time domain is only discussed in detail.

### 4.3 Measurement of Induced Polarization

IP effect is measured by injecting controlled current into the ground and measuring the change in voltage with respect to time. When the induced current is turned off, the primary voltage almost immediately drops to a secondary response level and then the transient voltage diminishes with time (Figure 4.2). Measurement of the secondary voltage is one means of measuring the polarization of a material. IP effect is normally measured in conjunction with apparent resistivity.

There are several different ways of measuring the IP effect in the time domain. The most commonly measured parameter is the Chargeability  $M$ , is the area (commonly in millivolt/volt) between the decay curve over a certain time interval ( $t_1-t_2$ ) and the zero-volt level (Figure 4.2). This value is usually normalized by dividing it by the peak charging voltage.

Chargeability (M) is defined as 
$$M = \frac{\int_{t_1}^{t_2} V_s}{V_i} \frac{1}{\Delta t} \dots\dots\dots (4.1)$$

Where,  $V_i$ ,  $V_s$  are the primary voltage and secondary voltages respectively.

The Figure 4.2 shows induced current waveform used in IP/Resistivity survey. Potential difference is measured during the ON time of the current and apparent resistivity computed by using the equation (4.3), here the decay voltage has been recorded during OFF time with pre-programmed ON-OFF times from 0.5 to 8 seconds by factor of 2. Thus, it is operating at a base frequency of 0.5 Hz, 0.25 Hz, 0.125 Hz, 0.0625 Hz and 0.03125 Hz with a duty cycle of 50%.

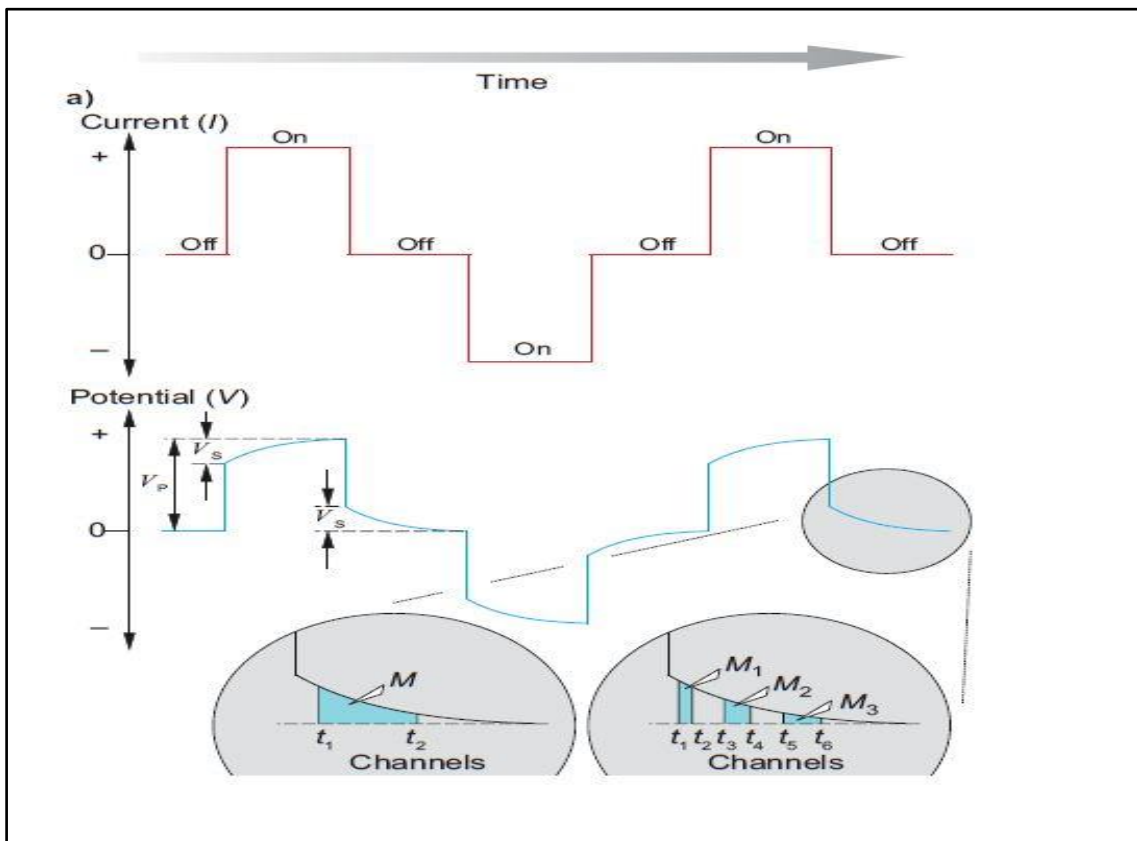


Figure 4.2 IP measurement (after Michael Dentith et al., 2014)

#### 4.4 Theory of DC Resistivity method

The resistivity of a material is defined as the resistance between the two opposite faces of a unit cube of the material. For a conducting cylinder of resistance  $\delta R$ , length  $\delta L$  and cross-sectional area  $\delta A$  (Figure 4.3) the resistivity  $\rho$  is given by,

$$\rho = \frac{\delta R * \delta A}{\delta L} \quad \dots\dots\dots (4.2)$$

Where,  $\rho$  represents the resistivity. SI unit of resistivity is Ohm.m and the reciprocal of this is conductivity whose unit is Siemens/m.

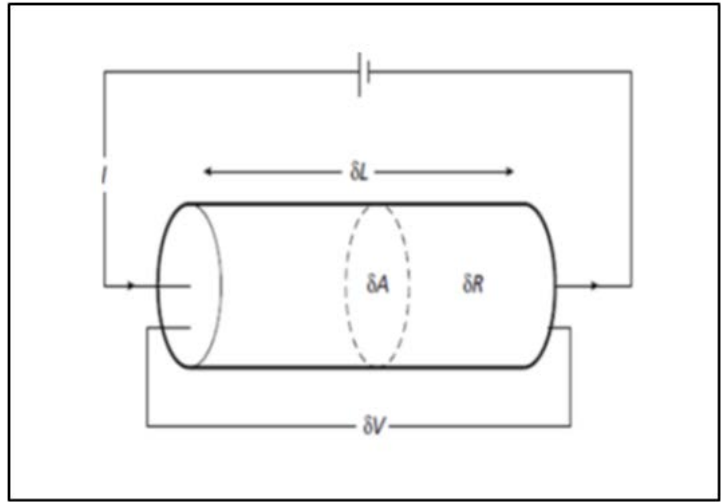


Figure 4.3 Schematic diagram for the resistivity( $\rho$ ) when current passes through a cylinder

Many factors influence the resistivity of a given material which are mineral grains, fluid content in the matrix, the degree of saturation in the pore spaces etc. The apparent resistivity can be calculated from the measurement of potential difference between the two potential electrodes When we injected the current into the ground through two current electrodes. For the homogeneous and isotropic half-space, the resistivity can be calculated for any electrode configuration. Resistivity  $\rho$  for electrode arrangement as shown in Figure 4.4

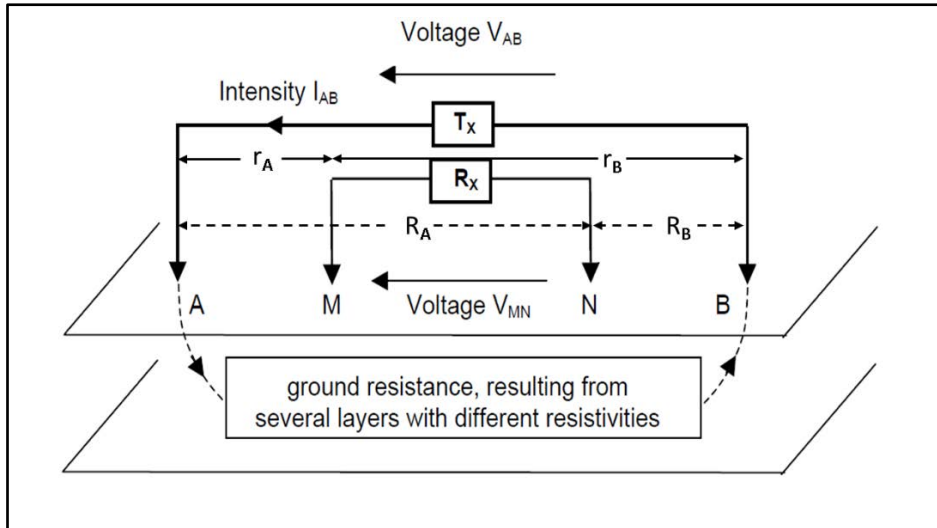


Figure 4.4 General electrode configuration used in resistivity survey (A, B current, and M, N are potential electrode respectively)

$$\rho = \frac{2\pi\Delta V}{I\left\{\left(\frac{1}{r_A} - \frac{1}{r_B}\right) - \left(\frac{1}{R_A} - \frac{1}{R_B}\right)\right\}} \dots\dots\dots (4.3)$$

Where,  $r_A$  is the distance between current electrode A and potential electrode M

$r_B$  is the distance between current electrode B and potential electrode M,

$R_A$  is the distance between current electrode A and potential electrode N,

$R_B$  is the distance between current electrode B and potential electrode N,

Resistivity values over homogenous and isotropic ground are constant and independent of electrode spacing and location on the surface and it is called as a true resistivity of the medium. but in general, we get the apparent resistivity values only in the field because of the fact that, in real conditions ground is always heterogenous and measured values are a function of the volume of earth beneath the sensors and the array geometry, and is not the actual value at the plotted point.

## 4.5 Data Acquisition of IP and Resistivity Data

### 4.5.1 Instrumentation

IP equipment of IRIS make is used for the present study ([www.irisinstruments.com](http://www.irisinstruments.com)). The transmitter is energized with a 3-phase voltage regulated motor generator (MG) operating at 20 kW, 220 V and 60 Hz frequency. The voltage is maintained between 180 V to 240 V. The instrument has got several safety features to prevent damage under abnormal conditions like unregulated or high voltages greater than 250 V. Figure 4.5 and 4.6 shows the images of IRIS IP Receiver and Transmitter respectively.



Figure 4.5 Multi electrode IRIS IP Receiver

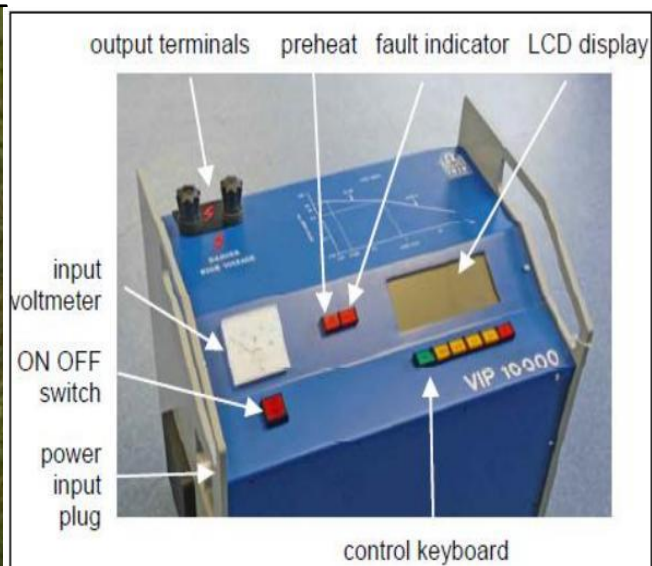


Figure: 4.6 IRIS IP Transmitter

### 4.5.2 Gradient array

The gradient array is used to measure the potential using a dipole M-N moving between two fixed current electrodes A and B as shown in the Figure 4.7. The current electrodes in the gradient array are fixed at the end of the line for that profile, while measurements are made with the potential electrodes at different positions along the line. Large volume of the ground is energized and the large parallel field region below the central part of the current dipole allows a large area to be surveyed rapidly. The uniform subsurface current flow in the measurement

region produces simple anomaly shapes. This array does not influence by topography effects, rapid data acquisition can be made along the profiling. This array is ideal for delineating geological contacts of vertical to subvertical and faults/fractures. In view of the above merits the gradient array is opted for the study to delineate conductive horizons and faults, fractures within the basement.

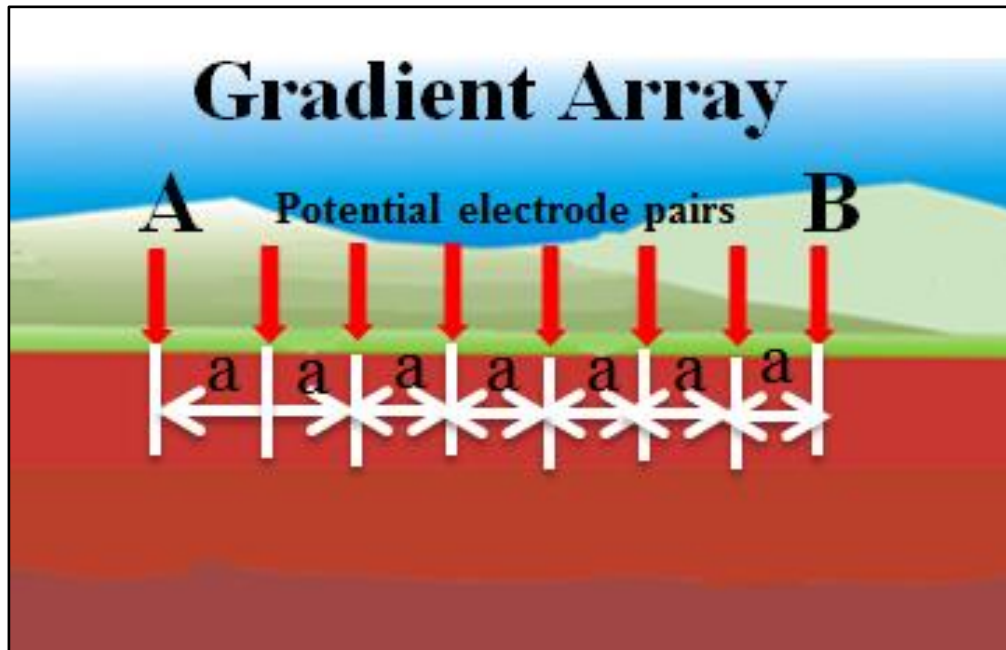


Figure 4.7 Gradient array configuration

(<https://www.agiusa.com/blog/comparison-11-classical-electrode-arrays>)

### 4.5.3 Data acquisition

IP/Resistivity traverses are planned with reference to earlier reported radioactive anomaly location (RW<sub>2</sub>), in the direction of N60°W accordingly as perpendicular to general trend of the geological features in the study area as shown in the Figure 4.8 IP/Resistivity profiles are posted over the reduced to pole magnetic anomaly map. Most of the IP/Resistivity data was acquired to the SW of the Chhota Udaipur radioactive anomaly to study the continuity of the high chargeability zone as NE portion is already covered by the earlier workers (Figure 1.4 and 1.5) and few profiles have been taken in the N-S direction to know the association of the sulphides with the NE-SW fracture as observed in magnetic anomaly map.

In the present study IP/Resistivity survey was carried out by using of multi-channel rectangular gradient array. Measurements are taken with a potential electrodes spacing of  $a=50$  m between the fixed current dipole separation of 1200m. The system calculates the apparent resistivity using obtained potential difference, applied current and geometrical factor of the array.

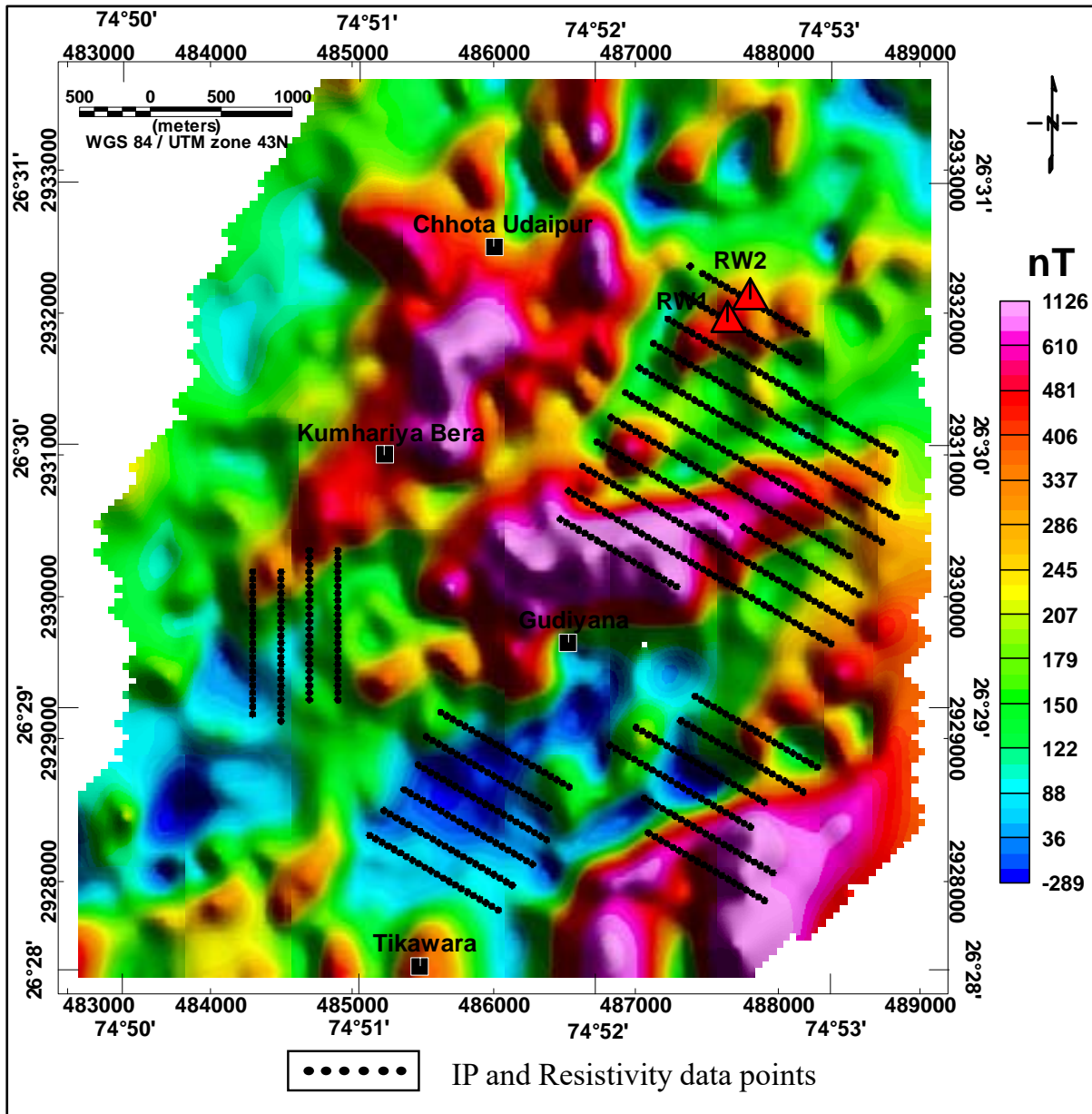


Figure 4.8 IP/Resistivity Profiles over RTP map, Chhota Udaipur area, Ajmer district, Rajasthan

## 4.6 Processing and interpretation of IP and Resistivity Data

Induced polarization and resistivity data were collected simultaneously by using IRIS IP 10K instrument. Processing of data is required in order to transform the IP/Resistivity data so that it can be interpreted geologically. In the initial stage of processing, automatic filtering technique was used to minimize the noise in the recorded data. For further analysis apparent resistivity  $\rho_a$  (Figure 4.9) and apparent chargeability  $m_a$  (Figure 4.10) maps have been prepared in Geosoft using minimum curvature gridding method with a cell size of 50 m. The principle of minimum curvature provides a method of two-dimensional interpolation which allows a computer to draw the smoothest possible surface while attempting to honor your data as closely as possible.

### 4.6.1 Apparent Resistivity Map

The order of variation in resistivity values is 90 to 5966 Ohm.m. The apparent resistivity map clearly shows the prominent low resistivity zones having resistivity values in the range of 90-862 Ohm.m in middle and eastern portion of the study area, this could be due to the fractures within banded gneissic complex (BGC).

Near the earlier reported Chhota Udaipur radioactive anomalies the high resistive zone gets splitted into two high resistive lineaments and separated by relatively low resistivity. This is may be due to the fracturing in BGC and radioactive anomalies are located along this resistivity gradient (< 1500 Ohm.m). The high resistivity values (>1500 Ohm.m) present in northern and eastern side of the study area are attributed to compact gneissic rocks, which continue towards south and this high resistivity trends are marked as black dashed line in the map (Figure 4.9).

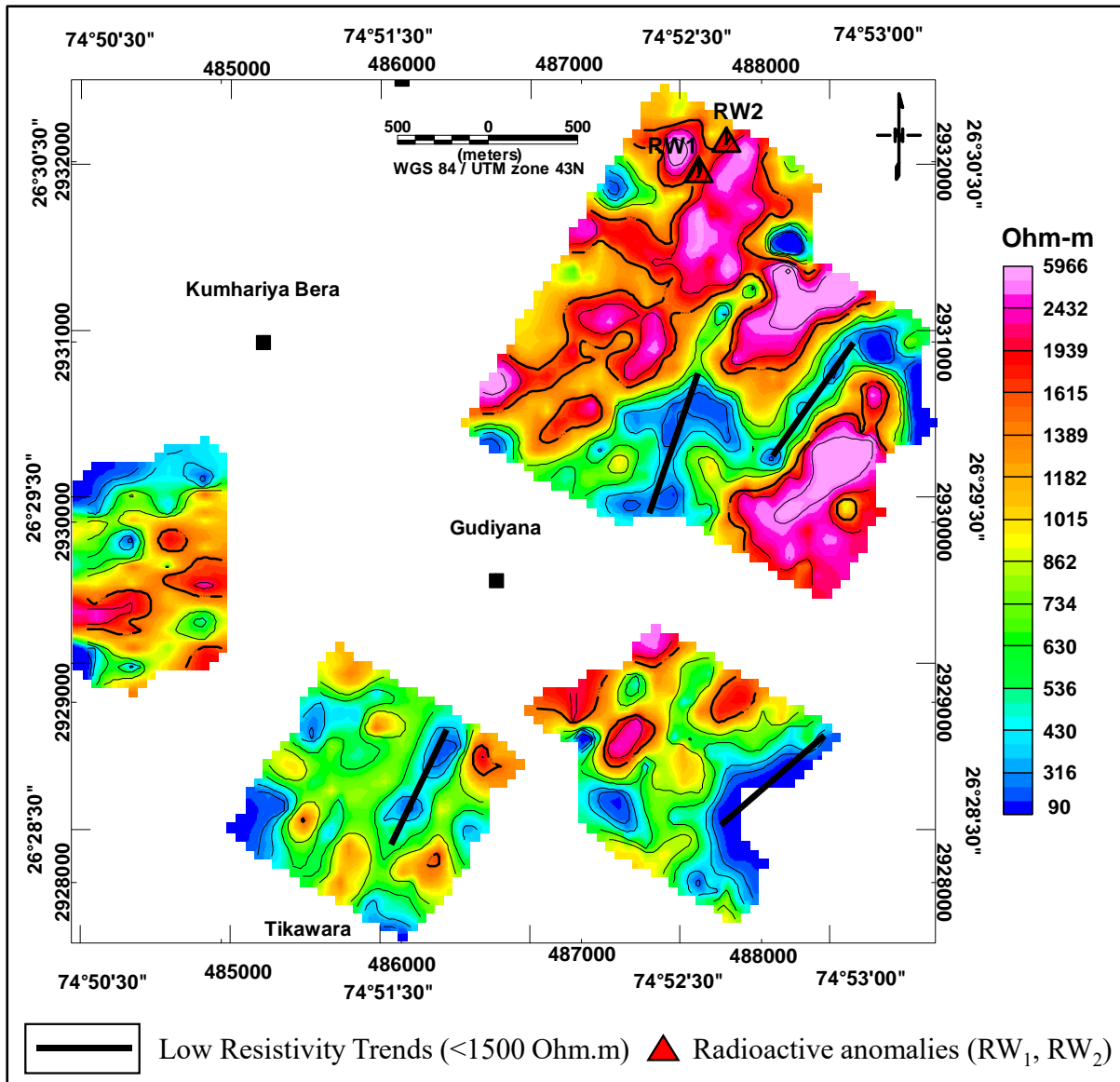


Figure 4.9 Apparent resistivity map, Chhota-Udaipur area, Ajmer district, Rajasthan

#### 4.6.2 Apparent Chargeability Map

The apparent chargeability values of the study area varying from 1mV/V to 19 mV/V as shown in the Figure 4.10. According to the magnitude of chargeability values, three high chargeability(>10mV/V) zones called Zone-M<sub>1</sub> in north, Zone-M<sub>2</sub> in middle and Zone-M<sub>3</sub> in southern portion have been identified. The zone-M<sub>1</sub> trending NE-SW has a strike length of around 600 m with width of 90 to 130 m further north-east. The earlier reported Chhota Udaipur radioactive anomalies are falling in zone-M<sub>1</sub> and associated with high chargeability of around 12 mV/V and moderate resistivity (< 1500 Ohm.m) signatures that may represent the NE-SW

fracture in BGC and filled with disseminated sulphides. The NNE-SSW trending high chargeability zone-M<sub>2</sub> has been observed towards the eastern side of the study area over strike length of around 1.5 km with width of 250 m to 380 m, which is associated with low to moderate resistivity (90 to 1500 Ohm.m) which may represent fracture zone within the BGC associated with disseminated sulphides. Another high chargeability anomaly is observed towards the south-eastern side of the Gudiyana village and which is associated with low resistivity (<500 Ohm.m) and moderate to high magnetic (350 to 963 nT) signatures. The chargeability values are not very high compared to high chargeability anomaly generally recorded in Aravalli fold belt (AFB) and North Delhi fold belt (NDFB) but they represent the presence of disseminated sulphides along the fracture zone/alteration zones/foliation planes within BGC. The host rock could be reason for the lower chargeability values is the presence of hard granitic-gneissic terrain with less overburden thickness (<15m). The low chargeability values (< 8 mV/V) towards the southern side of the Gudiyana village associated with low resistivity (< 800 Ohm.m) are interpreted as the acidic rocks of Gyangarh Asind acidic igneous suite with fractures likely to be water bearing.

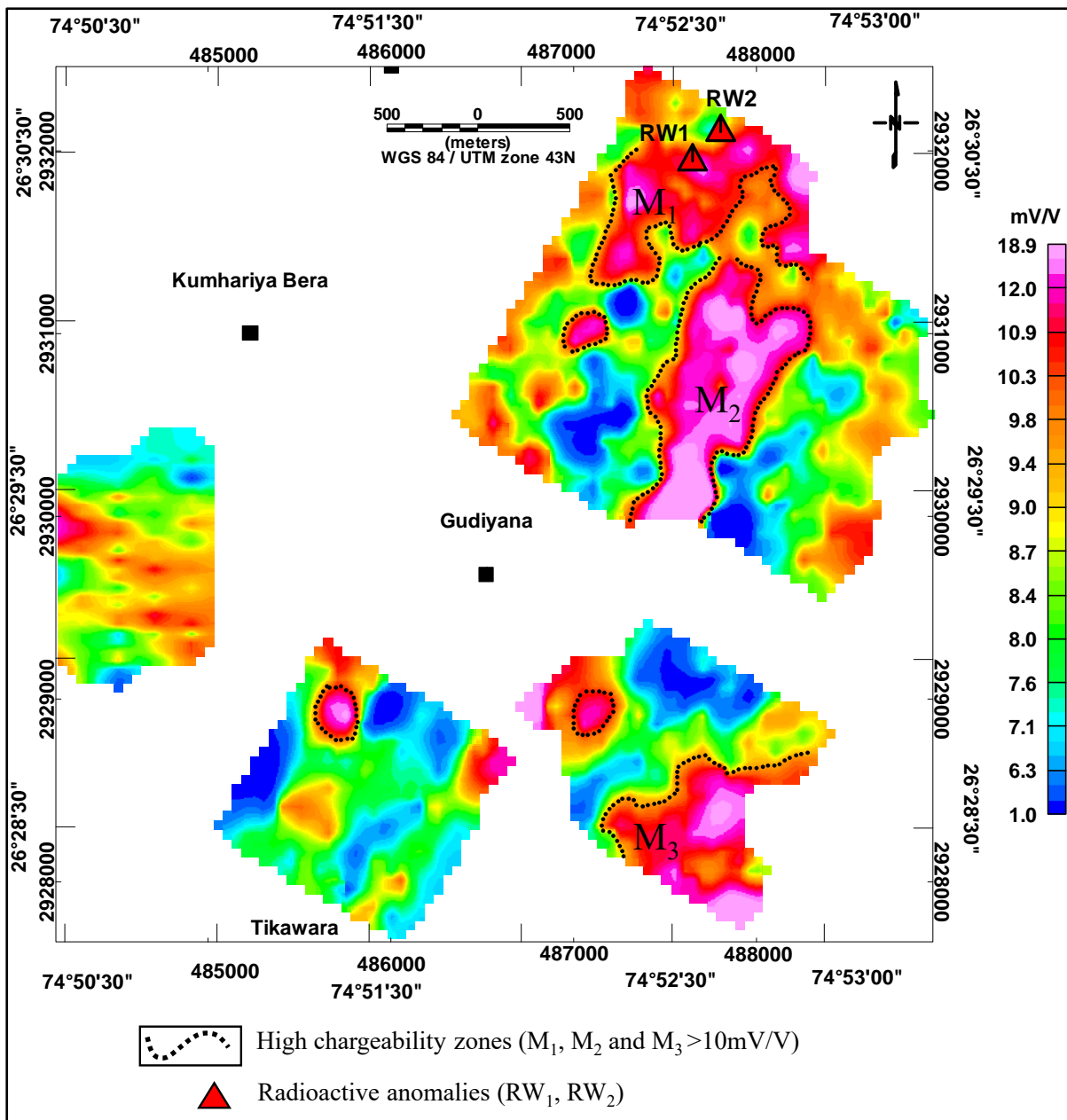


Figure 4.10 Apparent chargeability map, Chhota-Udaipur area, Ajmer district, Rajasthan

#### 4.6.3 Decay curve analysis of IP data

The Decay curve analysis of IP data has attempted over the high chargeability zones (>10mV/V) to understand the mineral distribution. Which is very effective when there is mono metallic mineral association and is useful to establish correlation of sulphides mineralization from known to unknown place. The country rock in the study area is biotite gneiss made up of alternating bands of quartz-felspathic and hornblende, biotite minerals. The previously reported

radioactive anomalies from Chhota Udaipur area has polymetallic character of uraninite, molybdenite, chalcopyrite, pyrite, magnetite, ilmenite and xenotime (Sinha et al., 2002).

The different order of decay time constant can be associated with different grain size and mineralization. As we can see in the Figure 4.11 there are two different orders of decay constant obtained by fitting the sum of two exponential series to the observed IP decay curve with a chi. square error of 0.10 at data point near radioactive anomaly (RW<sub>1</sub>). The decay constants obtained are 278 ms and 2077 ms. The first decay time constant 278 ms may represents the sulphide mineralization and the second decay time constant 2077 ms could be indicative of association of ferruginous material/ magnetite in gneiss. Similarly, for the IP data point near second radioactive anomaly (RW<sub>2</sub>) the decay time constant  $\tau_1$  and  $\tau_2$  are 175 ms and 1562 ms are obtained respectively, which represents less volume percentage of sulphides and magnetite mineralisation association than compared to the RW<sub>1</sub>. The decay curve analysis has been attempted for IP data points of 18 traverses of the high chargeability zone (>10 mV/V). The chargeability constants (a, b) and decay time constants ( $\tau_1$ ,  $\tau_2$ ) are estimated and bivariate plots are generated for 'a' against ' $\tau_1$ ' and 'b' against ' $\tau_2$ ' as shown in the Figure 4.13 & 4.14 respectively.

The horizontal trend of the bivariate plot (Figure 4.13) of chargeability constant(**a**) against decay time constant( $\tau_1$ ) signifies that the decay time constant values are varying over narrow range of chargeability. The horizontal trend may represent the increasing of grain size with less variation in sulphides concentration (Pelton et al., 1978). In the case of plot of chargeability constant(**b**) and decay time constant( $\tau_2$ ) (Figure 4.14), the trend of the points is near to vertical, which represents large variation of chargeability constant (b) values over limited variation in decay time constant, which implies the increase in concentration of ferruginous material/ magnetite in gneiss with less variation in grain size.

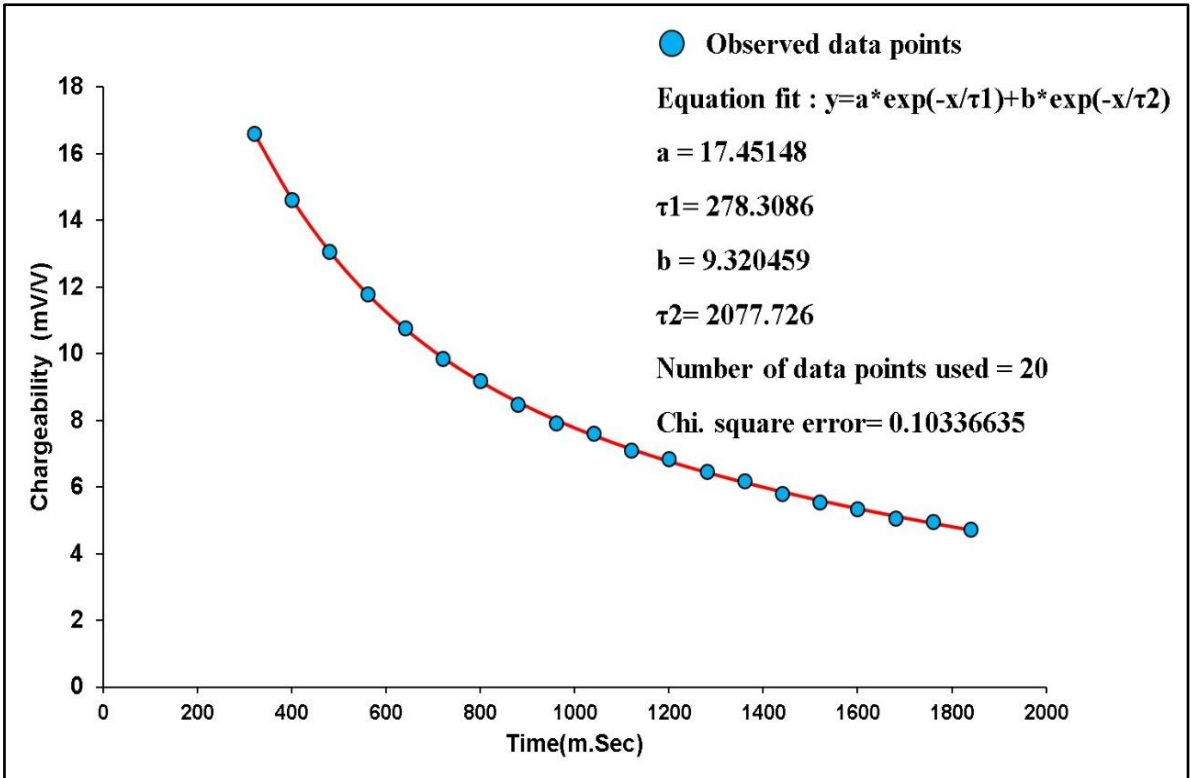


Figure 4.11 Chargeability decay curve analysis of IP data station near RW<sub>1</sub>

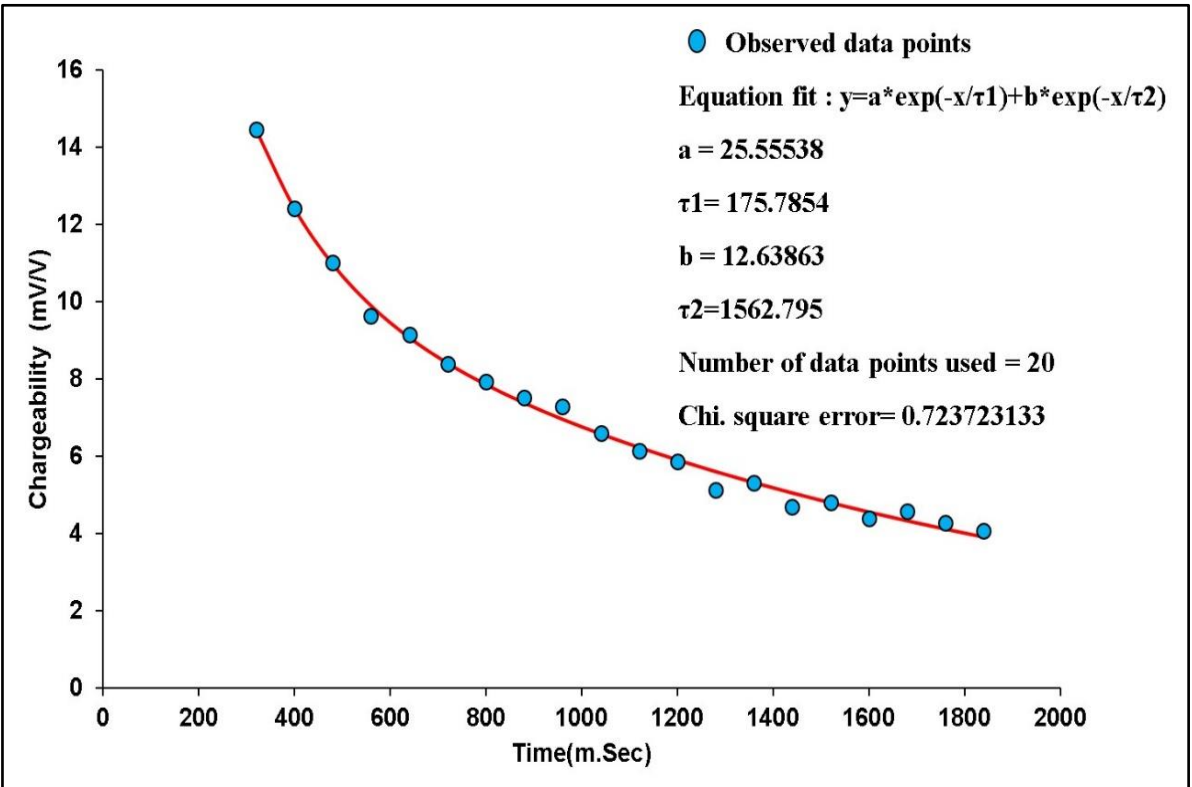


Figure 4.12 Chargeability decay plot analysis of IP data station near RW<sub>2</sub>

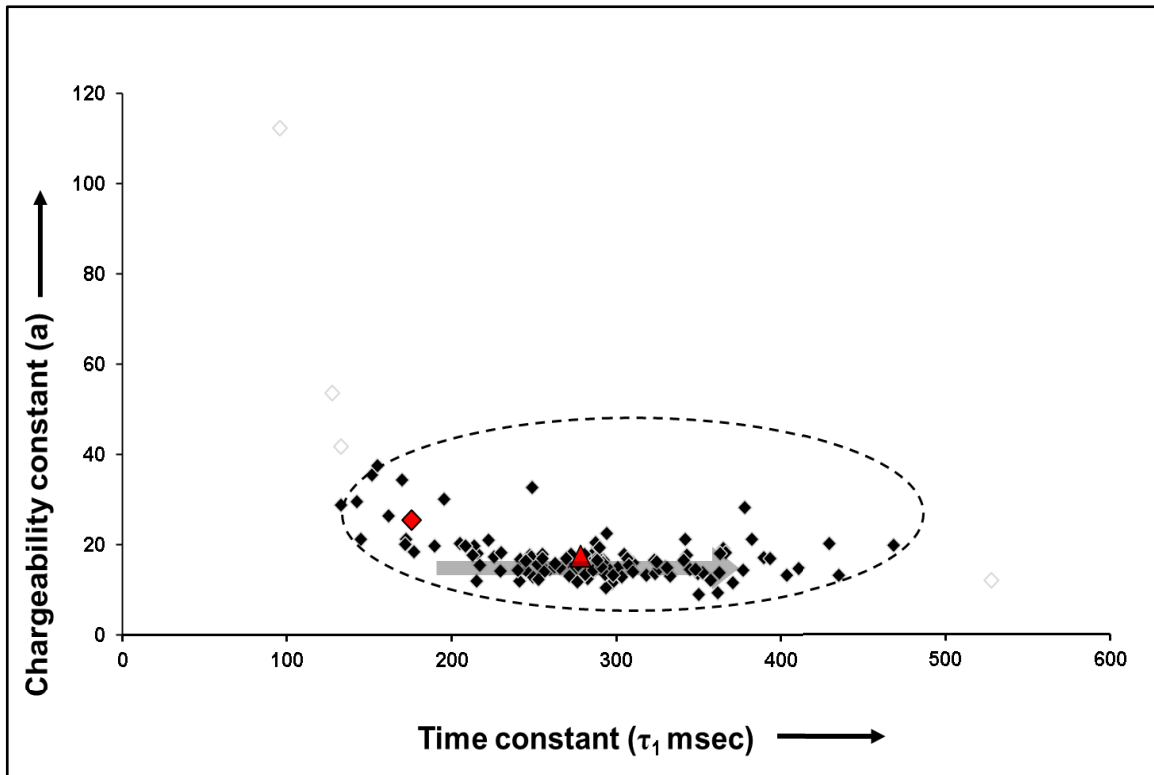


Figure 4.13 Bivariate plot of Chargeability constant(a) against Decay Time constant( $\tau_1$ )

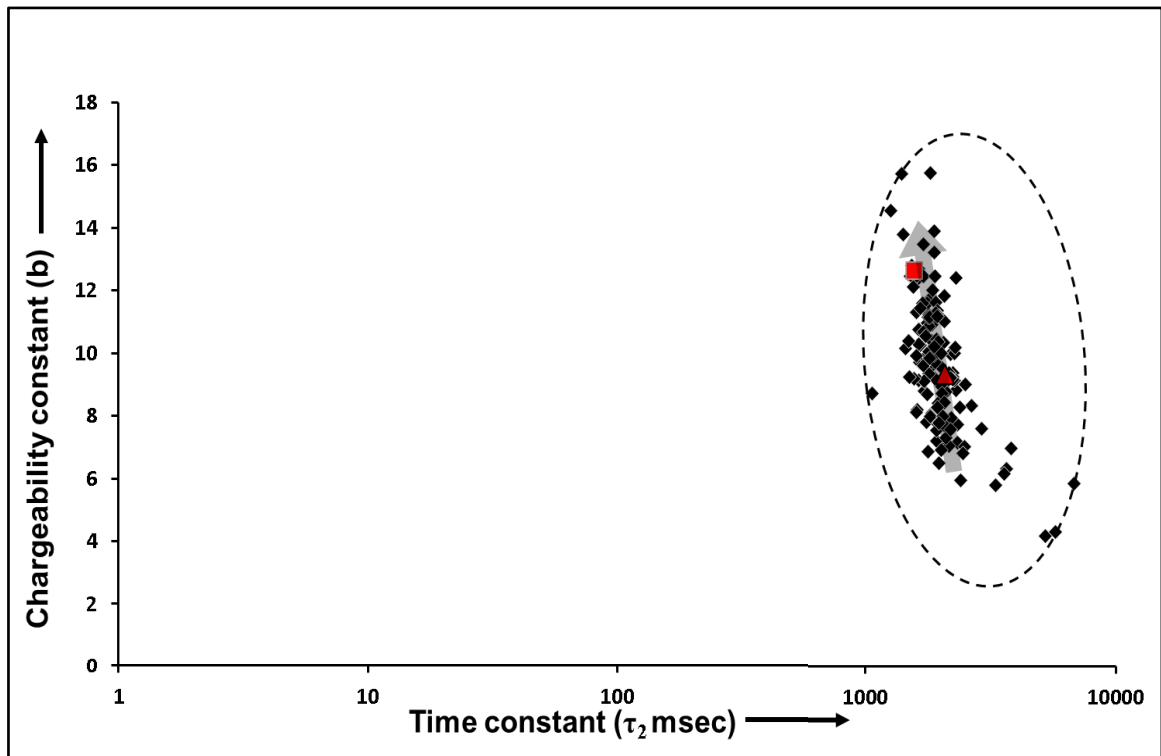


Figure 4.14 Bivariate plot of Chargeability constant (b) against Decay Time constant( $\tau_2$ )

#### 4.7 Inversion of IP/Resistivity Data

Inversion of apparent resistivity data enable to derive unambiguous interpretation of the earth's resistivity structure (Boonchaisuk et al., 2008). By modeling and inversion of the IP/resistivity data true resistivity and chargeability picture of the subsurface is derived.

Inverted model depth sections have been prepared from the IP/Resistivity data along the few traverses by using the RES2DINV program ([www.geotomosoft.com](http://www.geotomosoft.com)). The inversion program divides the subsurface into a number of small rectangular prisms and attempts to determine the resistivity and chargeability values of the prisms so as to minimize the difference between the calculated and observed apparent resistivity and chargeability values. The profile S8E covering a total length of 1200 m, interpreted up to a depth of 240 m is shown in Figure 4.15(A).

Table 4.1 Inversion parameters of chargeability and resistivity depth section of S8E line

S. No	Inversion parameters
1.	Line length is 1200m
2.	Electrode spacing is 50m
3.	Total no. of data points are 22
4.	The model has 8 layers and 102 blocks
5.	Absolute error is 10.90 for resistivity data and 1.52 for IP data
6.	Average sensitivity is 0.185

The 2-D interpreted geological model section can be characterized by low to high resistivity distributions in the range of 120-1970 Ohm.m, chargeability depth section corresponding to the same line is shown in Figure 4.15(B). As the study area is part of the banded gneissic complex (BGC) which contains high resistive compact metamorphic gneissic rocks exposed on the surface, the same is reflected in the depth section. Towards south-east

side of the section the high resistivity distribution start from surface and increases with depth. The progressive increase in formation resistivity indicate that the decrease in degree of weathering of the rock units from the surface to higher depth. A prominent low resistive zone (<179 Ohm.m) is observed in the north-west side of the section which is correlating with moderate chargeability (>10mV/V) signature in the chargeability depth section (Figure 4.15(Q)). the low resistivity and moderate chargeability zone indicate the fractures filled with sulphides within the BGC. The observed prominent low resistive and moderate chargeability zone in this section is reflected from 15m to up to the depth of 80m.

Inverted depth sections have been prepared for three traverses of S6, S7 and S8 to compare the resistivity and chargeability of three depth sections in order to know the depth as well as strike continuity and shown in Figures 4.16 and 4.17. As shown in the table 4.2 the following inversion parameters are utilized to prepare these inverted depth sections. In all the three sections, it is observed that the conductive zone starts from depth of around 15m and continues further up to 80m depth.

Table 4.2 Inversion parameters of chargeability and resistivity depth sections of S6, S7 and S8 lines

S. No	Parameters description	Parameters value		
		S6 Line	S7 Line	S8 Line
1.	Line length	1935	1978	1978
2.	Electrode spacing	50	50	50
3.	Total no. of data points	42	44	44
4.	No. of Model layers	12	11	11
6.	No. of model blocks	807	762	762
5.	Absolute error for resistivity data	3.29	4.95	2.23
	and IP data	0.19	1.71	1.96
6.	Average sensitivity	0.122	0.132	0.149

**Inverted 2D depth sections(P- resistivity; Q-Chargeability) of IP/Resistivity data, Chhota Udaipur area, Ajmer district, Rajasthan**

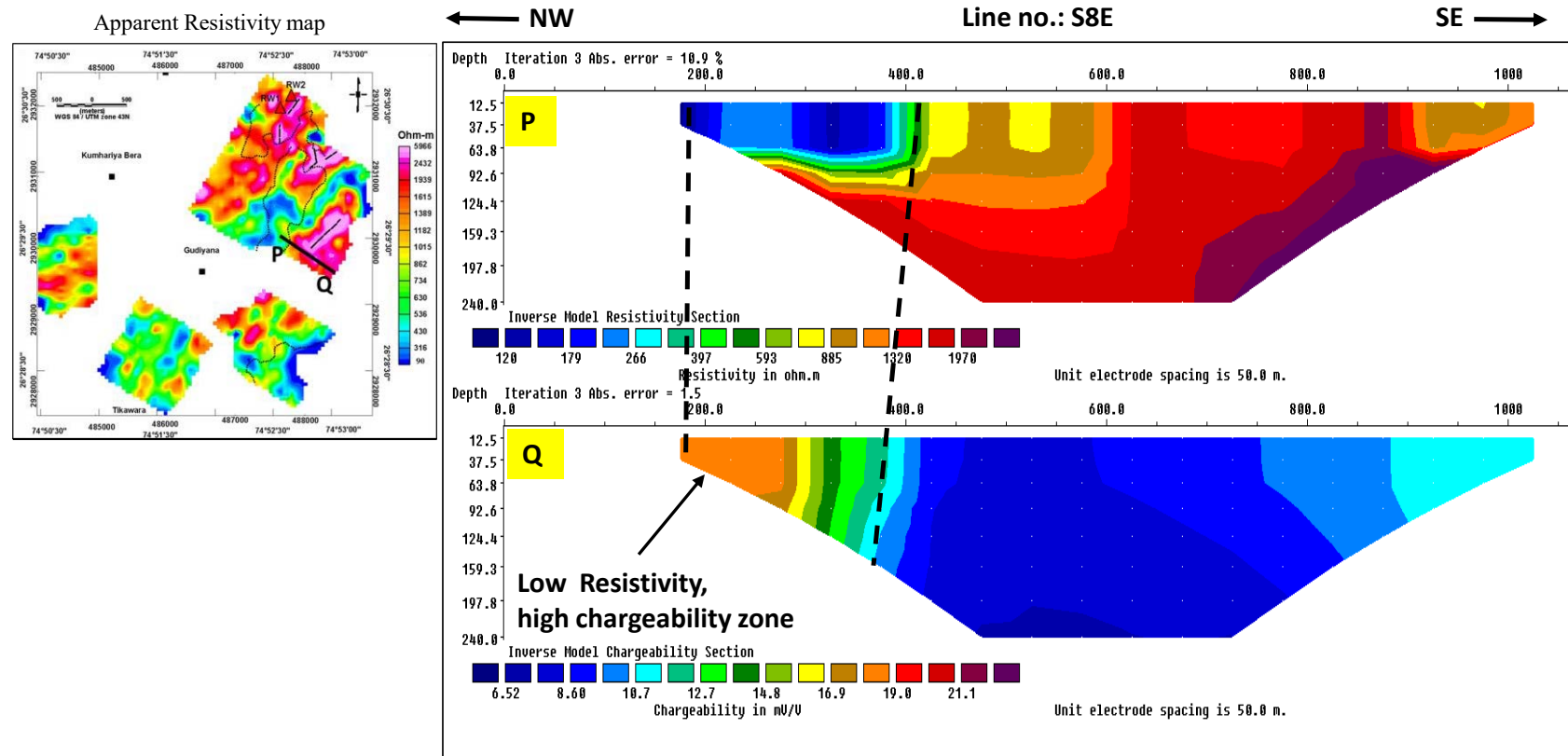
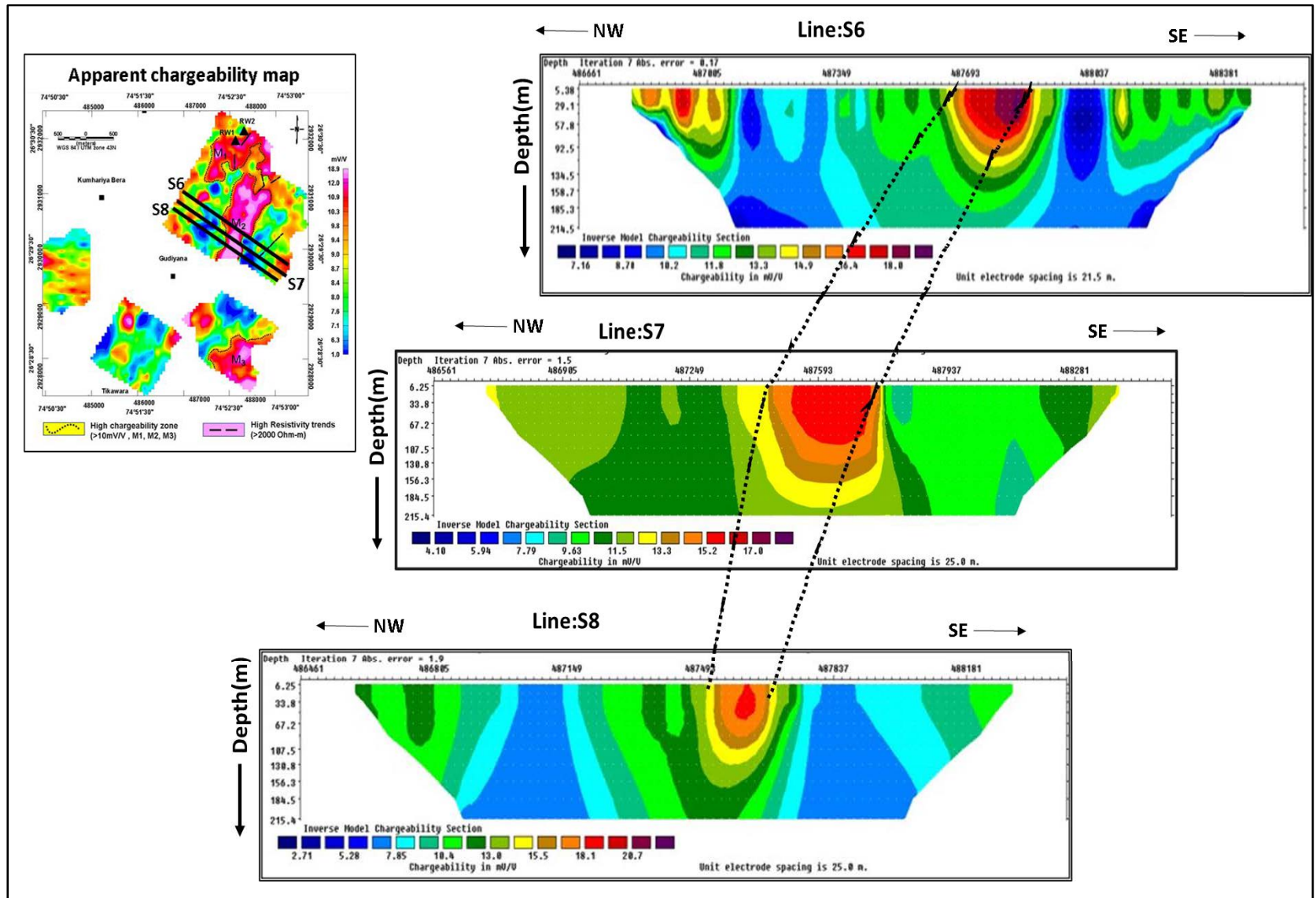


Figure 4.15 2D-Inverted depth sections (P) resistivity (Q) Chargeability of IP/Resistivity data along the traverse S8E



Figures 4.16 2-D Inverted depth-sections of Chargeability along the traverses S6, S7 and S8, Chhota Udaipur area, Ajmer district, Rajasthan

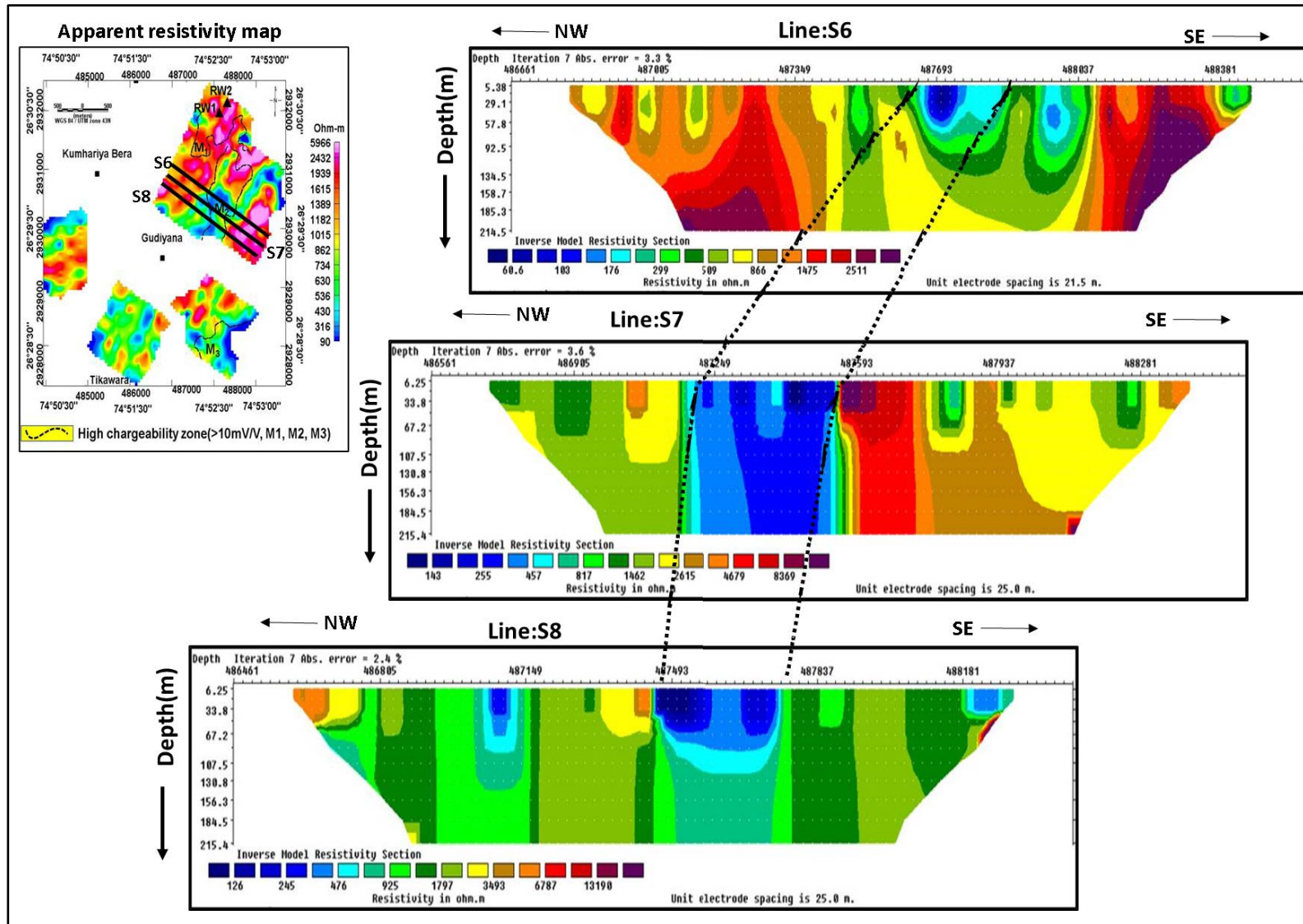


Figure 4.17 2-D Inverted depth-sections of Resistivity along the traverses S6, S7 and S8, Chhota Udaipur area, Ajmer district, Rajasthan

## CHAPTER 5

### INTEGRATED INTERPRETATION

The geophysical techniques are used as an indirect tool in uranium exploration. The study and analysis of multiple physical properties and laboratory information of different rock types in the study area along with geophysical signatures helps to resolve the ambiguities in interpretation. Laboratory analysis has been attempted for few grab samples which are representative of the different lithologies in the study area.

#### 5.1 Petrographic Study

Petrographic studies of grab samples from the study area has been carried out to derive additional information about nomenclature and mineralogy. The radioactive sample RW<sub>1</sub> (table 3.1) in hand specimen is greyish colour, hard and compact and it contains abundant biotite and sulphides. Under the microscope the rock is identified as hornblende biotite gneiss. The perfect lineation is made by the alignment of hornblende and biotite as well as stretching of quartz along the linear plane. The main ore minerals are magnetite, pyrrhotite, pyrite, and chalcopyrite.

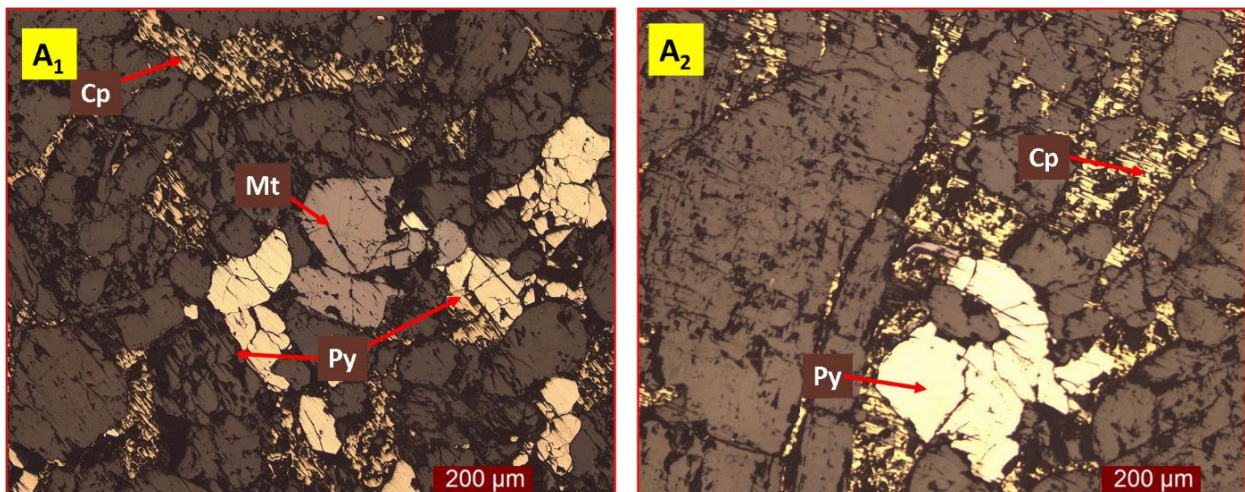
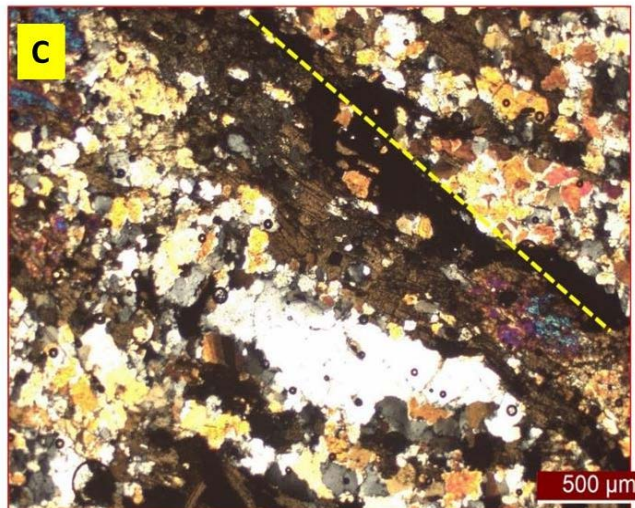
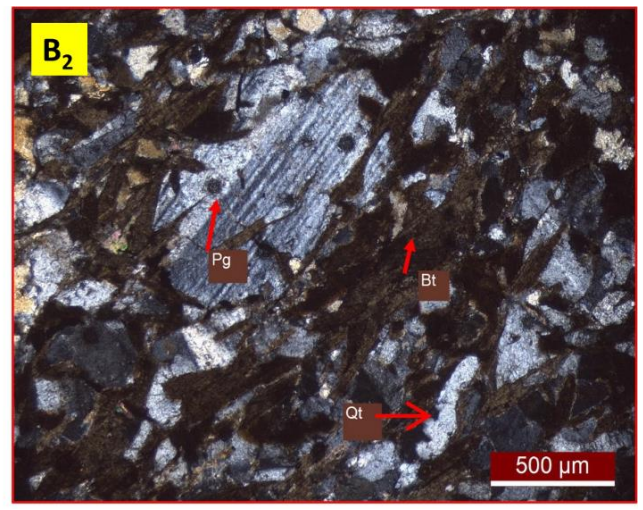
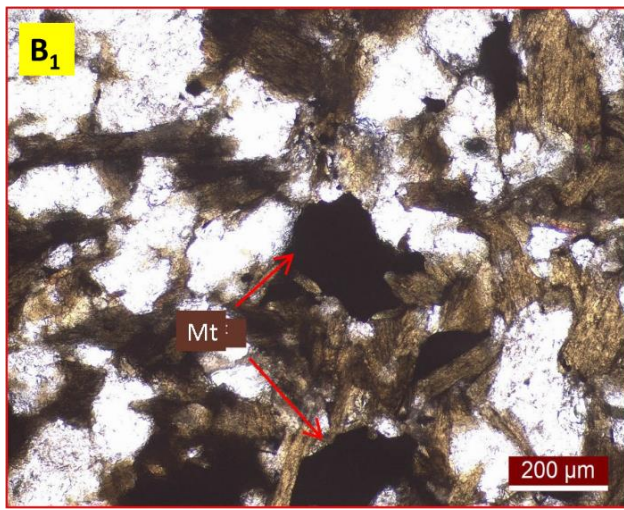


Figure 5.1 A<sub>1</sub> and A<sub>2</sub> Quartz biotite gneiss with Magnetite, Chalcopyrite and Pyrite.

Py = Pyrite, Cp = Chalcopyrite, Mt = Magnetite,

The thin sections of radioactive sample are shown in Figure 5.1. The sample has shown high susceptibility of 25-570 mSI.



Mt = Magnetite, Pg = Plagioclase felspar,  
Qt = Quartz, Bt = Biotite.

Figure 5.2 B<sub>1</sub> Quartz biotite gneiss with Magnetite in transmitted light and B<sub>2</sub>) plagioclase feldspars crystals

Figure 5.3 (C) Gneissose plane of gneiss

## 5.2 Hydrogeochemical study

The hydrogeochemical study provides direct information about concentration of elements in ground water implies subsurface and often able to test the distribution of uranium in the third dimension, giving evidence of the presence of buried deposits that may have no surface radiometric expression. In present study, along with the magnetic and IP/Resistivity surveys, radioactivity measurements have been made over the rock exposures using a scintillometer. The recorded readings were in the range of 25-15  $\mu R/hr$  which are not

significant. Hence, water sampling has been carried out in study area to know the anomalous radioactivity and to correlate its result with geophysical signatures.

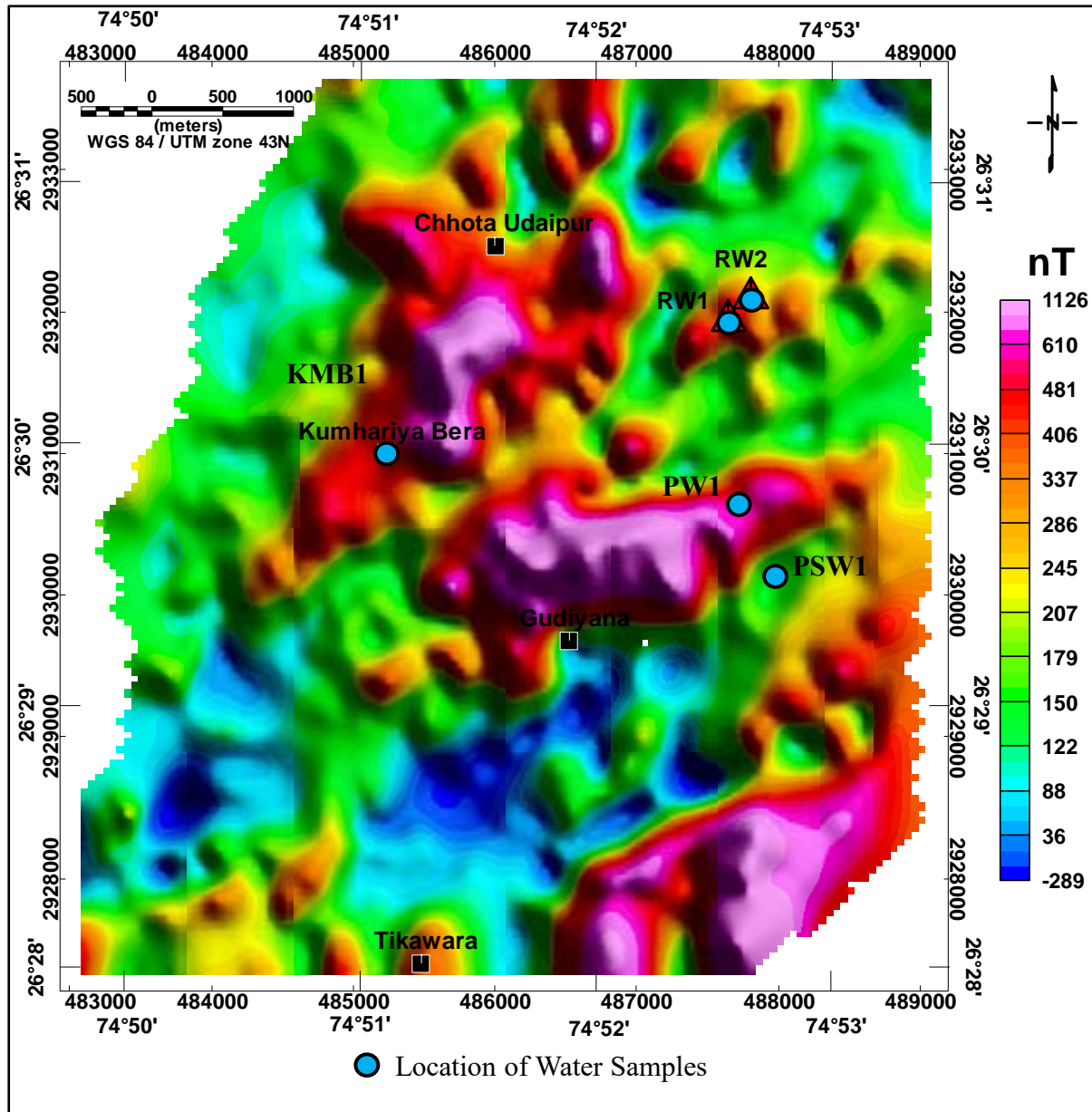


Figure 5.4 Water sample locations over the RTP map of Chhota Udaipur area, Ajmer district, Rajasthan

Total five water samples were collected from dug wells in the study area, among which two are collected from the two radioactive wells RW<sub>1</sub> and RW<sub>2</sub> and two are collected from the wells falling over high magnetic, high chargeability zones and one sample is collected from a well falling solely on alteration zones (malachite staining) (Figure 5.4). Generally, ground

water contains an order of 0.5- 2 ppb of uranium concentration which may be higher in granitic terrains (IAEA Vienna, 1988). Analysis of the water samples (table 5.1) shown less than 30 ppb uranium concentration. The water sample from near radioactive anomaly RW<sub>1</sub> has 28 ppb uranium concentration and another water sample from the well near kumariya bera village (KMB<sub>1</sub>) has 19 ppb uranium concentration, both are showing a positive correlation with Na<sup>+</sup>, HCO<sup>3-</sup>, Mg<sup>+2</sup>, TDS and relatively higher conductivity. The uranium values are not very significant but the dug well (RW<sub>1</sub>) is known for the association of radioactivity with up to 1.1% of eU3O8 from the grab samples. The crystalline gneissic complex rocks could be responsible for the less concentration of uranium in ground water. If considering 7-10 ppb as background value, hydrogeochemical anomalies in uranium at RW<sub>1</sub> and KMB<sub>1</sub> which may be related to fracture /alteration zones along which uranium bearing groundwaters may have reached the surface.

### **5.3 Geochemical analysis**

Correlation plot has been prepared for the major oxides of rock samples from the study area, it is observed that Iron oxide, phosphorous oxide and calcium oxides seems to have a negative correlation with silica oxide (Figure 5.5). The decreasing calcium with increasing silica content implies that some Ca bearing phase (Plagioclase) might have been fractionated from the parent magma, which is also supported by negative Strontium anomaly (Figure 5.4). From the Primitive Mantle normalized spider plot (Figure 5.6) it is observed that Barium showing a negative anomaly, it may be due to the hydrothermal fluid. Slightly negative Titanium anomaly signifies that metamorphism was moderate to high.

Table 5.1 Hydrogeochemical analysis of water samples, Chhota Udaipur area, Ajmer district, Rajasthan

S.No	Sample code	U (ppb)	Cond (mS/cm)	TDS (ppm)	Na <sup>+</sup> (ppm)	K <sup>+</sup> (ppm)	Ca <sup>2+</sup> (ppm)	Mg <sup>2+</sup> (ppm)	CO <sub>3</sub> <sup>2-</sup> (ppm)	HCO <sub>3</sub> <sup>3-</sup> (ppm)	Cl <sup>-</sup> (ppm)	SO <sub>4</sub> <sup>2-</sup> (ppm)	F <sup>-</sup> (ppm)	Cu (ppb)	Zn (ppb)	Ni (ppb)	Pb (ppb)
1.	RW1	28	2.8	1990	477	4	48	57	P.Nil	542	672	20	2	<10	18	<10	<20
2.	RW2	13	0.73	554	93	3	40	14	P.Nil	290	82	10	<0.5	<10	7	<10	<20
3.	KMB1	19	2.92	2010	352	10	128	86	P.Nil	602	640	59	1	<10	13	<10	<20
4.	PW1	14	1.69	1210	293	4	32	28	P.Nil	464	317	15	1.6	<10	18	<10	<20
5.	PSW2	7	1.02	774	139	2	48	19	P.Nil	433	93	20	1.4	<10	10	<10	<20

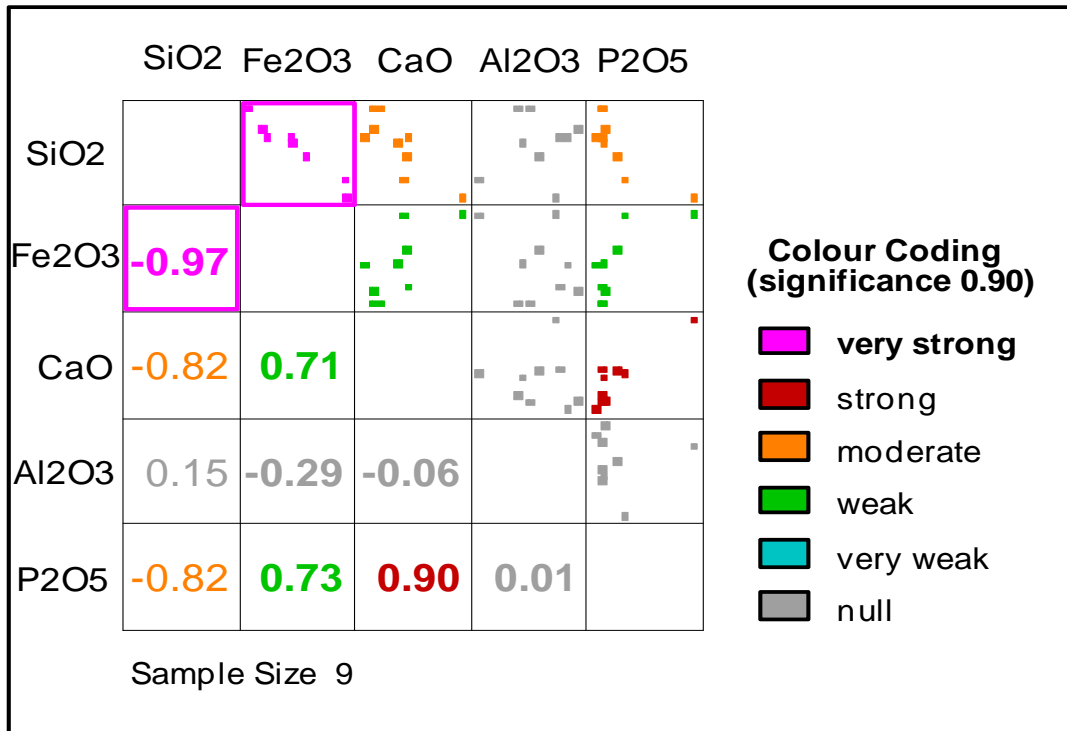


Figure 5.5 Correlation of major oxides

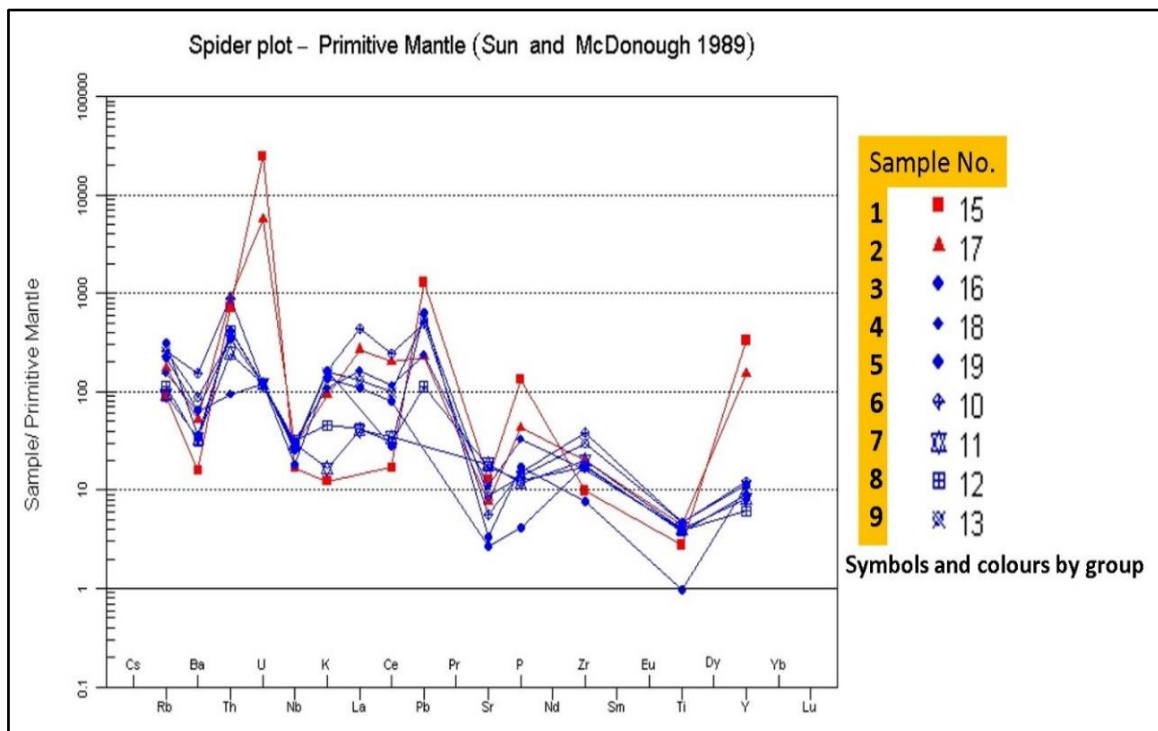


Figure 5.6 Primitive Mantle normalized spider plot

## 5.4 Profile analysis of Magnetic and IP/Resistivity data

In the image map preparation of the data, the interpolation of data by gridding techniques sometimes may create artifacts and mask the genuine anomalies. Profile analysis has been done for the better understanding of geophysical signatures at the two radioactive anomalies. Profiles are taken along the two radioactive anomaly locations in NW-SE direction perpendicular to the general trend of the geological features in the study area. Figure 5.7 shows the location of profiles over reduced to pole magnetic map and apparent chargeability map. As shown in Figure 5.8 the radioactive anomaly RW<sub>1</sub> is falling in the moderate low resistivity (~1460 Ohm.m), high magnetic (~460 nT) and moderate chargeability of 12 mV/V zone. The second radioactive anomaly RW<sub>2</sub> is falling in the high magnetic (~440 nT) and along gradient of the resistivity (1520 Ohm.m) and chargeability (8.5 mV/V) zone as shown in Figure 5.9.

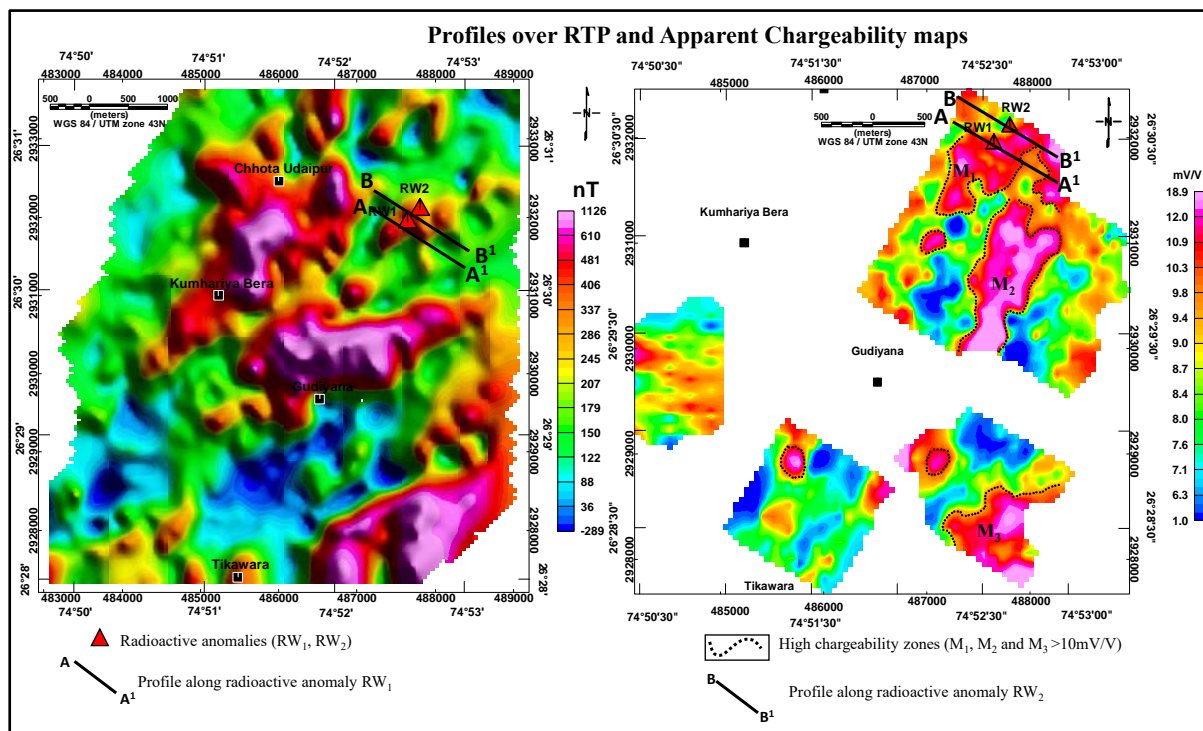


Figure 5.7 Profiles over RTP and Apparent chargeability maps

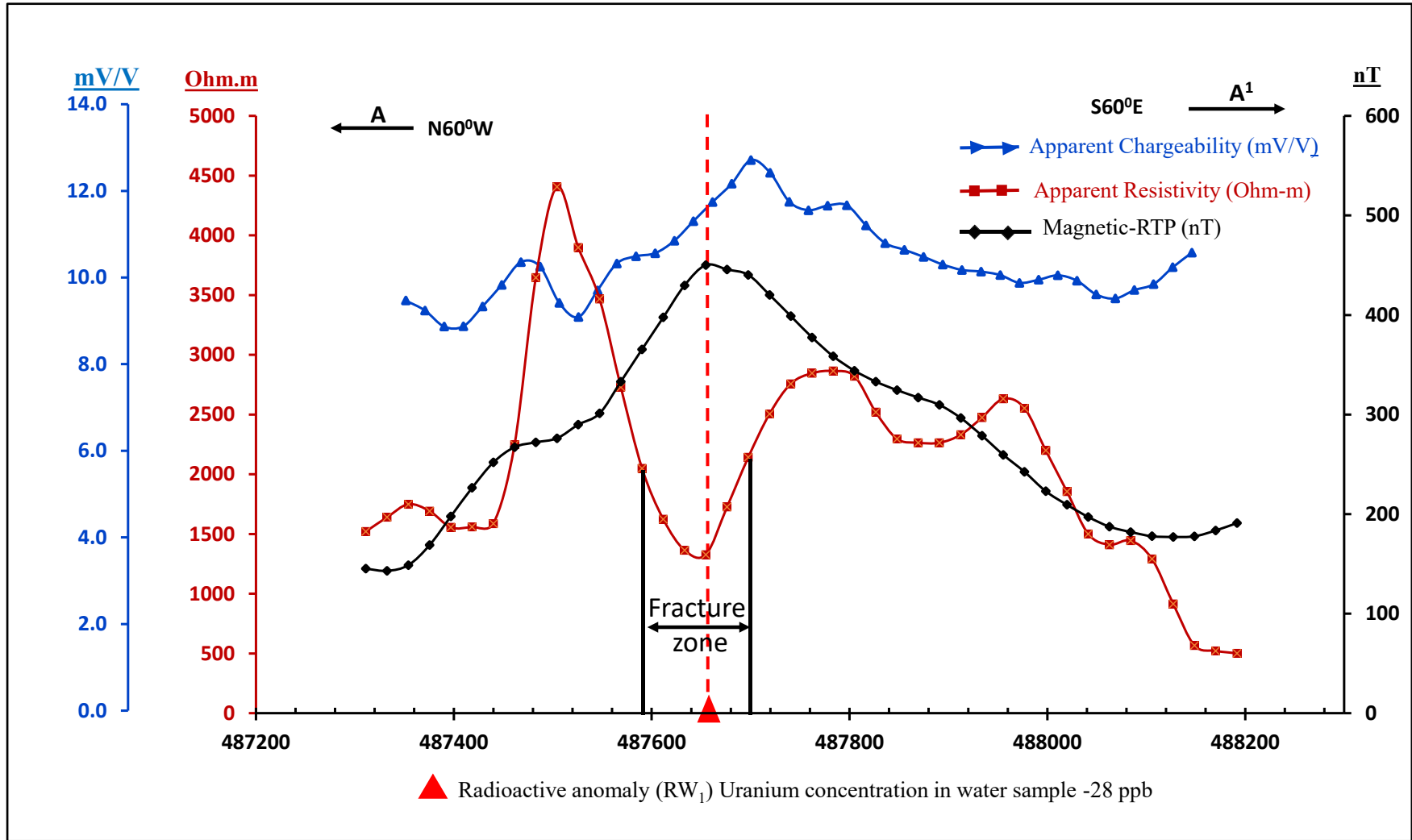


Figure 5.8 Profile analysis of magnetic and IP/Resistivity data along RW<sub>1</sub> line

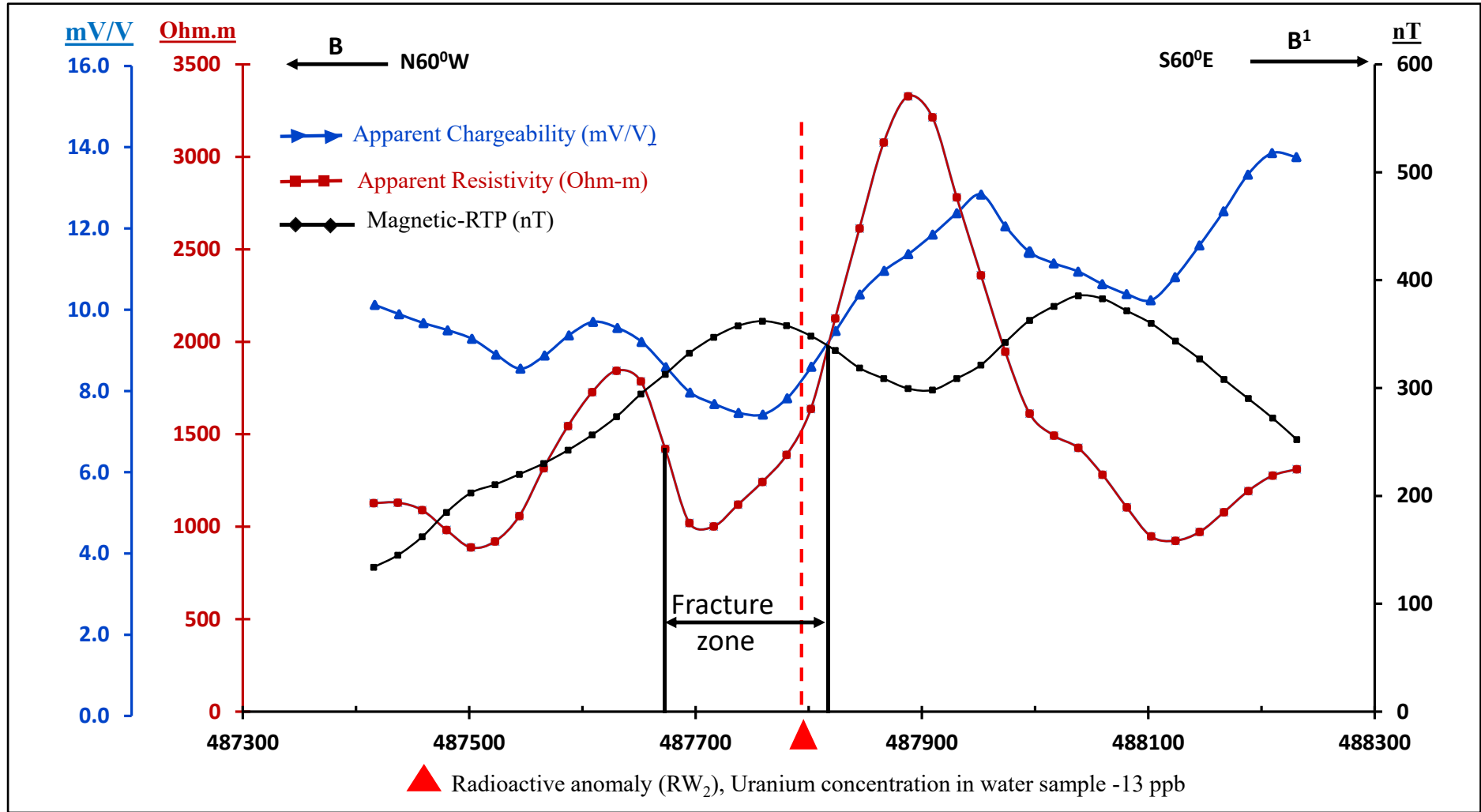


Figure 5.9 Profile analysis of magnetic and IP/Resistivity data along RW<sub>2</sub> line

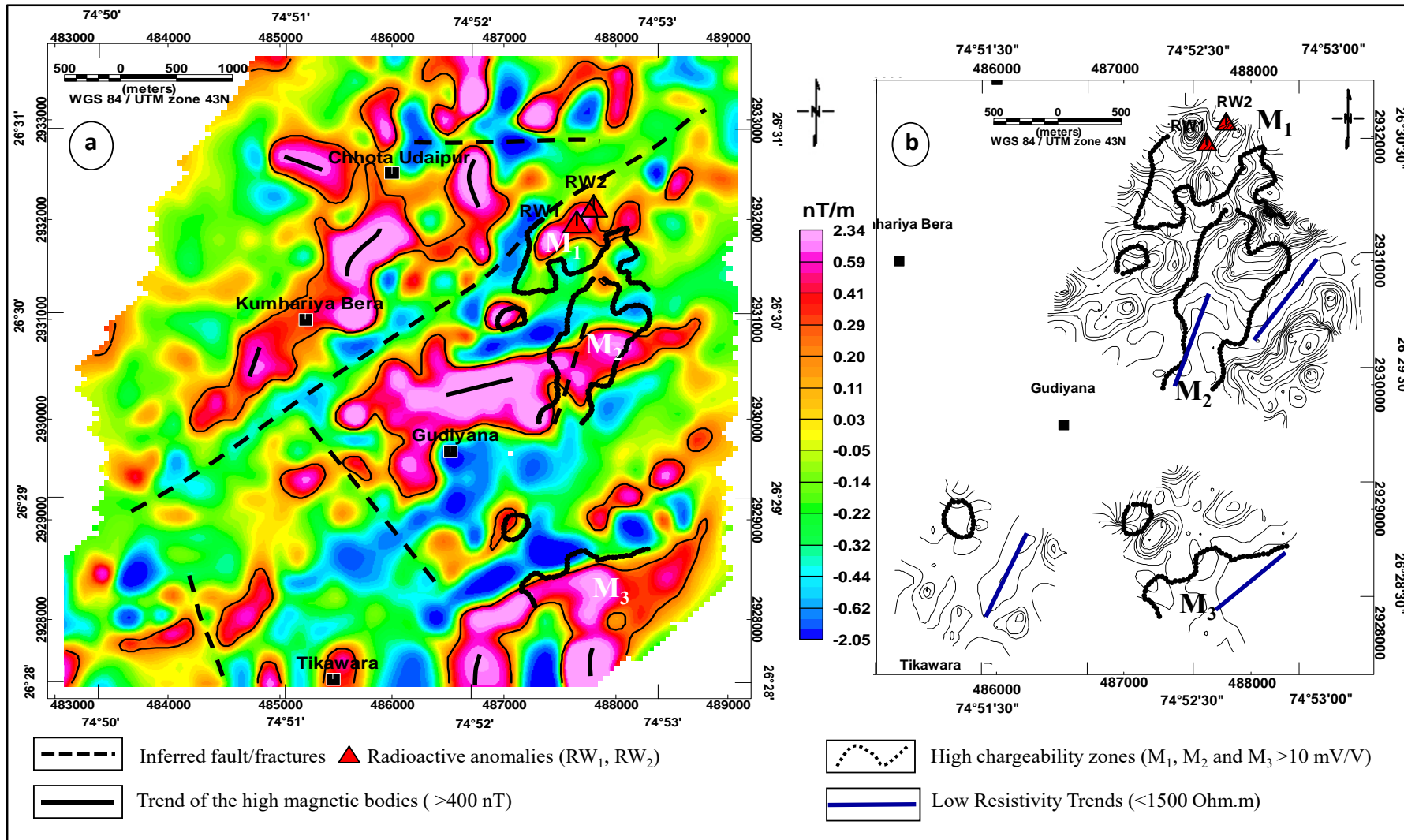


Figure 5.10 (a) Integrated structural features and high chargeability zones over FVD of RTP map  
 (b) Resistivity contour map of Chhota Udaipur area, Ajmer district, Rajasthan

The combined analysis of chargeability, resistivity and magnetic data of the area is shown in Figure 5.10(A) and 5.10(B). By integrating of the high chargeability zone ( $>10$  mV/V) with first vertical derivative of RTP and resistivity contour maps indicated that the high chargeability zones ( $M_1, M_2, M_3$ ) are coinciding with the low to moderate resistivity values (90-1500 Ohm.m). The high chargeability zone-  $M_1$  is correlating with moderate high magnetic values (380-440 nT) which is vindicated by the petrographic study of grab sample (Figure 5.1A<sub>1</sub> and A<sub>2</sub>) as the magnetite mineralization is present in the fractured/altered BGC is responsible for high magnetic, while presence of Chalcopyrite and pyrite for high chargeability. The association of similar geophysical signatures that are high magnetic, low resistivity and high chargeability values have been observed in the south east of the study area and demarcated as target zone.

Geochemical analysis of grab samples also revealed that the alteration and hydrothermal activity might have been taken place and iron oxide gets precipitated along with other minerals along the fractures. Based on the petrographic and hydrogeochemical studies, high magnetic signatures near kumariya bera ( $KMB_1$ ) village is caused by ilmenite and magnetite mineralisation in biotite gneiss which may be significant as it has anomalous anion and cation concentrations which are comparable with that of sample from  $RW_1$ .

Integrated interpretation of magnetic and IP/resistivity data including geophysical profile analysis, laboratory analysis and physical property measurements of grab rock samples and hydro geochemical studies, it is found that high chargeability zones ( $>10$  mV/V) which are well correlated with the moderate to low resistivity ( $< 1500$  Ohm.m) and moderate high magnetic zones ( $>400$  nT) could be favourable locales for uranium mineralization in this area



## CHAPTER 6

### CONCLUSIONS

Detailed ground geophysical surveys comprising of Induced polarization/Resistivity and Magnetic surveys were conducted in and around Chhota-Udaipur area, Ajmer district, Rajasthan. The study area is geologically highly deformed and contains moderate to high grade metamorphic rocks of Sandmata complex of Archean age, which has been subjected to hydrothermal alteration as revealed by the laboratory studies of grab samples and supported by the field observations.

Magnetic data over 30 sq. km area facilitated in demarcating faults/fractures trending in E-W, NE-SW and NW-SE directions. Three prominent high magnetic anomalies have been recorded and interpreted in terms of mafic intrusive bodies/magnetite mineralization in banded gneissic complex. 2-D and 3-D modeling of magnetic data enabled in deciphering the location and geometry of the structures in the study area. The derived plausible geological models provided useful information for further planning of sub surface exploration program.

From IP/Resistivity surveys, three high chargeability zones ( $M_1$ ,  $M_2$  and  $M_3$ ) have been successfully delineated. The NE-SW trending zone- $M_1$  has strike length of around 600 m with width of 90 to 130 m and continues further north-east. The radioactive anomalies are located in this high chargeability zone and associated with the geophysical signatures of moderately low resistivity (1460 Ohm.m) and high magnetic (460 nT). The second zone- $M_2$  in the eastern side of the study area has strike length of 1.5 km with width of 300 to 350 m and third zone- $M_3$  in the south east of the study area. The high chargeability zones are correlating with low resistivity and interpreted as the fracture/alteration zones filled with disseminated sulphides in BGC. Inverted depth sections of high chargeability zones yielded necessary information regarding the size, depth and width of the conductive body in the sub surface.

Based on integrated interpretation of geophysical data including profile analysis, laboratory analysis and physical property measurements of grab rock samples and hydro geochemical studies it is inferred that high chargeability zones ( $>10$  mV/V) associated with the moderate to low resistivity ( $< 1500$  Ohm.m) and moderate high magnetic zones ( $>400$  nT) represents alteration zones which could be favourable locales for uranium mineralization in the area

The present study has brought out the structural features and favourable target zones for uranium mineralisation in the study area by employing Magnetic and IP/Resistivity techniques. Future work includes after drilling of these anomalous zone, geophysical multiparameter logging has to be carry out to record the physical properties of formations against depth, which directly provides the subsurface information. The integration of surface and borehole database will provide detail understanding and genesis of the geology of the area and also this results will be used for precise subsurface modeling which also facilitate in adapting new techniques to define the subsurface structures and ore body with improved accuracy.

**PUBLICATION TITLE:**

**“Application of Magnetic and IP/Resistivity methods to Delineate the Structural Features and conductive zones: A case study from Chhota-Udaipur area, Ajmer district, Rajasthan”**

\*The above titled paper would be prepared for publication



## REFERENCES

- Austin, Jim., Andreas Björk., Ben Patterson., (2019). Structural controls of the Ernest Henry IOCG deposit: Insights from integrated structural, geophysical and mineralogical analyses. AEGC, From Data to Discovery – Perth, Australia.
- Baranov, V., Naudy, H., (1964). Numerical calculation of the formula of reduction to the magnetic pole. *Geophysics*. vol. 29, pp. 67-79.
- Boonchaisuk, S., Vachirastienchai, C., and Siripunvaraporn, W., (2008). Two Dimensional direct current (DC) resistivity inversion: Data space Occam`s approach: *Physics of the Earth and Planetary Interiors*, vol. 168, p. 204-211.
- Borner, F.D., Schopper, W. and Weller, A., (1996), Evaluation of transport and storage properties in the soils and groundwater zone from induced polarization measurements, *Geophysical Prospecting*, vol. 44(4), pp. 583-601.
- Briggs, I.C., (1974). Machine contouring using minimum curvature. *Geophysics*, vol. 39, pp. 39-48.
- Clark, D, A., French, D. H., Lackie, M. A., and Schmidt, P. W., (1992). Magnetic petrology: Application of integrated rock magnetic and petrological techniques to geological interpretation of magnetic suveys. *Exploration geophysics*, vol. 23, pp. 65-68.
- Crawford, A.R., (1970). The Precambrian geochronology of Rajasthan and Bundelkhand, northern India, *Can. J. Earth Sci.* vol. 7, pp. 91–110.
- Cull, J.P. & Massie, D., (2002). Aquifer mapping and groundwater quality in faults and fractures. *Exploration Geophysics*, vol. 33(2), pp. 122-126.
- Dash, J. K., S. Sethuram, V. Ramesh Babu and M. N. Chary, (2006). Target delineation for uranium exploration in the southern margin of Bhima basin – A Geophysical case study,

- Third International seminar and exhibition on exploration geophysics: Journal of Geophysics, AEG, pp. A18.
- Dentith, M., Mudge, S.T., (2014). Geophysics for the mineral exploration Geoscientist, Cambridge University press.
- Dhirenda Kumar Pandey., Alfred Uchman., Vineet Kumar., Rajesh Singh Shekhawat., (2014). Cambrian trace fossils of the Cruziana ichnofacies from the Bikaner-Nagaur Basin, north western Indian Craton. Journal of Asian Earth Sciences, Vol. 81, pp. 129–141.
- Dobrin, M.B., Savit, C.H., (1988). Introduction to Geophysical Prospecting. Fourth edition, McGraw-Hill, New York. p. 882.
- Esdale Donald., Pridmore, Don F., Coggon, John., Philip Muir, Peter Williams., Frank Fritz., (2003). The Olympic Dam copper-uranium-gold-silver-rare earth element deposit, South Australia: A geophysical case history, ASEG Extended Abstracts, pp. 147-168.
- GEM System., (2008). GSM-19 v7.0 Instruction manual. Manual release 7.4, GEM Systems, Canada.
- Gupta, S. N., Arora, Y. K., Mathur, R. K., Iqbaluddin, Parsad, B., Sahai, T. N., and Sharma, S. B., (1997). The Precambrian geology of the Aravalli region, Southern Rajasthan and northeastern Gujarat, Geological Survey of India, pp. 123.
- Henkel, H., Guzman, M., (1977). Magnetic features of fracture zones. Geoexploration, vol. 15(3), pp. 173-181.
- Heron, A.M., (1953). The Geology of central rajaputhana. Geological society of India, vol. 79, p.389

- Hong-Rui Fan., Kui-Feng Yang., Fang-Fang Hu., Shang Liu., Kai-Yi Wang., (2016). The giant Bayan Obo REE-Nb-Fe deposit, China: Controversy and ore genesis. *Geoscience Frontiers* vol.7, pp. 335-344.
- International Atomic Energy Agency, Vienna, (1988). *Geochemical Exploration for Uranium*, technical reports series no. 284.
- Kamlesh Kumar., (2018). Uranium mineralization in the Khetri sub-basin, North Delhi fold belt, India. poster, URAM-2018.
- Kearey, P., Brooks, N., Hill, I., (2002). *An Introduction to Geophysical Exploration*. 3<sup>rd</sup> edition, Blackwell Science. p. 281.
- Khandelwal, M.K., Bisht, B.S., Tiwary, A., Dash, S.K., Mundra, K.L., Padhi ,Ajoy.K., Nanda, L.K. and Maithani, P.B., (2008). Uranium-copper–molybdenum association in the Rohil Deposit, North Delhi Fold Belt, Rajasthan. *Mem. Geological society of India*, vol. 73, pp. 117-130.
- Loke, M. H., (2016). Tutorial: 2-D and 3-D electrical imaging surveys, pp. 207.
- Loke, M. H., (2011). Electrical resistivity surveys and data interpretation. In *Encyclopedia of Solid Earth Geophysics*, Springer, Dordrecht. pp. 276-283.
- Loke, M.H., (2000). *Electrical imaging surveys for environmental and engineering studies: A practical guide to 2-D and 3-D surveys*, p. 61
- Lopez-Loera, H., U.-Fucugauchi, J., A-Valdivia, L.M., (2010). Magnetic characteristics of fracture zones and constraints on the subsurface structure of the Colima Volcanic Complex, Western Mexico. *Geosphere*, vol. 6 (1), pp. 35–46.
- Lowrie, W., (2007). *Fundamentals of Geophysics*, Second edition: Cambridge University Press, New York. p. 393.

- Marshall, J.D., and Madden, T.R., (1959). Induced, polarization, a study of its causes, Geophysics, Vol. 24, pp. 790-816.
- Miller, H. G., and Singh, V., (1994). Potential field tilt: A new concept for location of potential field sources. Journal of Applied Geophysics, vol. 32, pp. 213–217.
- Mishra, B., Kumar, K., Khandelwal, M.K., and Nanda, L.K., Uranium mineralization in the Khetri sub-basin, North Delhi fold belt, India. Geological Society of India, pp 285 to 288.
- Nabighian, M.N., Grauch, V.J.S., Hansen, R.O., LaFehr, T.R., Li, Y., Peirce, J.W., Phillips, J.D. & Ruder, M.E., (2005). The historical development of the magnetic method in exploration. Geophysics, vol. 70 (6), pp. 33-61.
- Paterson, N.R., Reeves, C.V., (1985). Applications of gravity and magnetic surveys: the state of the-art in 1985. Geophysics, vol. 50, pp. 2558–94.
- Pedersen, L. B., (1979). Constrained inversion of potential field data: Geophysical Prospecting, Vol. 27, pp. 726–748.
- Pelton, W.H., Ward, S.H., Hallof, P.G., Sill, W.R., and Nelson, P.H., (1978). Mineral discrimination and removal of inductive coupling with multi-frequency IP, Geophysics, Vol. 43, pp. 588-609.
- Peters, L.J., (1949). The direct approach to magnetic interpretation and its practical application. Geophysics, vol. 14, pp. 290–320.
- Powell, B., Wood, G., Bzdel, L., (2007), Advances in Geophysical Exploration for Uranium Deposits in the Athabasca Basin, Proceedings of Exploration 07, pp. 771-790
- Radhakrishna murthy, I.V., and Rama Rao, B.S., (1978). Gravity and Magnetic methods of prospecting. Gulab vazirani publishers -India, p. 390.
- Ramakrishnan, M., Vaidyanathan, R., (2010). Geology of India. Geological society of India.

- Ramesh Babu, V., 2007. Modeling and Inversion of Magnetic and VLF-EM data for Uranium Exploration, Raigarh district, Chhattisgarh, India: PhD Thesis, Osmania University.
- Reid, A. B., J. M. Allsop, H. Granser, A. J. Millett, and I. W. Somerton, (1990). Magnetic interpretation in three dimensions using Euler deconvolution: *Geophysics*, vol. 55, pp. 80–91
- Roberts, C.L., Smith, S.G., (1994). A new magnetic survey of Lundy Island, Bristol Channel. *Proceedings of the Ussher Society*, vol. 8 (3), pp. 293-297.
- Salem Ahmed., Simon Williams , Derek Fairhead, Richard Smith, and Dhananjay Ravat, (2008). Interpretation of magnetic data using tilt-angle derivatives. *Geophysics*, Vol. 73, pp. L1–L10.
- Satyanarayana, K. V., Mahender, S., and Rama Rao, J. V., (2018). Multi parameter geophysical Surveys for Identification of Geological Environment favorable for base metal mineralization in mallapuram block, Markapur base metal Belt, Cuddapah Basin. *Jour. of Geophysics*, Vol. XXXIX No.2, pp 51-56.
- Satyanarayana, M. V., Subhash Ram., Navin Goyal, Srinivasan, S., Srinivas, R., Nanda, L. K., and Chaturvedi, A. K., (2014). Delineation of Structure over Karara-Tavidar Volcanics of Jalore District, Rajasthan, by Magnetic and Gravity Investigations - An Appraisal of the Integrated Results. *Jour. of Geophysics*. XXXV No.4, pp 159-165.
- Seigel, H.O., (1959). Mathematical formulation and type curves for induced polarization, *Geophysics*, Vol. 24, No. 3, pp. 547-565.
- Seigel, H.O., Vanhala, H., and Sheard, S.N., (1997). Some case histories of source discrimination using time-domain spectral IP, *Geophysics*, Vol. 62, No. 5, pp. 1394- 1408.
- Shrajala Pitla., SrinivasaRao, B., Allipeera, P., Subhash Ram., Chaturvedi, A.K., (2015). Application of geophysical techniques in uranium exploration along the albitite line,

- Kerpura-Karoi area, Sikar district, Rajasthan. Jour. of Geophysics, Vol. XXXVI No.2, pp 95-102.
- Sinha, D. K., SohailFahmi, Sarkar, B.C., and Roy, M.K., (2002). Discovery of the uraniferous polymetallic veins in the gneisses of Chhota-Udaipur, Ajmer District, Rajasthan. Geological Society of India, Vol.59, pp. 469 - 472.
- Sinha-Roy, S., Malhotra, G., Mohanty, M., (1998). Geology of Rajasthan. Geological Society of India. p.278
- Spector, A., Grant, F.S., (1970). Statistical models for interpreting aeromagnetic data: Geophysics, vol. 35. pp. 293-3302.
- Srinivasa Rao, S., Krishna chaithanya, K., Deepak Kumar., (2018). Annual report on detailed induced polarization (IP) / resistivity and magnetic surveys in the west and east of Rohil deposit, Sikar district, Rajasthan. Unpublished report, AMD/DAE.
- Srinivasa Rao, B., Subashram., Shaik Roshan Ali., Viney Kumar., Dash, J. K., Purohit, R. K., and Chaturvedi, A. K., (2016). Application of Integrated Geophysical Techniques to Delineate Favourable Structures and Conductive Zones for Uranium Mineralization in Narasinghpuri-Salwari Areas, Sikar District, Rajasthan. Jour. of Geophysics, Vol. XXXVII No.4, pp. 191-196
- Subash Ram., Nepal Singh., Kumar, B.V.L., Srinivas, R., (1999). Brief annual report on detailed geophysical surveys at Chhota Udaipur area, Ajmer district , Rajasthan.. Unpublished report, AMD/DAE.
- Sumner, J.S., (1976). Principles of induced polarization for geophysical exploration: Elsevier Science Publ. Co., Inc. p. 276

Sumit Kumar Ray., (1987). Albitite occurrences and associated Ore Minerals in the Khetri Copper belt, North-Eastern Rajasthan. Geological Society of India, Vol. 113-7, pp.41-49.

Telford, W.M., Geldart, L.P., and Sheriff, R.E., (1990). Applied Geophysics, Cambridge University Press, 2nd edition, pp. 289-291.

Thompson, D. T. (1982), A new technique for making computer-assisted depth estimates from magnetic data: Geophysics, vol.47, pp.31–37.

Tuncer Volkan , Martyn J. Unsworth<sup>1</sup> , Weerachai Siripunvaraporn , and James A. Craven., (2006). Exploration for unconformity-type uranium deposits with audiomagnetotelluric data: A case study from the McArthur River mine, Saskatchewan, Canada, Geophysics, vol. 71, pp. 201–209.

Vijaya Kumar, V., Shrajala Pitla., Siva Krishna, Y., Shashank Shekar Mishra., (2015). Annual report on regional magnetic and detailed ip/resistivity surveys in mawata-jahaz-bera ki dhani block, Jhunjhunu district, Rajasthan. Unpublished report, AMD/DAE.

<https://www.agiusa.com/blog/comparison-11-classical-electrode-arrays>

<https://www.eoas.ubc.ca>

<http://www.gemsys.ca/versatile-proton-magnetometer>

<http://www.geosoft.com>

<http://www.iris-instruments.com>

<http://www.tensor-research.com.au>

<https://www.yumpu.com/user/terraplus.ca>

<https://www.world-nuclear.org>